

Aus dem Institut für kardiovaskuläre Physiologie und
Pathophysiologie
im Walter Brendel Zentrum für experimentelle Medizin, WBex
Institut der Ludwig-Maximilians-Universität München
Komm. Direktor: Prof. Dr. med. Markus Sperandio
Ehem. Direktor: Prof. Dr. med. Ulrich Pohl

Differential Role of the AMP-Kinase's α Subunits in Controlling Microvascular Smooth Muscle Tone

Dissertation
zum Erwerb des Doktorgrads der Medizin
an der Medizinischen Fakultät der
Ludwig-Maximilians-Universität zu München

vorgelegt von
Margarethe Wiedenmann, geb. Gangkofner
aus
München

Mit Genehmigung der Medizinischen Fakultät
der Universität München

Berichterstatter: Prof. Dr. med. Ulrich Pohl
Mitberichterstatter: Prof. Dr. rer. nat. Alexander
Faußner
PD Dr. med. Andreas Lechner
Mitbetreuung durch die
promovierten Mitarbeiter: Kai-Michael Schubert, PhD
Dr. med. Holger Schneider
Dekan: Prof. Dr. med. dent. Reinhard HICKEL

Tag der mündlichen Prüfung: 06.06.2019

Table of contents

<u>TABLE OF CONTENTS</u>	<u>I</u>
<u>LIST OF FIGURES</u>	<u>IV</u>
<u>1. INTRODUCTION</u>	<u>1</u>
1.1. REGULATION OF THE CIRCULATORY SYSTEM	1
1.1.1. RELEVANCE OF RESISTANCE ARTERIES	1
1.1.2. REGULATION OF VASCULAR TONE	4
1.2. AMP-KINASE	7
1.2.1. DISCOVERY AND STRUCTURE OF THE AMP-KINASE	7
1.2.2. RELEVANCE OF THE AMP-KINASE	9
1.2.3. REGULATION OF THE AMP-KINASE	11
1.3. AIM OF THIS STUDY	13
<u>2. MATERIAL</u>	<u>14</u>
2.1. ANIMALS	14
2.2. EXPERIMENTAL SETUP AND DEVICES	14
2.3. MATERIAL	15
2.4. SOFTWARE	16
2.5. BUFFER SOLUTIONS AND AGENTS	16
2.5.1. BUFFER SOLUTIONS	16
2.5.2. AGENTS	17
2.5.3. PCR	19
<u>3. METHODS</u>	<u>20</u>
3.1. VESSEL PREPARATION AND CANNULATION	20
3.1.1. PREPARATION OF THE MESENTERIC ARTERIES	20
3.1.2. PREPARATION OF THE SKELETAL MUSCLE ARTERIES	20
3.1.3. VESSEL CANNULATION	21
3.2. CALCIUM MEASUREMENT WITH FURA-2AM	22

3.2.1. INCUBATION WITH FURA-2AM	22
3.2.2. MODE OF ACTION OF FURA-2AM	23
3.2.3. MEASUREMENT OF INTRACELLULAR CALCIUM	23
3.2.4. STRUCTURE OF THE CALCIUM WORKSTATIONS	25
3.2.5. MEASUREMENT OF VESSEL DIAMETER	26
3.3. ABBREVIATIONS	27
3.4. PROTOCOLS	29
3.4.1. PCR	29
3.4.2. ADDITION OF AGONISTS	30
3.4.3. VESSEL-DEPENDENT DISQUALIFYING FACTORS	30
3.4.4. BLOCKING THE ENOS AND THE COX	31
3.4.5. DOSE-RESPONSE CURVES	31
3.4.6. CALCIUM-DESENSITIZATION CURVES	33
3.4.7. ANALYSIS	34
4. RESULTS	38
4.1. COMPARISON OF SKELETAL MUSCLE ARTERIES AND MESENTERIC ARTERIES	38
4.1.1. GENERAL VESSEL CHARACTERISTICS	38
4.1.2. CONSTRICTION	38
4.1.3. RELAXATION	39
4.2. AMP-KINASE IN MESENTERIC ARTERIES	42
4.2.1. EXPRESSION OF AMP-KINASE'S SUBUNITS IN MESENTERIC ARTERIES	42
4.2.2. INFLUENCE OF A76/PT1 ON MESENTERIC ARTERIES	43
4.2.3. CALCIUM SENSITIVITY	45
4.2.4. THE RELATIVE ROLE OF THE DIFFERENT AMP-KINASE'S A SUBUNITS AS STUDIED IN KNOCKOUT MICE	47
5. DISCUSSION	60
5.1. FINDINGS	60
5.2. CHARACTERIZATION OF MOUSE ARTERIES	60
5.3. THE AMP-KINASE IN MOUSE MESENTERIC ARTERIES	62
5.3.1. THE EFFECT OF THE AMP-KINASE'S A SUBUNITS ON DECREASING INTRACELLULAR CALCIUM LEVELS	65

5.3.2. THE EFFECT OF THE AMP-KINASE'S A SUBUNITS ON CALCIUM SENSITIVITY	66
5.4. CONSEQUENCES OF THESE FINDINGS FOR VASCULAR CONTROL	68
<u>6. SUMMARY</u>	<u>A</u>
<u>7. ZUSAMMENFASSUNG</u>	<u>C</u>
<u>8. REFERENCES</u>	<u>F</u>
8.1. BOOKS	F
8.2. ARTICLES	F
<u>ACKNOWLEDGEMENTS</u>	<u>- 1 -</u>
<u>EIDESSTATTLICHE VERSICHERUNG</u>	<u>- 2 -</u>

List of figures

Figure 1 “Changes in blood pressure, velocity, and the area of the arteries, capillaries, and veins of the circulatory system”	2
Figure 2: Mechanisms of vasoconstriction and vasodilation in smooth muscle cells	7
Figure 3: The far-reaching influence of the AMP-kinase and how it self-regulates	9
Figure 4: Regulation of the AMP-kinase (adapted from original of Kreutz (2013))	12
Figure 5: First, second and third generation of mesenteric arteries after preparation	20
Figure 6: Set-up for vessel cannulation.....	22
Figure 7: Excitation and emission spectrum of Fura-2	24
Figure 8: Structure of workstation 1 (modified original of Kreutz (2013))	27
Figure 9: Effect of U46 on skeletal muscle arteries and mesenteric arteries.....	39
Figure 10: Dose-dependent effects of acetylcholine (ACh) in skeletal muscle arteries and mesenteric arteries	40
Figure 11: Influence of L-NAME on ACh-induced dilation in skeletal muscle arteries	41
Figure 12: Effects of nifedipine on skeletal muscle arteries and mesenteric arteries	42
Figure 13: Relative expression levels of AMPK subunits in mesenteric arteries	43
Figure 14: Dose-dependent dilation and Fura decrease on addition of A76	44
Figure 15: A76-induced dose-dependent dilation and decrease of the Fura ratio.....	45
Figure 16: PT1-induced dose-dependent dilation	45
Figure 17: Dose-dependent constriction and Fura increase on addition of increasing doses of extracellular Ca ²⁺ in a mesenteric artery with and without additional A76	46
Figure 18: Effect of A76 on Ca ²⁺ sensitivity.....	47
Figure 19: Effect of norepinephrine on α_1 and α_2 wild type and knockout vessels	48
Figure 20: Effect of depolarization on α_1 and α_2 wild type and knockout vessels.....	49
Figure 21: Effect of PT1 on α_2 wild type and knockout vessels.....	50
Figure 22: Effect of PT1 on α_1 wild type and knockout vessels.....	51
Figure 23: Effect of A76 on α_2 wild type and knockout vessels.....	52
Figure 24: Effect of A76 on α_1 wild type and knockout vessels.....	52

List of figures

Figure 25: Effect of iberiotoxin (IbTX) on A76-related dilation and decrease of the Fura ratio in α_2 wild type and knockout vessels.....	54
Figure 26: Effect of iberiotoxin (IbTX) on A76-related dilation and decrease of the Fura ratio in α_1 wild type and knockout vessels.....	55
Figure 27: Dose-dependent dilation on addition of increasing doses of A76 in both BkCa wild type and knockout vessels	56
Figure 28: Effect of thapsigargin (TG) on A76 (100 μ M)-induced dilation and decrease of Fura ratio in α_1 knockout and wild type vessels	57
Figure 29: Effect of thapsigargin (TG) on A76 (100 μ M)-induced dilation and decrease of Fura ratio in α_2 knockout and wild type vessels	57
Figure 30: Effect of A76 on Ca^{2+} sensitivity in α_2 knockout vessels	58
Figure 31: Effect of A76 on Ca^{2+} sensitivity in α_1 wild type and knockout vessels.....	59

1. Introduction

1.1. Regulation of the Circulatory System

1.1.1. Relevance of Resistance Arteries

Small arteries or arterioles with a diameter smaller than 400 μm constitute the main flow resistance in the vascular system and are therefore characterized as arterial resistance vessels (Intengan and Schiffrin (2000)). They reduce the blood pressure and the blood flow in capillaries to ensure the possibility of gas and nutrient exchange. A blood pressure of about 35 mmHg and a blood flow of about 0.03 cm/sec prove to be a good setting for gas and nutrient exchange between the capillaries and the surrounding tissue.

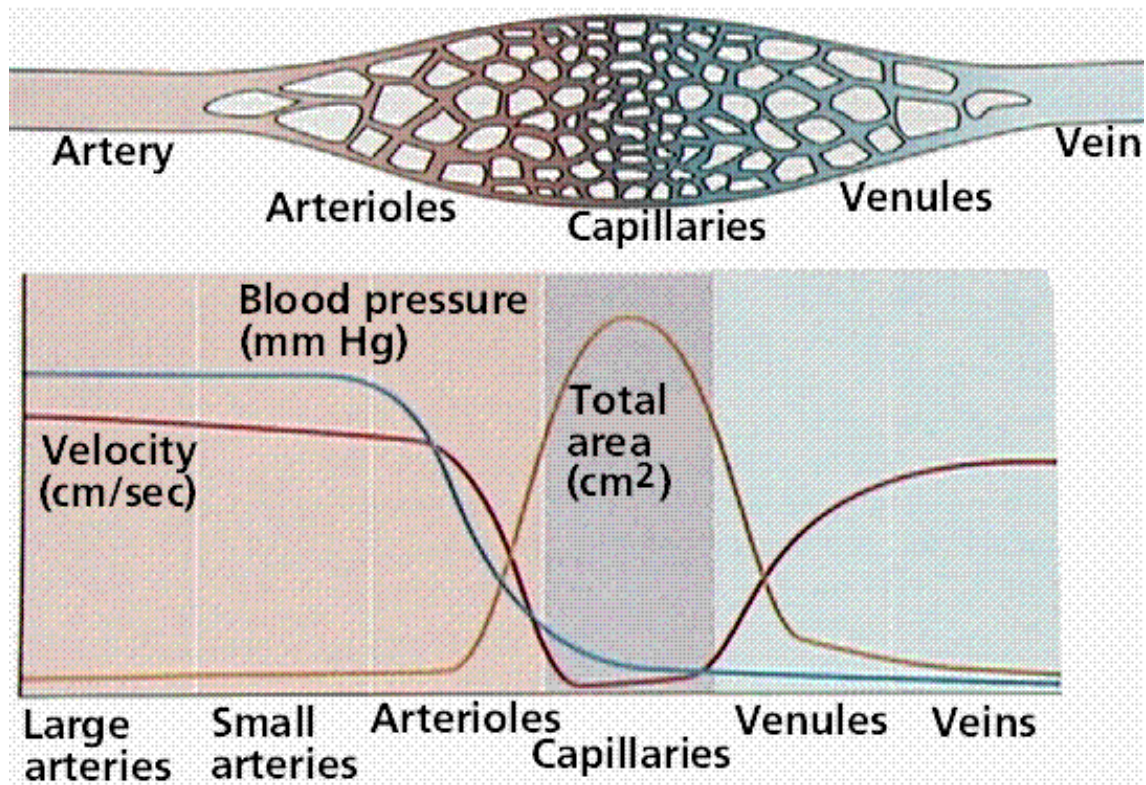


Figure 1 “Changes in blood pressure, velocity, and the area of the arteries, capillaries, and veins of the circulatory system”

(<http://www2.estrellamountain.edu/faculty/farabee/BIOBK/BioBookcircSYS.html>, last accessed May 25th 2015)

Velocity and blood pressure are high, while the total area is small in both large and small arteries as seen on the left side of the graph. Due to Ohm's law and the Hagen-Poiseuille equation there is a decrease in blood pressure as soon as there is an increase in vascular resistance, which is inversely dependent on the 4th power of the vessel's radius, thereby explaining the decrease of blood pressure in arterioles and capillaries compared to larger arteries. The reduction of blood velocity in arterioles and capillaries is explained by the continuity equation, which describes the relation between velocity and total area (cross section) of all blood vessels. As this relation is constant, the increase in cross section of all small blood vessels leads to a decrease in velocity. As per Kirchhoff's 2nd law, the inverse of the total vessel resistance of one vascular bed is equal to the sum of the individual inverse artery's resistance (see below).

(Hick and Hick (2013), chapter 4.2.2.1; Pape, Kurtz et al. (2014), chapter 6.4)

Ohm's law describes the relationship between blood vessel resistance, blood pressure and blood flow.

$$R = \frac{\Delta P}{I}$$

R	Vascular resistance
ΔP	Difference in blood pressure along the blood vessel
I	Blood flow

The Hagen-Poiseuille equation, which Gotthilf Heinrich Ludwig Hagen and Jean Léonard Marie Poiseuille discovered independently of each other, describes the relationship between vascular resistance and blood viscosity, vessel diameter and vessel length. For physiological analysis this equation therefore allows a more detailed analysis of vascular resistance than Ohm's law.

$$R = \frac{8 * \eta * l}{r^4 * \pi}$$

R	Vascular resistance
η	Blood viscosity
l	Length of the blood vessel
r	Radius of the blood vessel
π	Mathematical constant

Since blood viscosity only changes slowly and slightly due to a change of the hematocrit and the vessel length usually stays the same, the vessel diameter is the only parameter that can be changed quickly to adjust vascular resistance.

As it can be seen in the Hagen-Poiseuille equation above, the resistance is inversely proportional to the fourth power of the radius (r^4), which explains the importance of small arteries in adjusting vascular resistance. The equation requires laminar and constant flow, long straight tubes with a circular diameter and a Newtonian fluid. Even if some of these factors are not fulfilled in blood vessels, the equation is important in understanding the concept of vascular resistance and the influence of the changing vessel diameter.

The continuity equation explains the reduction of the blood flow velocity caused by the increase in total cross-section of the capillaries.

$$A * v = const.$$

Or

$$A_1 * v_1 = A_2 * v_2$$

A	Cross section of all blood vessels
v	Blood velocity

Kirchhoff's 2nd law describes the relationship between the total resistance of a parallel vascular bed and the sum of the single artery's resistance. The inverse of the total vessel resistance of one vascular bed is equal to the sum of the individual inverse artery's resistance. This means that the total resistance of a parallel vascular bed is always smaller than the smallest single artery's resistance.

$$\frac{1}{R_{total}} = \frac{1}{R_1} + \frac{1}{R_2} + \frac{1}{R_3} + \dots + \frac{1}{R_n}$$

R _{total}	Vascular resistance of all arteries of a vascular bed
R _{1/2/3/...n}	Vascular resistance of singular arteries of a vascular bed

(Hick and Hick (2013), chapter 4.2.2.1; Pape, Kurtz et al. (2014), chapter 6.4)

1.1.2. Regulation of Vascular Tone

Vasoconstriction and vasodilation are the only parameters for rapidly adjusting vascular resistance and consequently vascular tone¹. There are two mechanisms for regulating vascular tone, the first being calcium-dependent and the second calcium-independent. The calcium-dependent regulation of vascular tone (i.e. smooth muscle tone) occurs either via receptors or depolarization/hyperpolarization, while the calcium-independent regulation occurs via the myosin-light chain kinase (MLCK) and the myosin-light chain phosphatase (MLCP), which phosphorylate and dephosphorylate the myosin-light chain (MLC) independently of the intracellular

¹ Vascular tone: "degree of constriction experienced by a blood vessel relative to its maximal dilated state" (<http://www.cvphysiology.com/Blood%20Flow/BF002.htm>; last accessed July 20th 2015)

calcium levels. Phosphorylation of the MLC leads to vasoconstriction, while dephosphorylation induces vasodilation.

1.1.2.1. Calcium-Dependent Regulation

Calcium-dependent vasoconstriction increases intracellular calcium by releasing calcium from cytosolic stores, like the sarcoendoplasmic reticulum (SERCA), and by increasing the influx from the extracellular space through ligand-gated or voltage-gated calcium channels.

Depolarization opens voltage-dependent calcium channels (VDCCs), mainly L-type Ca^{2+} channels, to increase intracellular calcium and to induce constriction, while the receptor mediated constriction works via the G-Protein/PLC/DAG and IP_3 cascade. IP_3 releases calcium from the sarcoplasmic reticulum and thus increases the cytosolic calcium, while DAG has several target proteins and can amongst others boost constriction by activating L-type Ca^{2+} channels and thus increase the intracellular calcium concentration (Webb (2003)).

The normal cytosolic calcium concentration in relaxed smooth muscle cells is 10^{-7} mol/l. As soon as intracellular calcium levels increase to 10^{-5} mol/l, up to four calcium ions can attach to and activate the calcium sensor calmodulin (CaM) (Teo and Wang (1973); Adelstein and Eisenberg (1980)). The myosin light-chain kinase (MLCK) is activated by an activated calmodulin (Dabrowska, Sherry et al. (1978); Adelstein and Eisenberg (1980)). MLCK in turn phosphorylates and thus activates the myosin light-chain (MLC), which enables the cross-bridging of myosin and actin and results in vasoconstriction (Dabrowska, Aromatorio et al. (1977)).

1.1.2.2. Calcium-Independent Regulation

For a long time, calcium-dependent regulation of vascular tone was thought to be the only mechanism that could induce vasoconstriction until additional pathways were discovered that could evoke vasoconstriction without a change in intracellular calcium levels, but by directly regulating the MLCP and the MLCK.

MLCP is predominantly inhibited by two pathways, the RhoA/ROCK/MYPT1 and the $\text{PLC}\beta/\text{PKC}/\text{CPI-17}$ pathway (Mizuno, Isotani et al. (2008); Kitazawa, Eto et al. (2000)). Since these pathways lead to vasoconstriction without increasing the intracellular calcium levels, this induced calcium-independent vasoconstriction is often called calcium sensitization. RhoA is a small GTPase-protein that activates ROCK, which in turn phosphorylates the MYPT1 protein that is also called the myosin-binding subunit

(MBS) of the myosin phosphatase. The phosphorylation of the MYPT1 inhibits MLCP action. (Kimura, Ito et al. (1996))

The PLC β /PKC/CPI-17 pathway also works via phosphorylation of its target protein, CPI-17, which is only expressed in smooth muscle cells and blocks the action of the MLCP when phosphorylated. There is a connection between both pathways as CPI-17 is also activated via ROCK. (Eto, Kitazawa et al. (2001))

In addition to these inhibiting pathways, the MLCP is activated by NO via cGMP, which consequently induces calcium desensitization (Bolz, Vogel et al. (2003)). Calcium desensitization can however also be achieved by directly inhibiting the MLCK via phosphorylation by a kinase, such as the AMPK (Horman, Morel et al. (2008)).

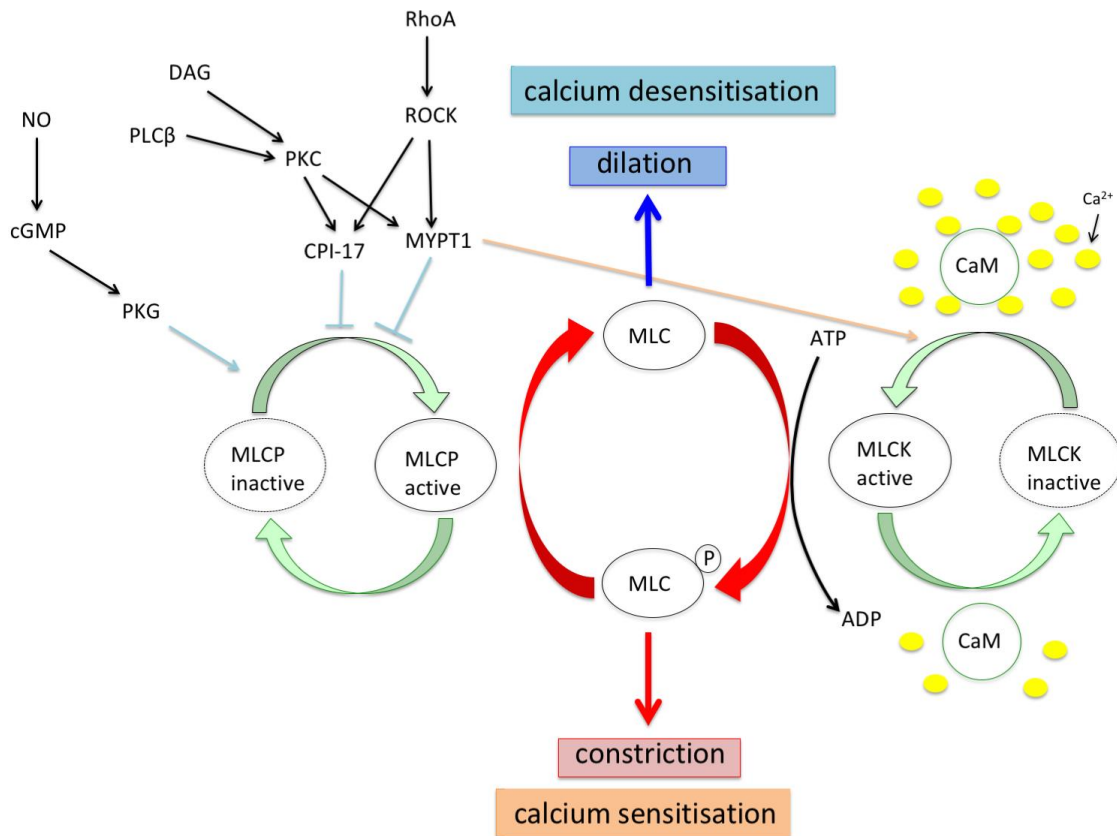


Figure 2: Mechanisms of vasoconstriction and vasodilation in smooth muscle cells

Vasoconstriction and vasodilation are influenced by calcium-dependent and calcium-independent pathways. The balance of the activities of the MLCK and MLCP is important, as an increase in one will lead to phosphorylation (MLCK) or dephosphorylation (MLCP) of the MLC. When intracellular calcium levels increase, a calcium calmodulin complex is formed which activates the MLCK. This induces calcium-dependent vasoconstriction. However, there is also a calcium independent-mechanism to induce or enhance vasoconstriction. Via the RhoA/ROCK/MYPT1 and PLC β /PKC/CPI-17 pathways the MLCP is blocked and dephosphorylation of the MLC is inhibited. This is called calcium-sensitization. When the MLCP is activated by PKG, vasodilation is induced, which is equivalent to calcium-desensitization.

1.2. AMP-Kinase

1.2.1. Discovery and Structure of the AMP-Kinase

Reactions catalyzed by the AMP-kinase were first described in 1973, inhibiting both the HMG-CoA reductase and the acetyl-CoA carboxylase, which are important enzymes in the synthesis of cholesterol and fatty acids (Hardie, Carling et al. (1998)). Both the HMG-CoA reductase kinase and the acetyl-CoA carboxylase kinase are found to be activated by an increase in the AMP/ATP ratio (Ferrer, Caelles et al. (1985); Yeh, Lee et al. (1980)). Further experiments led to the conclusion that these two kinases were indeed the same and it was then named „AMP-activated protein kinase“ (Carling, Zammit et al. (1987); Munday, Campbell et al. (1988); Sim and

Hardie (1988); Hardie and Carling (1997)). Today the AMP-kinase is a well-known enzyme regulating not only sterol or fatty acid synthesis but also energy homeostasis and is being referred to as a cellular “fuel gauge” (Hardie and Carling (1997)).

The AMP-kinase is a heterotrimeric serine/threonine kinase consisting of three subunits, one catalytic α subunit and two regulatory subunits, the β and γ subunit (Mitchelhill, Stapleton et al. (1994); Stapleton, Gao et al. (1994)). There are two isoforms of the α and of the β subunit (α_1 and α_2 ; β_1 and β_2) and three isoforms of the γ subunit (γ_1 , γ_2 and γ_3) (Stapleton, Mitchelhill et al. (1996); Thornton, Snowden et al. (1998); Cheung, Salt et al. (2000)). The genes encoding for the AMPK subunits and isoforms are the PRKA genes (Hardie (2007)). Latest DNA sequencing technology has shown that the PRKA genes are universally existent in all eukaryotic cells, except a few parasites (Hardie 2018).

1.2.2. Relevance of the AMP-Kinase

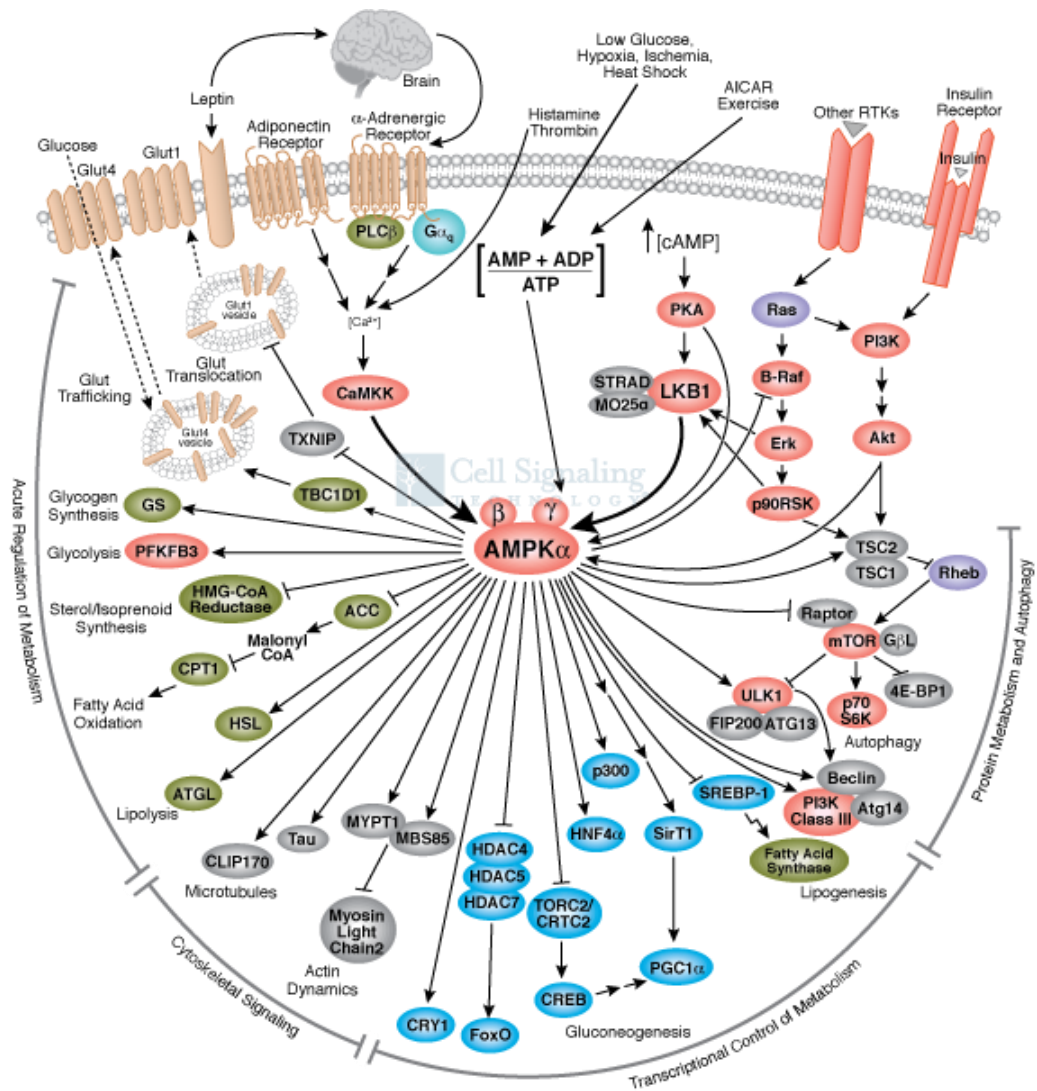


Figure 3: The far-reaching influence of the AMP-kinase and how it self-regulates (Illustration reproduced courtesy of Cell Signaling Technology, Inc. (www.cellsignal.com))

As can be seen in Figure 3, the AMP-kinase influences a huge variety of pathways. It is an important enzyme for energy homeostasis as it influences these pathways to switch to an energy saving mode. By phosphorylating both HMG-CoA reductase and acetyl-CoA carboxylase the AMP-kinase inhibits both sterol and fatty acid synthesis, processes requiring ATP, and it even induces ATP producing pathways (e.g. fatty acid oxidation and glycolysis). Being activated by an anabolic increase in AMP, the AMP-kinase induces catabolic pathways to conserve ATP, which led to it being named the “fuel gauge of the mammalian cell” (Hardie and Carling (1997)).

1.2.2.1. Influence of the AMP-Kinase on Vascular Tone

The AMP-kinase was also shown to influence vascular tone via Ca²⁺-dependent and independent pathways explained in sections 1.1.2.1 Calcium-Dependent Regulation and 1.1.2.2 Calcium-Independent Regulation.

It has been reported that the AMP-kinase inhibits the RhoA/Rock/MYPT1 pathway via two mechanisms. The first mechanism is the phosphorylation of serine of p190-GAP, which binds and inhibits RhoA while the second mechanism is direct phosphorylation of RhoA on Ser¹⁸⁸. The AMP-kinase thus activates the MLCP and consequently induces Ca²⁺-independent vasodilation. (Wang, Liang et al. (2011); Gayard, Guilluy et al. (2011)) The AMP-kinase has also been shown to inactivate the MLCK by phosphorylation of the CaM binding site at Ser⁸¹⁵ inducing a vasodilation (Horman, Morel et al. (2008)). Furthermore, it can affect the actin cytoskeleton by depolymerizing the F-actin, thus affecting another pathway inducing Ca²⁺-independent vasodilation (Schubert, Qiu et al. 2017).

In addition the AMP-kinase is now also known to influence calcium decreasing mechanisms by BkCa-channel mediated membrane hyperpolarization and by indirectly activating the SERCA (Schneider, Schubert et al. (2015)).

The AMP-kinase does, however, not only regulate vascular tone by influencing smooth muscle cell contractility but has also been reported to play an important role in the endothelial regulation of vascular tone. It is considered to not only induce vasodilation by influencing the endothelium-dependent hyperpolarization (EDH) but also by phosphorylating the eNOS leading to an increased production of NO (Enkhjargal, Godo et al. (2014); Chen, Mitchelhill et al. (1999); Chen, Peng et al. (2009)).

1.2.2.2. Pathophysiological Relevance of the AMP-Kinase

Not only the metabolic pathways like sterol and fatty acid synthesis and gluconeogenesis, but also vascular functions are deeply impaired in the metabolic syndrome. As the AMP-kinase has favorable effects on patients affected by the metabolic syndrome by improving insulin resistance and regulating hypertension, it is seen as a new possibility not only in the treatment of the metabolic syndrome but also of cardiovascular diseases especially when they are related to the metabolic syndrome (Fogarty and Hardie (2009); Wang, Liang et al. (2011); Cao, Luo et al. (2014); Dong, Zhang et al. (2010); Wang, Zhang et al. (2010)). This is also supported by evidence showing that the well-known anti-diabetic drug Metformin can, in addition

to AMP-kinase independent anti-diabetic mechanisms, activate the AMP-kinase and thus increases hepatic insulin sensitivity (Zhou, Myers et al. (2001); (Rena, Hardie et al. 2017)).

Both catalytic AMPK α subunits have a different influence on the AMP-kinase's metabolic effects. When mice globally lack the AMP-kinase's α_2 subunit, not only do they present with an elevated blood pressure, but also glucose intolerance and insulin resistance (Wang, Liang et al. (2011); Viollet, Andreelli et al. (2003)). The global α_1 knockout in mice is not characteristic for influencing glucose homeostasis (Viollet, Andreelli et al. (2003)). In contrast, the α_1 knockout mice are anemic, develop splenomegaly and a shortened erythrocyte life span (Wang, Dale et al. (2010)).

In contrast to skeletal and cardiac muscle, the AMP-kinase α_1 subunit is described to be the predominant subunit in porcine vascular smooth muscle cells and the major vasodilative subunit in large conductance vessels like the carotid artery and the aorta (Rubin, Magliola et al. (2005); Goirand, Solar et al. (2007)). There is however not yet any indication on which subunit regulates the vascular tone of resistance arteries. It is also not known which mechanisms are used by the two α subunits to regulate vascular tone.

1.2.3. Regulation of the AMP-Kinase

The AMP-kinase is part of a cascade of protein kinases, which means that the AMP-kinase itself is regulated by upstream kinases (AMPK kinases) and phosphatases. The upstream kinases that activate the AMP-kinase via phosphorylation are LKB1, CaMKK β and Tak1, with LKB1 being the most potent of them and the one that is influenced by metabolic changes and an increase in the AMP/ATP ratio. AMP-kinase's phosphorylation site is to be found at Thr¹⁷² on the α subunit (Hawley, Davison et al. (1996)). The AMP-kinase is consequently deactivated by dephosphorylation of Thr¹⁷² via the protein phosphatase 2C α (PP2C α). (Suter, Riek et al. (2006); Woods, Johnstone et al. (2003); Shaw, Kosmatka et al. (2004); Woods, Dickerson et al. (2005); Momcilovic, Hong et al. (2006))

AMP-kinase is also activated allosterically by AMP, which binds to the γ subunit. AMP does not only activate the AMP-kinase allosterically, but also by decreasing the dephosphorylation by blocking the phosphatase (Sanders, Grondin et al. (2007); Suter, Riek et al. (2006)).

While AICAR, a well-known AMP-kinase activator, works by imitating AMP and thus activates the AMP-kinase, the regulators used in this thesis, A769662 (A76) and PT1, activate the AMP-kinase differently and more effectively.

Like AMP described above, A76, as first described by Cool, Zinker et al. (2006), is said to allosterically activate the AMP-kinase by inhibiting its dephosphorylation. It can bind to the β_1 subunit inducing an allosteric AMP-kinase activation (Sanders, Ali et al. (2007); Scott, van Denderen et al. (2008); Goransson, McBride et al. (2007); (Timmermans, Balteau et al. 2014)). Later evidence however indicates that A76 can also activate the AMP-kinase independently of the Thr¹⁷² phosphorylation (Scott, Ling et al. 2014; Huang, Smith et al. 2017).

The second AMPK activator used in this thesis, PT1, allosterically activates the catalytic α subunit directly by inhibiting the autoinhibitory domain that lies on the α subunit (Pang, Zhang et al. (2008)).

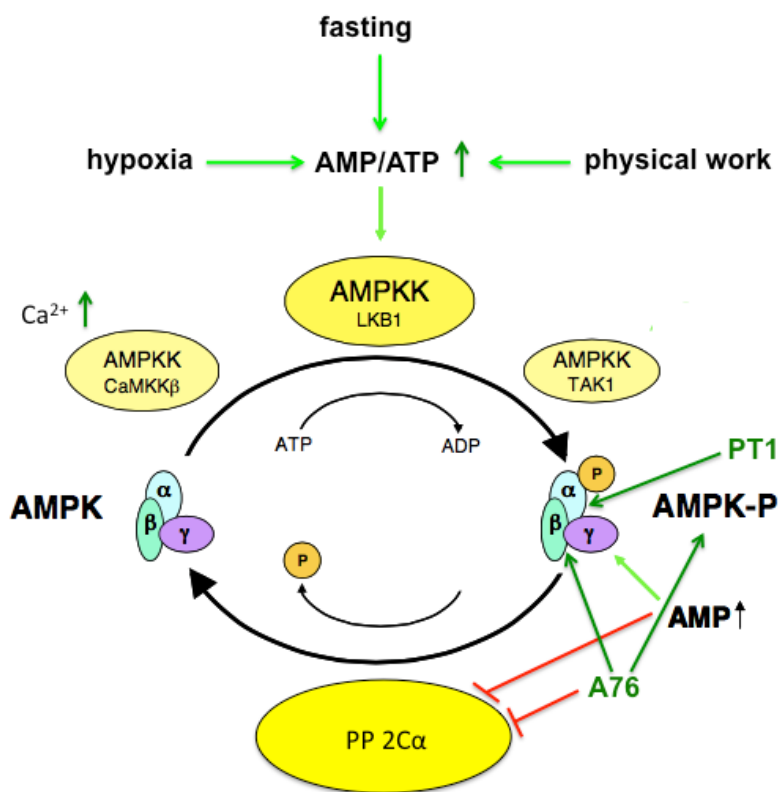


Figure 4: Regulation of the AMP-kinase (adapted from original of Kreutz (2013))

AMP-kinase is activated by phosphorylation via three AMPK upstream kinases, the CaMKK β , the LKB1 and the TAK1, while dephosphorylation via the protein phosphatase 2 α (PP2C α) inactivates it. It can also be activated allosterically by an increase in AMP or by its specific activators A76 and PT1.

1.3. Aim of this Study

While the AMP-kinase has been described as an important enzyme for energy homeostasis, there is high interest in how it affects blood flow regulating resistance arteries. Our group previously worked on hamster skeletal muscle arteries, but as knockout models are mainly available for mice, it was of major importance to:

- Study whether mouse skeletal muscle arteries present with a significant AMP-kinase induced regulation of the vascular tone as previously described for hamster skeletal muscle arteries
- Study whether this AMP-kinase induced regulation of the vascular tone can also be seen in another kind of vascular bed, e.g. the vascular bed of mesenteric arteries
- Study which α subunits are involved in the regulation of vascular tone and whether these subunits have a different effect on calcium-dependent and calcium-independent vasodilative mechanisms

2. Material

2.1. Animals

C57Bl/6 mice were received from Charles River, Sulzfeld, Germany. Global AMPK α_1 and α_2 knockout and wild type mice as generated and previously described by Viollet, Andreelli et al. (2003); Viollet, Andreelli et al. (2003); Jorgensen, Viollet et al. (2004) were derived from Ingrid Fleming, Frankfurt, and further bred in our animal facility. Mice were aged 8-44 weeks and age-distribution was comparable in all experimental groups. Both male and female mice were used for the experiments with a similar gender distribution in treatment and control groups.

2.2. Experimental Setup and Devices

Micromanipulator	Dual Tool Holder Micromanipulator, World Precision Instruments, Berlin, Germany
Microscope for preparing mesenteric and skeletal muscle arteries	Fully automated Leica M205 A, Leica, Wetzlar, Germany
Organ bath	Produced by the workshop of the Walter-Brendel-Centre, Munich, Germany
Pipette Puller System	Laser Based Micropipette Puller System P-2000, Sutter Instruments, distribution by Science Products, Hofheim, Germany
Water bath	GFL® 1083, GFL, Burgwedel, Germany

Workstation 1 for calcium and diameter measurements

Bryte Box	Bryte Box, PTI®, Edison, United States of America
Camera for diameter registration	WAT-902B; Watec, Japan
DeltaScan™	DeltaScan™, PTI®, Edison, United States of America
Inverted microscope	Diaphot 300, Nikon, Düsseldorf,

	Germany Objective: DApo 20UV/340, Olympus
Lamp Power Supply	Lamp Power Supply LPS-220, PTI®, Edison, United States of America
Motor driver	Motor driver MD-5020; PTI®, Edison, United States of America
Optical Chopper	Optical Chopper OC-4000, PTI®, Edison, United States of America
Photomultiplier	Photomultiplier Detection System 710, PTI®, Edison, United States of America
Power Module	Power Module DeltaRAM, PTI®, Edison, United States of America
Shutter controller	Shutter controller SC-500, PTI®, Edison, United States of America

Workstation 2 for calcium and diameter measurements

DeltaRAM V™	DeltaRAM V™, PTI®, Edison, United States of America
Camera for diameter registration	CCD-camera: XC-ES50 Type XC-ES50CE, Sony, Japan
Inverted microscope	Eclipse TS 100, Nikon, Düsseldorf, Germany Objective: S Fluor, Nikon
Lamp Power Supply	Lamp Power Supply LPS-220B; PTI®, Edison, United States of America
Photomultiplier	Photomultiplier Detection System 814, PTI®, Edison, United States of America

2.3. Material

Glass cannulas	Borosilicate glass with filament (GB100F-10), Science Products GmbH, Hofheim, Germany
----------------	---

Filters (0.22 µm pore size)	Filter-System Capacity 1 l, sterile, Sigma-Aldrich International GmbH, Schnelldorf, Germany
Perfusor® Line	Original-Perfusor® Line, B. Braun, Melsungen, Germany
Silicone tubes	Flexible silicone tubing Tygon®, Neolab, Heidelberg, Germany
Stopcock	Discofix® C, B. Braun, Melsungen, Germany
Surgical scissors and forceps	Fine Science Tools, Heidelberg, Germany
Surgical threads	Ethilon polyamide monofil 11-0, Ethicon, Norderstedt, Germany
Syringes	BD Discardit™ II, Becton Dickinson, Fraga, Spain
Scalpel	Carbon Steel Safety Scalpel, Aesculap AG/B. Braun, Tuttlingen, Germany
StepOne™ Real Time PCR System	StepOne™ Real Time PCR System, Applied Biosystems provided by Fisher Scientific GmbH, Schwerte, Germany

2.4. Software

BVA 300 (Blood Vessel Analyzer)	Blood Vessel Analyzer 300, Hasotec, Rostock, Germany
FeliX32™	FeliX32™, PTI®, Edison, United States of America

2.5. Buffer Solutions and Agents

2.5.1. Buffer Solutions

2.5.1.1. MOPS Buffer

	Concentration	Company
CaCl ₂ * 2 H ₂ O	3 mM	AppliChem, Darmstadt, Germany
Distilled water		
EDTA	0.02 mM	AppliChem, Darmstadt, Germany
Glucose	5 mM	AppliChem, Darmstadt, Germany

KCl	4.7 mM	AppliChem, Darmstadt, Germany
MgSO ₄ * 7 H ₂ O	1.17 mM	AppliChem, Darmstadt, Germany
MOPS	3 mM	AppliChem, Darmstadt, Germany
NaCl	145 mM	AppliChem, Darmstadt, Germany
NaH ₂ PO ₄ * 1 H ₂ O	1.2 mM	AppliChem, Darmstadt, Germany
Pyruvate	2 mM	Sigma-Aldrich, Steinheim, Germany

To avoid insoluble complexes of CaCl₂ with NaH₂PO₄, CaCl₂ was added at the end. The pH-value was adjusted by adding NaOH (1 M) until the neutral pH of 7.4 was reached. After sterile filtration, the MOPS buffer was stored at 4°C.

2.5.1.2. Incubation Solution (with Fura-2am)

	Concentration	Company
CaCl ₂ * 2 H ₂ O	3 mM	AppliChem, Darmstadt, Germany
Distilled water		
EDTA	0.02 mM	AppliChem, Darmstadt, Germany
Fura-2am	2 µM	Life Technologies, Darmstadt, Germany
Glucose	5 mM	AppliChem, Darmstadt, Germany
KCl	4.7 mM	AppliChem, Darmstadt, Germany
MgSO ₄ * 7 H ₂ O	1.17 mM	AppliChem, Darmstadt, Germany
MOPS	3 mM	AppliChem, Darmstadt, Germany
NaCl	145 mM	AppliChem, Darmstadt, Germany
NaH ₂ PO ₄ * 1 H ₂ O	1.2 mM	AppliChem, Darmstadt, Germany
Pyruvate	2 mM	Sigma-Aldrich, Steinheim, Germany

2.5.2. Agents

Agent	Stock solution	Company
A769662	100 mM in DMSO	Tocris, distribution by Bio-Techne, Wiesbaden-Nordenstadt, Germany
Acetylcholine	100 mM in distilled water	Sigma-Aldrich, Steinheim, Germany
Dimethylsulfoxide (DMSO) (>99.99%)		Carl Roth, Karlsruhe, Germany
Fura-2am	1 mM in DMSO	Life Technologies, Darmstadt,

		Germany
Iberiotoxin	0.1 mM in distilled water	Tocris, distribution by Bio-Techne, Wiesbaden-Nordenstadt, Germany
Indometacin	100 mM in ethanol	Fluka, distribution by Sigma-Aldrich, Steinheim, Germany
N ω -Nitro-L-Arginine Methyl-Ester	10 mM in distilled water	Sigma-Aldrich, Steinheim, Germany
Manganese chloride	1 M in MOPS	Merck, Darmstadt, Germany
Nifedipine	10 mM in DMSO	Sigma-Aldrich, Steinheim, Germany
Norepinephrine	Serial dilution in MOPS buffer	Aventis, Frankfurt am Main, Germany
PT1	100 mM in DMSO	Tocris, distribution by Bio-Techne, Wiesbaden-Nordenstadt, Germany
Thapsigargin	10 mM in DMSO	Sigma-Aldrich, Steinheim, Germany
U46619	10 mM in DMSO	Tocris, distribution by Bio-Techne, Wiesbaden-Nordenstadt, Germany
Isoflurane		Forene® 100% (V/V), AbbVie Deutschland GmbH, Ludwigshafen, Germany
Bacillol		Bacillol 1 I, AF Bode Chemie GmbH, Hamburg, Germany

All agents were stored at the conditions requested by the manufacturer. The agents were freshly diluted from aliquots of the stock solutions to the requested concentration on the day of the experiments. These dilutions were not kept overnight.

2.5.3. PCR

Protein/Gene	Primer	Sequence
AMPK- α 1/prkaa1	Forward Reverse	CCTTCGGGAAAGTGAAGGT GAATCTTCTGCCGGTTGAGT
AMPK- α 2/prkaa2	Forward Reverse	CGACTACATCTGCAAACATGG CAGTAATCCACGGCAGACAG
AMPK- β 1/prkab1	Forward Reverse	GGACACGGGCATCTCTTG TGCATAGAGGTGGTTCAGCA
AMPK- β 2/prkab2	Forward Reverse	GATCATGGTGGGGAGCAC CTGCTGCCAGGGTACAAACT
AMPK- γ 1/prkag1	Forward Reverse	CATCAACATTTTGCACCGATA TGCAGGTACACCTCTCTCCA
AMPK- γ 2/prkag2	Forward Reverse	GTGGAGAATTCAGAAAAGCATT GGCCTCTGGAGAAGAGTCCT
AMPK- γ 3/prkag3	Forward Reverse	TCTTTGTGGACCGACGTGT AGTAGAGGCCACGACCTG
HPGRT/hprt1	Forward Reverse	TCCTCCTCAGACCGCTTTT CCTGGTTCATCATCGCTAATC
YWHAZ/ywhaz	Forward Reverse	TAAAAGGTCTAAGGCCGCTTC CACCACACGCACGATGAC
SDHA/sdha	Forward Reverse	CCCTGAGCATTGCAGAATC TCTTCTCCAGCATTTCCTTA

All primers were obtained from Eurofins MWG Operon, Ebersberg, Germany.

In addition, the following substances were used for the PCR process:

Substance	Company
REVERTAID reverse transcriptase	Fermentas, Sankt Leon-Rot, Germany
Tri Reagent®	Sigma-Aldrich, Steinheim, Germany
SYBR® Green reagent	Power SYBR Green, LifeTechnologies, Carlsbad, CA, USA

3. Methods

3.1. Vessel Preparation and Cannulation

Mice were anesthetized with isoflurane before being killed by cervical dislocation. To avoid spreading germs and contamination of the preparation area, the abdomen was disinfected with Bacillol before dissection.

3.1.1. Preparation of the Mesenteric Arteries

In order to get to the mesenteric vessels, the abdominal cavity was opened by cutting through the abdominal muscles. The mesentery was first separated from the large and small intestine starting at the rectum and afterwards from the big vessels (superior mesenteric artery and vein). After extracting the mesentery from the mouse, it was stored in MOPS buffer at a constant temperature of 4°C. The mesentery was subsequently placed into a petri dish also filled with MOPS that was kept on ice. The second order mesenteric arteries were then dissected from the surrounding fatty tissue and the mesenteric veins using a preparation microscope.

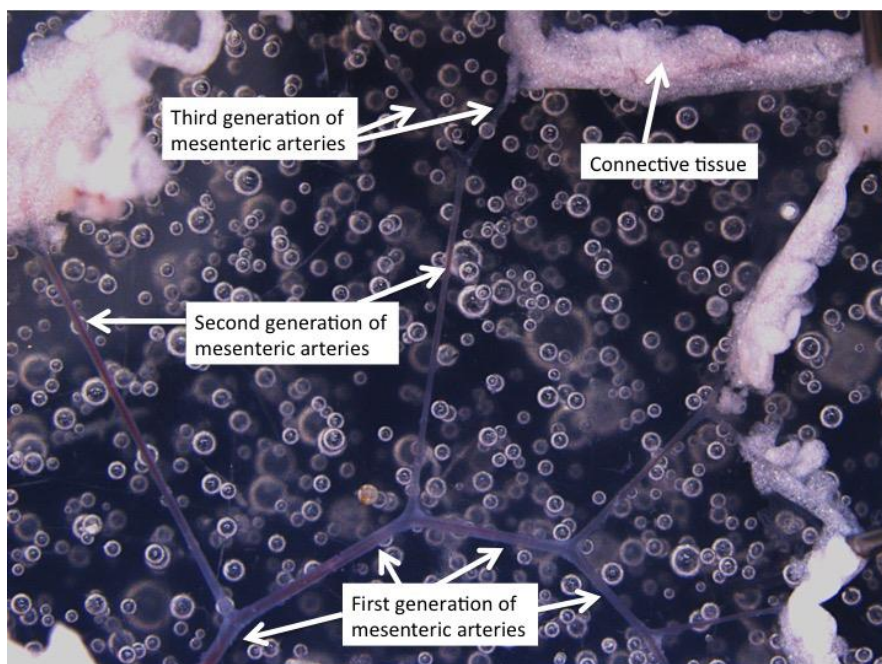


Figure 5: First, second and third generation of mesenteric arteries after preparation

3.1.2. Preparation of the Skeletal Muscle Arteries

In order to dissect the skeletal muscle arteries from the gracilis muscle, the mouse's hind legs were fixed on a board made of styrofoam. After exposing the femoral muscles, the thigh was cut off the trunk and the lower leg using a scalpel. The thigh was then spread out in a petri dish filled with MOPS buffer. Here, the gracilis artery

was prepared after the accompanying vein, the gracilis muscle and the surrounding connective tissue had been removed using a preparation microscope.

These arteries were then stored in an organ bath (also filled with MOPS) at 4°C until the set-up was prepared for cannulation.

Both mesenteric and skeletal muscle arteries were extracted using microsurgical instruments. To ensure minimal risk of damaging the arteries, all vessels were touched as little as possible. Fatty and connective tissue was removed from the artery in the gentlest way as well.

3.1.3. Vessel Cannulation

After preparation, both mesenteric and skeletal muscle arteries were pulled onto the pointed ends of glass cannulas that were attached to micromanipulators and filled with MOPS. The micromanipulators ensured the precise movements of the cannulated vessels segments in the three dimensions of the organ bath that was filled with MOPS.

The glass cannulas were obtained when the middle of a glass micropipette was heated by a CO₂-Laser (pipette puller). By pulling from both ends the micropipette could then be broken in the middle so that two glass cannulas with sharp points and a diameter of about 40 µm became available.

The other blunt end of the glass cannula was connected with a stopcock via a silicone tube. The stopcock was linked to a syringe cavity (without plunger) via a Perfusor® line. The syringe cavity was filled with 10-15 ml MOPS and could be attached to the wall in various heights. This way a hydrostatic pressure of 45 mmHg or 60 mmHg could be achieved for the cannulated vessels thus behaving like a pressure myograph.

Now the vessel was pulled onto the first cannula, fixed there with surgical threads and perfused at a hydrostatic pressure of 45 mmHg. This way MOPS would flow through the vessel and clean it of the remaining blood. Potential holes in the vessel wall (due to side branches having been cut off) could be seen when blood leaked from them. Afterwards the vessel was pulled onto the second cannula and was likewise fixed there with surgical thread. The cannulated vessel was further tested for leaks by closing the first stopcock. If a hole was present MOPS would leak through it and the hydrostatic pressure would no longer be maintained resulting in the vessel's shrinking. Such a vessel was either discarded or a shorter segment of it was used by pulling the vessel further along one of the cannulas.

Afterwards the vessel was stretched to its original length by using the micromanipulators and was again tested for leakage, as described before.

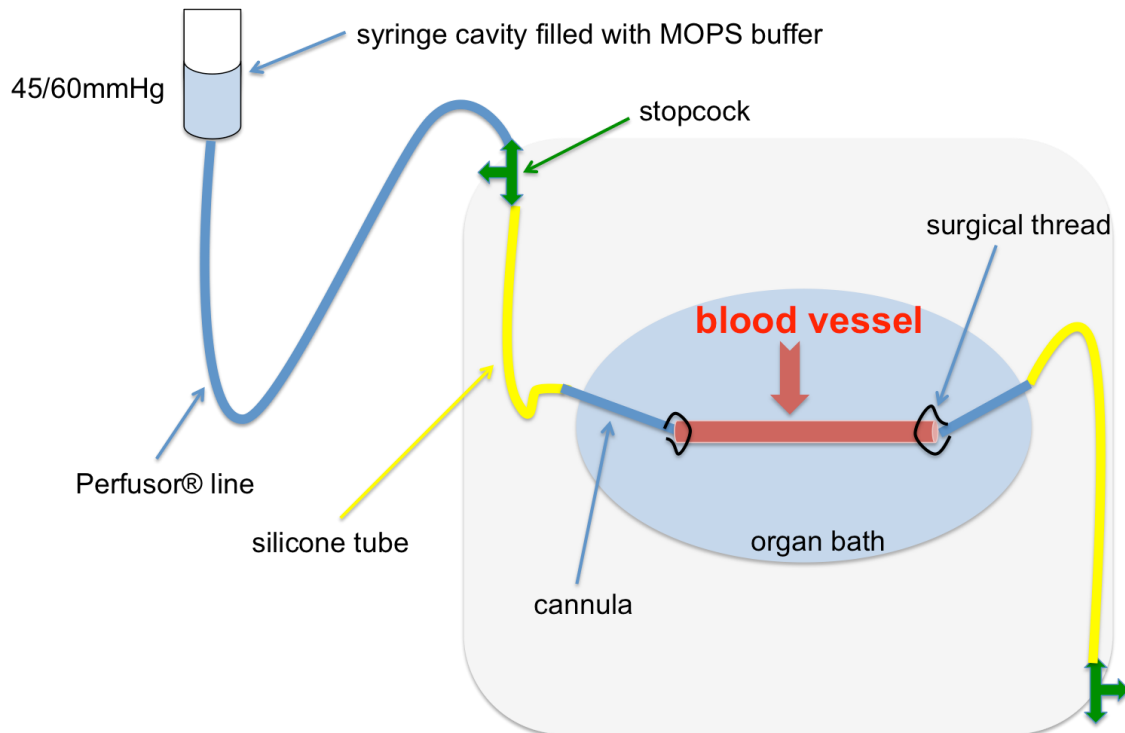


Figure 6: Set-up for vessel cannulation

The cannulas are attached to micromanipulators to ensure precise movement of the blood vessel in all three dimensions of the organ bath. A transmural pressure of 45/60 mmHg was achieved by fixing a syringe cavity filled with MOPS at an appropriate height.

3.2. Calcium Measurement with Fura-2am

3.2.1. Incubation with Fura-2am

After successfully cannulating the blood vessels, the whole set-up (as described in section 3.1.3 Vessel Cannulation) was transported to the calcium workstations. There, the MOPS buffer in the organ bath was substituted with 3 ml of the incubation solution with the calcium dye Fura-2am (2 μ M) (see section 2.5.1.2 Incubation Solution (with Fura-2am)). The vessel was incubated for two hours at a physiological temperature of 37°C and a transmural pressure of 45 mmHg. After one hour of incubation another 2 ml of the incubation solution was added to the organ bath to compensate for evaporation. The COX inhibitor indometacin and the eNOS inhibitor L-NAME were added to these 2 ml to block potential endothelium-dependent vasodilation in the following experimental protocols (see chapter 3.4.4. Blocking the eNOS and the COX) except for the experiments described in section 3.4.5.1 Acetylcholine Dose-Response Curve, where the effects of the COX and eNOS were analyzed separately.

After two hours of incubation the organ bath solution was exchanged with normal MOPS two times before the start of the experiments.

To avoid bleaching of Fura-2am, both incubation and the following experiments were performed in a darkened room.

3.2.2. Mode of Action of Fura-2am

Fura-2am, a fluorescent calcium indicator, was first described by Grynkiewicz, Poenie et al. (1985). Since Fura-2 itself is hydrophilic and thus cannot pass the cell membranes it was applied as an acetoxymethyl ester. The acetoxymethyl ester Fura-2am is lipophilic and can thus easily pass the smooth muscle cells' membranes when applied to the organ bath (Roe, Lemasters et al. (1990)). The ester group is then removed by the intracellular esterases. As soon as the ester group is removed, Fura-2 can bind free intracellular calcium ions leading to changes in its fluorescence.

Adding Fura-2am externally (i.e. to an organ bath) ensures selective loading of smooth muscle cells and negligible loading of endothelial cells (Meininger, Zawieja et al. (1991)).

3.2.3. Measurement of Intracellular Calcium

As described by Tsien, Rink et al. (1985) the emission spectrum of Fura-2 changes when it binds to calcium. Fura-2 (calcium free) has an emission maximum when excited at 380 nm, whereas Fura-2 (calcium bound) has this maximum at an excitation wavelength of 340 nm.

Both kinds of Fura-2 (calcium bound and calcium free) emit at the same wavelength of 510 nm.

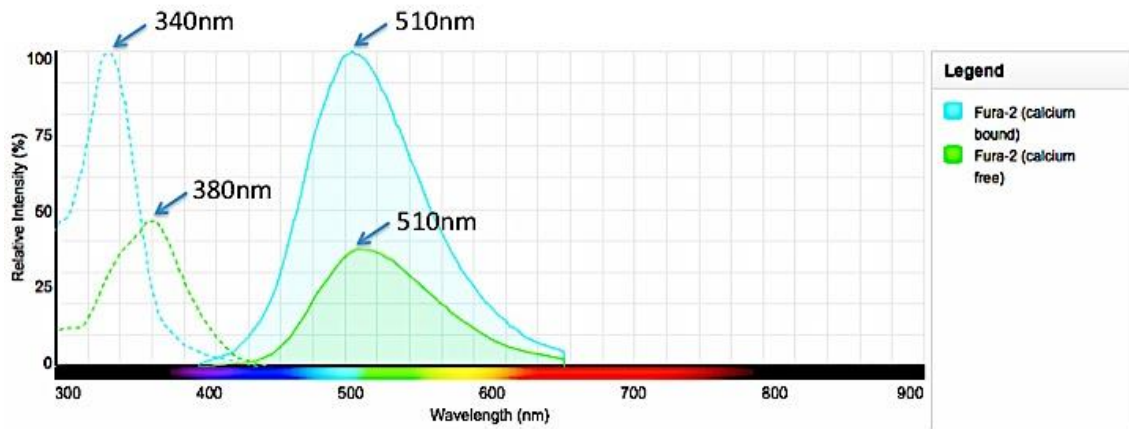


Figure 7: Excitation and emission spectrum of Fura-2

The excitation spectrum of Fura-2 depends on the concentration of free versus bound calcium, whereas the emission wavelength is not altered by calcium. (Figure created with Fluorescence SpectraViewer provided by www.lifetechnologies.com)

Various factors like bleaching or an increase in tissue volume (e.g. in vessel constriction) induce changes in the absolute excitation spectrum and the emission intensity. These effects can be avoided by using the ratio of the fluorescence intensities emitted after excitation at 340 nm and 380 nm (F_{340} , F_{380}), as both of them are proportionally affected (Meininger, Zawieja et al. (1991)).

The absolute values of intracellular calcium can then be calculated by using the ratios and the dissociation constant K_d and the following formula of Grynkiewicz, Poenie et al. (1985):

$$[Ca^{2+}]_i = K_d * \left(\frac{R - R_{min}}{R_{max} - R} \right) * \left(\frac{S_{f2}}{S_{b2}} \right)$$

$[Ca^{2+}]_i$	Intracellular calcium concentration
K_d	Dissociation constant for Fura-2
R	Ratio at any Ca^{2+} concentration
$R_{min/max}$	Ratios at maximum and minimum Ca^{2+} saturation
S_{f2}	Free dye at λ_2 (for Fura-2 $\lambda_2=380$ nm)
S_{b2}	Calcium-bound dye at λ_2 (for Fura-2 $\lambda_2=380$ nm)

The absolute values are thus heavily dependent on $R_{min/max}$, which are further dependent on filters and the lamp used. Small changes therefore lead to a large over-

or underestimation of the absolute calcium concentration. In addition to this, it is difficult to determine the K_d in living cells. Calculating the ratio values (after subtracting background fluorescence) instead of absolute values avoided these problems but still allowed for changes of intracellular calcium concentrations to be measured reliably and reproducibly. (Benham (1989))

The ratio values were therefore mainly used throughout this thesis instead of calculating the calcium values because the dissociation constant (K_d) for the smooth muscle of mouse arteries is not known and depends, amongst others, on local ionic strength and pH (Uto (1991)). Ratio values were considered to satisfactorily allow the analysis of changes in intracellular calcium levels.

As each blood vessel has a unique autofluorescence, these autofluorescence values needed to be subtracted when calculating the ratio to have vessel-independent calcium ratios. Manganese chloride ($MnCl_2$: 8 mM) was used to measure autofluorescence as metal ions are described to quench fluorescence dyes as they have a much higher affinity to Fura-2 than calcium (Grynkiewicz, Poenie et al. (1985)).

$$R = \frac{(F_{340} - A_{340})}{(F_{380} - A_{380})}$$

R:	Ratio independent of autofluorescence
$F_{340/380}$:	Fluorescence intensity at 340 nm or 380 nm
$A_{340/380}$:	Autofluorescence values at 340 nm or 380 nm after quenching with $MnCl_2$

3.2.4. Structure of the Calcium Workstations

3.2.4.1. Structure of Workstation 1

The intracellular calcium that was bound to Fura-2 was detected by the DeltaScan™ system, which was structured as follows.

A light beam generated by a xenon lamp (75 W) was diverted to a monochromator for either a wavelength of 340 nm or 380 nm by the chopper wheel, which was rotating with a frequency of 50 Hz. The monochromatic light beams were then channeled to the optical path of an inverted microscope via two different optical fibers. Aperture diaphragms were used to eliminate possible artefacts of sutures or tissue residues. Fura-2 was alternately excited by the two different wavelengths (340 nm or 380 nm).

As discussed in chapter 3.2.3 Measurement of Intracellular Calcium, both calcium bound and calcium free Fura-2 emitted light at the same wavelength (510 nm). Due to a band-pass filter, only light of this wavelength was detected by a photomultiplier and the resulting signal was sent to the primary data reception unit, the Bryte Box. The Bryte Box was connected to a computer, which analyzed the signals with the FeliX32™ software. The software related the signal intensities to the exciting wavelengths (340 nm and 380 nm) and recorded five values per second. The values of autofluorescence had to be subtracted from the fluorescence intensities in an excel sheet afterwards.

A shutter in the light path of the photomultiplier, which was also directly operated by the software minimized bleaching of the vessels during experimental breaks.

3.2.4.2. Structure of Workstation 2

A second system, the DeltaRAM V™, was also used to measure the calcium-dependent Fura ratio. The structure was similar to that of the DeltaScan™ of workstation 1, except that there was only one monochromator, which produced alternating light beams of either 340 nm or 380 nm.

3.2.5. Measurement of Vessel Diameter

Both inner and outer vessel diameters were measured using a high-resolution camera. A halogen lamp illuminated the vessel. To avoid interference with the calcium measurement, a red-light filter was installed to eliminate all wavelengths below 610 nm.

Using the blood vessel analyzer software BVA 300, both diameters were recorded once per second. As the outer diameter was more precise especially when the vessel was highly constricted, it was used throughout this dissertation. The diameter values were equally recorded by the Bryte Box and were synchronized with the results from the fluorescence intensity measurements. The diameter values were translated to their original unit (μm) during analysis following calibration of the system.

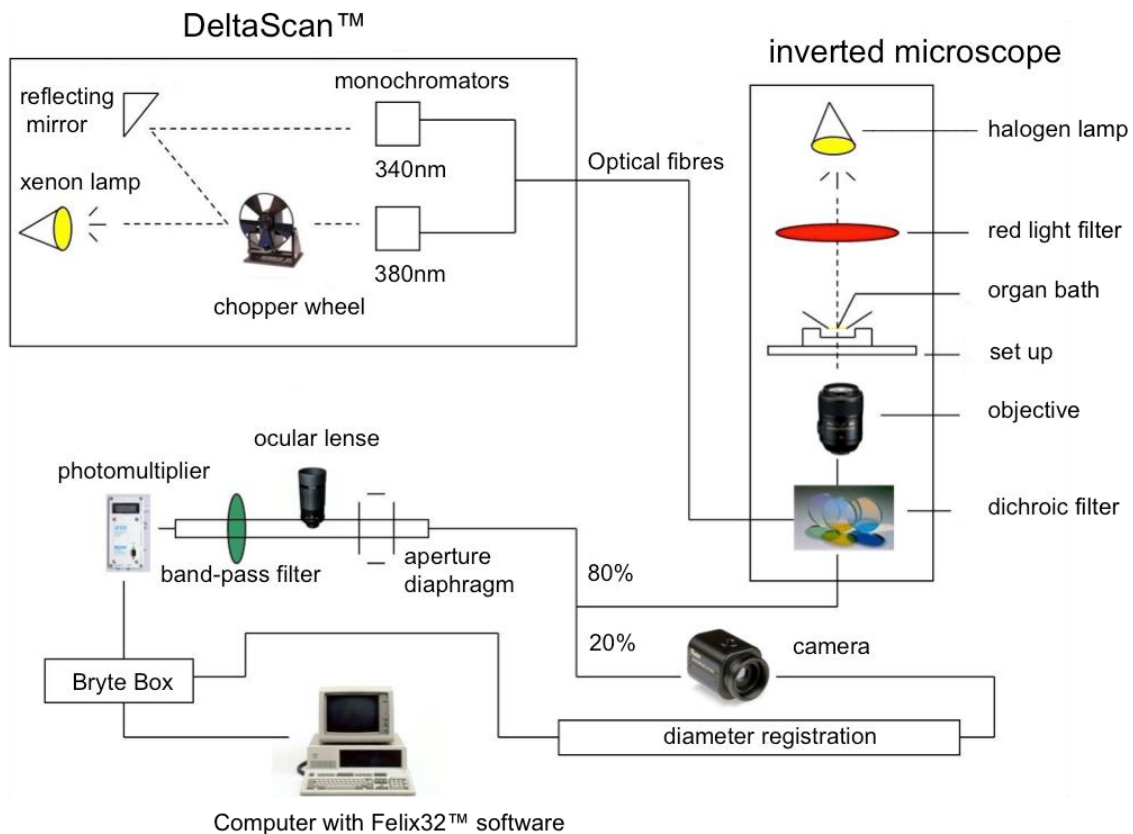


Figure 8: Structure of workstation 1 (modified original of Kreutz (2013))

Producing two monochromatic light beams (at 340 nm and 380 nm), the DeltaScan™ excites both calcium-bound Fura-2 with 340 nm and calcium-free Fura-2 with 380 nm. Both kinds of Fura-2 emit a wavelength of 510 nm. Due to specific filters, it is ensured that only this wavelength is recorded by the photomultiplier and consequently transmitted to the Bryte Box. The vessel diameter is registered using a high-resolution camera and using a red-light filter to avoid interference with the calcium measurement. The data for the diameter is equally transmitted to the Bryte Box, transformed to Volt values and continuously recorded using the Felix32™ software.

3.3. Abbreviations

Abbreviations for substances	
A76	A769662
ACh	Acetylcholine
IbTX	Iberiotoxin
MnCl	Manganese Chloride
Nif	Nifedipine
L-NAME	N _ω -nitro-L-arginine methyl ester
U46	U46619
MOPS	3-(N-morpholino)propanesulfonic acid

TG	Thapsigargin
----	--------------

General Abbreviations	
ADP	Adenosine diphosphate
AMP	Adenosine monophosphate
AMPK	AMP-kinase
AMPKK	AMPK-kinase
ATP	Adenosine triphosphate
BkCa-channels	Large conductance Ca ²⁺ -activated K ⁺ channels
Ca ²⁺	Calcium
CaM	Calmodulin
CaMKK β	Ca ²⁺ /CaM-dependent protein kinase kinase β
cAMP	Cyclic AMP
cGMP	Cyclic GMP
COX	Cyclooxygenase
DAG	Diacyl-Glycerol
eNOS	Endothelial nitric oxide synthase
GMP	Guanosine monophosphate
hprt1/HPRT1	hypoxanthine phosphoribosyltransferase1
IP ₃	Inositol trisphosphate
K ⁺	Potassium
K _{ATP} channel	ATP-sensitive potassium channel
K _d	Dissociation constant
KO	Knockout
LKB1	Liver kinase B1
MLC	Myosin light chain
MLCK	Myosin light chain kinase
MLCP	Myosin light chain phosphatase
MYPT1	Myosin phosphatase targeting subunit-1
NO	Nitric oxide
p190-GAP	p190-guanosine triphosphatase-activating

	protein
PCR	Polymerase chain reaction
PKC	Protein kinase C
PKG	Protein kinase G
PLC	Phospholipase C β
PP2C α	Protein phosphatase 2C α
RhoA	GTPase protein of the Ras homolog gene family, member A
ROCK	Rho-associated protein kinase
sdha/SDHA	Succinate dehydrogenase complex, subunit A
SERCA	Sarco/endoplasmic reticulum Ca ²⁺ -ATPase
TAK1	Transforming growth factor β activated kinase-1
WT	Wild type
ywhaz	Tyrosine 3-monooxygenase/tryptophan 5-monooxygenase activation protein, zeta polypeptide

3.4. Protocols

3.4.1. PCR

PCR was performed to analyze the presence and the relative amount of the AMPK subunits in mesenteric arteries. The StepOne™ Real Time PCR System and the SYBR® Green reagent were used in conjunction with the following primer pairs:

Gene	Protein	Primer sequence
prkaa1	AMPK α_1 subunit	CCTTCGGGAAAGTGAAGGT
prkaa2	AMPK α_2 subunit	CGACTACATCTGCAAACATGG
prkab1	AMPK β_1 subunit	GGACACGGGCATCTCTTG
prkab2	AMPK β_2 subunit	GATCATGGTGGGGAGCAC
prkag1	AMPK γ_1 subunit	CATCAACATTTTGCACCGATA
prkag2	AMPK γ_2 subunit	GTGGAGAATTCAGAAAAGCATTC
prkag3	AMPK γ_3 subunit	TCTTTGTGGACCGACGTGT

Three reference primers were also applied:

Gene	Protein	Primer sequence
hprt1	HPRT	TCCTCCTCAGACCGCTTTT
ywhaz	14-3-3 protein zeta/delta	TAAAAGGTCTAAGGCCGCTTC
sdha	SDHA	CCCTGAGCATTGCAGAATC

As many mesenteric arteries as possible were extracted from one mouse and RNA was isolated using the Tri Reagent®. First strand synthesis was then conducted using REVERTAID reverse transcriptase together with unspecific primers. (Blodow, Schneider et al. (2013))

The following protocol was used for first and seconds strand synthesis: 95°C for 10 minutes (denaturing), which was then followed by 45 cycles of 95°C for 15 seconds and 65°C for 60 seconds (annealing and extension). The melting curve was obtained from another 15 seconds of 95°C being followed by 60 seconds of 60°C. Fluorescence was registered at 95°C.

3.4.2. Addition of Agonists

All agents (NE, U46, ACh, A76, PT1 and the increasing Ca²⁺-concentrations) were kept as standardized stock solutions and freshly diluted in MOPS on the day of the experiments. The different substances were then added to the organ bath (filled with 3 ml of MOPS) using 1000 µl pipettes to obtain the final concentrations.

The solutions were kept in a water bath before administration to avoid any change in the temperature of the organ bath which was set at 37°C.

An equilibration period of 20 minutes after the end of Fura incubation was kept before starting (further) experiments.

3.4.3. Vessel-Dependent Disqualifying Factors

Only the results of vessels that passed a vitality test and constricted by at least 20% of the resting outer diameter (on either NE or U46) were included in the final statistical evaluation. This constriction was considered as a sign of an intact function of smooth muscle cells. Vessels that presented with a Fura-induced fluorescence that did not show a relevant decrease between the beginning and ending of the experiments were also excluded and not studied further.

3.4.4. Blocking the eNOS and the COX

To exclude the potential influence of the AMPK on the endothelium-dependent vasomotor response, both the endothelial NOS (eNOS) and the production of prostacyclin were blocked before the start of the experiments (Horman, Morel et al. (2008); Chen, Mitchelhill et al. (1999); Chen, Peng et al. (2009); Chang, Wang et al. (2011)). L-NAME (30 μ M) was used to block the eNOS and indomethacin (30 μ M) was used to block the COX and both were added with the second two milliliters of Fura-2 in the second hour of incubation (see chapter 3.2.1 Incubation with Fura-2am).

3.4.5. Dose-Response Curves

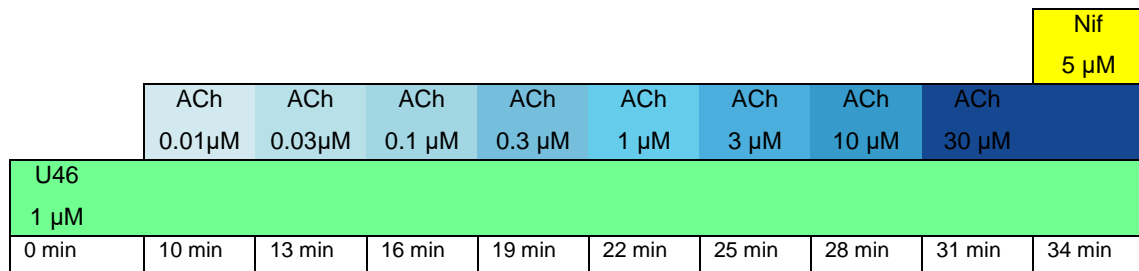
Substances were added in volumes of 1 ml each, while at the same time 1 ml was pipetted off the 3 ml (basal) fluid of the organ bath. This method ensured a constant fluid level while it also avoided excessive stress on the vessels by exchanging all 3 ml of the surrounding fluid in the organ bath. Adding 1 ml and pipetting off another 1 ml diluted the added 1 ml of fluid by one third. To compensate for this dilution, the concentration of the added substances had to be three times as high as the desired concentration in the organ bath. All concentrations mentioned in this thesis were the concentrations present in the organ bath.

After the vasoconstrictors, norepinephrine (NE) or U46, were administered, we waited either five minutes in the case of U46 or ten minutes in the case of norepinephrine for the vasoconstriction to reach a steady state before starting the dose-response experiments. In order to not dilute the constrictors during the dose-response curves, they were added simultaneously to the vasodilators in one third of the concentration that they were originally pipetted into the organ bath.

Please note that in all dose-response and calcium desensitization figures that follow the darker colors represent higher concentrations and the lighter colors lower concentrations.

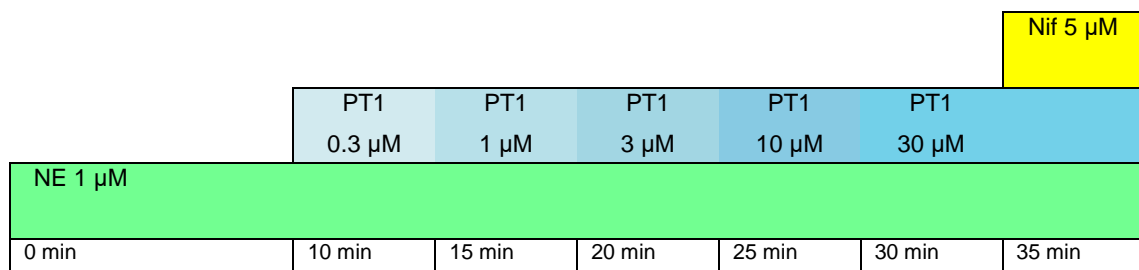
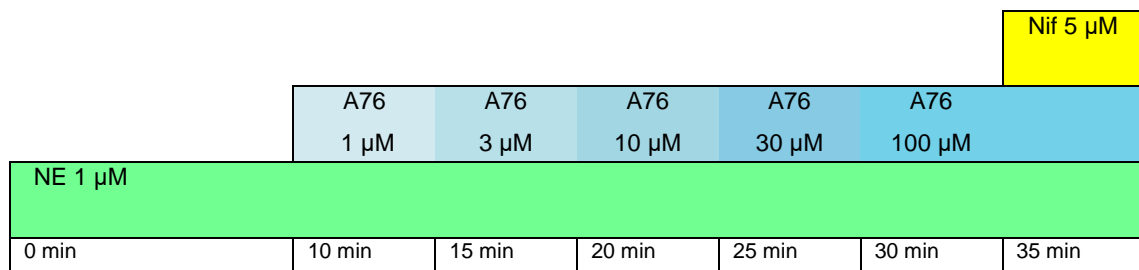
3.4.5.1. Acetylcholine Dose-Response Curve

To test the effect of the endothelial stimulus acetylcholine in skeletal muscle and mesenteric arteries, cumulative dose-response curves were obtained in the absence of L-NAME and indometacin. For these curves the vessels were pre-constricted with the thromboxane analogue U46 (1 μ M) and afterwards the concentration of acetylcholine was increased every 3 minutes (0.01 μ M – 30 μ M). Maximal dilation was achieved by adding nifedipine (5 μ M) at the end of the experiments.



3.4.5.2. A76/PT1 Dose-Response Curve

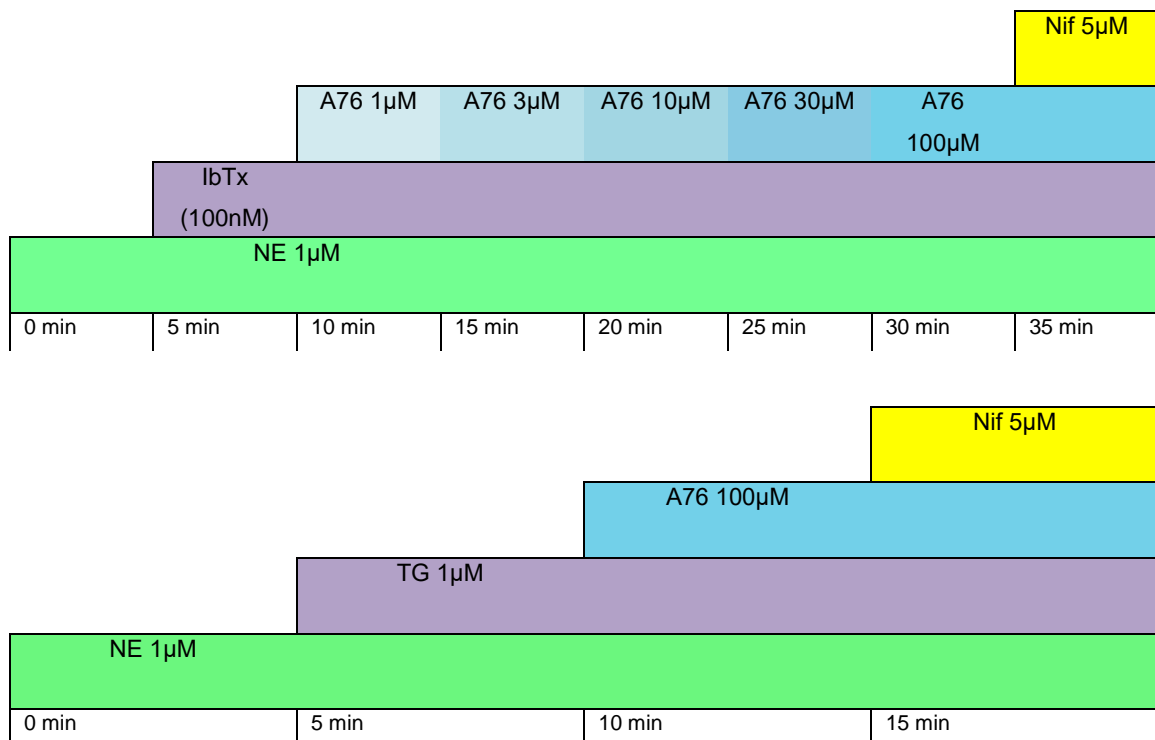
To analyze the vasomotor effects of AMP-kinase stimulation, dose-response curves were performed on vessels pre-treated with L-NAME and indometacin (see chapter 3.4.4 Blocking the eNOS and the COX). The vessels were pre-constricted with norepinephrine (1 μ M). The concentration of the substance that was tested (A76: 1 μ M – 100 μ M; PT1: 0.3 μ M – 30 μ M) was increased every 5 minutes. In order to relate these results to maximal dilation, nifedipine (5 μ M) was added at the end of the experiments.



When testing the effect of SERCA inhibitor TG and BkCa-channel blocker IbTx on the dilation mediated by either of the two AMPK α subunits, these substances were added 5 minutes after the addition of the vasoconstrictor NE (1 μ M). They were added to the organ bath together with one third of the NE concentration to ensure a continuous level of NE. In the case of IbTx (100 nm) the A76 dose-response was done as described before, but with an added level of one third (30 nm) of IbTx at every step of A76.

TG (1 μM), however, induced a substantial dilation of around 90% 8 to 10 minutes after administration, starting at around 3-4 minutes after application and due to the fact that A76 took 3 to 5 minutes to reach a dilatory steady state, only a single concentration of A76 of 100 μM was used to analyze the effect of SERCA on the respective subunits. A third of the aforementioned TG (1 μM) was added to the 100 μM A76 dosage to ensure a continuous level of TG.

Just as described before nifedipine (5 μM) was added at the end of the experiments in order to relate the results to maximal dilation.



3.4.6. Calcium-Desensitization Curves

To test the effect of the AMPK on calcium desensitization, the vessels' calcium stores were initially depleted by keeping the vessels in calcium-free MOPS for 3 minutes. The vessel was then depolarized for another 3 minutes using a potassium-rich (125 mM) MOPS (0 mM Ca^{2+}) to open voltage-dependent calcium channels. By increasing the extracellular calcium concentration step by step, a corresponding increase of the intracellular concentration was achieved (Bolz, Galle et al. (2000)). MOPS with increasing calcium concentrations (0.5 mM, 1 mM, 2 mM, 3 mM) was added every 3 minutes. In contrast to the dose-response curves all 3 ml of the respective MOPS had to be exchanged.

After administrating the MOPS with the highest calcium concentration (3 mM), the organ bath was washed with normal MOPS buffer and the vessel was equilibrated for

20 minutes before the start of the second part of the experiment testing the effect of AMPK stimulation by A76. A76 was added to the organ bath during the equilibration period and to all the substances used in the experiment.

		Ca ²⁺ 0.5mM	Ca ²⁺ 1mM	Ca ²⁺ 2mM	Ca ²⁺ 3mM
Ca ²⁺ 0mM	K ⁺ 125mM, Ca ²⁺ 0mM				
0 min	3 min	6 min	9 min	12 min	15 min

3.4.7. Analysis

The quantitative analysis was performed with Microsoft Office Excel 97-2004 and SigmaPlot 12.0 (Systat Software Inc).

SigmaPlot was also used to generate the graphs presented in this thesis. All results are presented as mean values \pm SEM. For all analyses, steady state values were used.

3.4.7.1. Analysis of PCR

The relative amount of the AMP-kinase's subunits as obtained by PCR was normalized to the mean of the three reference primers (Blodow, Schneider et al. (2013)).

3.4.7.2. Analysis of Dose-Response Curves

The constriction induced by NE or U46 was normalized to the maximal diameter obtained at a steady state at the end of the experiment after administration of nifedipine (in mesenteric arteries) or the highest concentration of ACh (in skeletal muscle arteries, since in these arteries the highest concentration of ACh already induced maximal dilatation).

$$\text{constriction}(\%) = \frac{\text{diameter}_{NE \text{ or } U46}(\mu\text{m}) - \text{diameter}_{max}(\mu\text{m})}{\text{diameter}_{max}(\mu\text{m})}$$

diameter _{NE or U46}	Diameter (μm) after administration of vasoconstrictor (NE or U46)
diameter _{max}	Diameter (μm) after administration of nifedipine or highest concentration of ACh in skeletal muscle arteries

The accompanying increase of the Fura ratio was also normalized to the minimal ratio.

$$Fura\ ratio(\%) = \frac{Fura\ ratio_{NE\ or\ U46} - Fura\ ratio_{min}}{Fura\ ratio_{min}}$$

Fura ratio _{NE or U46}	Fura ratio after administration of vasoconstrictor (NE or U46)
Fura ratio _{min}	Fura ratio after administration of nifedipine or highest concentration of ACh in skeletal muscle arteries

For the analysis of the dose-response curves, the relative dilation initiated by a particular agonist's concentration was calculated by normalizing absolute dilation to the maximal possible dilation (as obtained after administration of nifedipine/ACh (in skeletal muscle arteries)). In the case of skeletal muscle arteries, maximal dilation and maximal decrease of calcium was usually already obtained at the highest concentration of ACh (1 μ M). Here, nifedipine did not increase the diameter further.

$$dilation(\%) = \frac{diameter_{agonist}(\mu m) - diameter_{NE/U46}(\mu m)}{diameter_{max}(\mu m) - diameter_{NE/U46}(\mu m)}$$

diameter _{agonist}	Diameter (μ m) after administration of agonists (ACh, A76 or PT1)
diameter _{NE/U46}	Diameter (μ m) after administration of vasoconstrictor (NE or U46)
diameter _{max}	Diameter (μ m) after administration of nifedipine (Exception: diameter (μ m) after administration of the highest concentration of ACh in ACh dose-response curves of skeletal muscle arteries)

The relative decrease of the Fura ratio initiated by a particular agonist's concentration was equally normalized to the minimal values obtained after application of nifedipine. As mentioned before, the only exceptions to this rule were the acetylcholine dose-response curves of the skeletal muscle arteries, which were compared to the maximal decrease on addition to the highest concentration of ACh (1 μ M).

$$Fura\ ratio(\%) = - \frac{Fura\ ratio_{agonist} - Fura\ ratio_{NE/U46}}{Fura\ ratio_{min} - Fura\ ratio_{NE/U46}}$$

Fura ratio _{agonist}	Ratio after administration of agents (ACh, A76 or PT1)
Fura ratio _{NE/U46}	Ratio after administration of vasoconstrictor (NE or U46)
Fura ratio _{min}	Ratio after administration of nifedipine (Exception: ratio after administration of the highest concentration of ACh in ACh dose-response curves of skeletal muscle arteries)

Autofluorescence values were subtracted from the original fluorescence intensities beforehand.

Statistical analysis was performed using SigmaPlot 12.0. Differences between the tested groups were assumed to be relevant at a significance level of 5% ($p < 0.05$).

Possible differences of constriction or dilation between two independent groups were examined using a two-tailed t-test for unpaired data. A Shapiro-Wilk test was performed beforehand to check for normal distribution and a Brown-Forsythe test to check for equal variance. If either of these two tests failed, a Mann-Whitney rank sum test was performed.

A two-way Anova (Holm-Sidak test) was performed to find significant differences in dose-response curves. The two-way Anova tested normally distributed data with a Holm-Sidak test and in case the data was not normally distributed, a Kruskal Wallis test was applied. Both of these tests compare two independent variables (concentration of the stimulator and the kind of vessel/genotype) with a dependent variable (diameter/ratio).

3.4.7.3. Analysis of Calcium Desensitization Curves

The effect of A76 on AMPK-induced calcium desensitization was analyzed by plotting the absolute instead of relative data of the blood vessel diameter and its Fura ratio. The need for absolute data resulted from bleaching artefacts that tainted the relative data sets.

A non-linear regression analysis was used to compare the changes in both diameter and Fura ratio. For a non-linear regression analysis, two individual exponential curves had to be obtained from the two original data sets (before and after adding A76) and then be compared to a combined curve resulting in a pooled data set. If the separate curves were a significantly better fit than the combined curve, this equaled a significant difference between the data sets. Via regression analysis, sum of square data (SS) and degrees of freedom (df) were acquired. Using the following formulas, F values were calculated, which were then transformed to p values using the Graphpad software², whereby p values smaller than 0.05 represented a significant difference between two groups. (Bolz, de Wit et al. (1999); Motulsky and Ransnas (1987))

$$F = \frac{(SS_{pool} - SS_{sep}) / (df_{pool} - df_{sep})}{SS_{sep} / df_{sep}}$$

$$SS_{sep} = SS_1 - SS_2$$

$$df_{sep} = df_1 - df_2$$

<i>F</i>	F value
<i>SS_{pool}</i>	Sum of squares for pooled data
<i>SS_{sep}</i>	Added sum of squares for individual data
<i>SS_{1/2}</i>	Individual sum of squares before (1) and after (2) A76
<i>df_{pool}</i>	Degrees of freedom for pooled data
<i>df_{sep}</i>	Added degrees of freedom for individual data
<i>df_{1/2}</i>	Individual degrees of freedom before (1) and after (2) A76

² Graphpad software: www.graphpad.com

4. Results

4.1. Comparison of Skeletal Muscle Arteries and Mesenteric Arteries

4.1.1. General Vessel Characteristics

The experiments for this doctoral thesis were performed from February 2011 until September 2015 with the first 6 months being used to learn the preparation technique. In the following months 166 vessels were prepared for the experiments. 127 mesenteric and skeletal muscle arteries could finally be analyzed using the criteria described before (see chapter 3.4.3 Vessel-Dependent Disqualifying Factors). From the 39 vessels that could not be used, 18 constricted less than 20% of the original diameter on addition of norepinephrine or U46, while the rest had to be discarded due to technical or vessel related problems (e.g. broken organ baths, no decrease of the Fura ratio on addition of nifedipine or ongoing vasomotion).

The average maximal diameter for all mesenteric arteries studied in this thesis was $224.4 \pm 4.3\mu\text{m}$ while skeletal muscle arteries had an average maximal diameter of $183.0 \pm 8.3\mu\text{m}$. In order to analyze potential differences between the smaller skeletal muscle arteries and mesenteric arteries, a subgroup of smaller mesenteric arteries was chosen to insure comparability (diameter of skeletal muscle arteries (n=4): $183.0 \pm 8.3 \mu\text{m}$; diameter of comparable mesenteric arteries (n=7): $186.4 \pm 11.6 \mu\text{m}$).

4.1.2. Constriction

In both mesenteric and skeletal muscle arteries, the thromboxane analogue U46 (1 μM) induced virtually the same relative vasoconstriction in relation to maximal diameter (skeletal muscle arteries: $-29.4 \pm 3.0\%$; mesenteric arteries: $-30.9 \pm 2.1\%$). The Fura ratio was, however, significantly increased in the skeletal muscle arteries despite comparable starting levels (skeletal muscle arteries: $+62.1 \pm 10.0\%$; mesenteric arteries: $+33.7 \pm 7.1\%$).

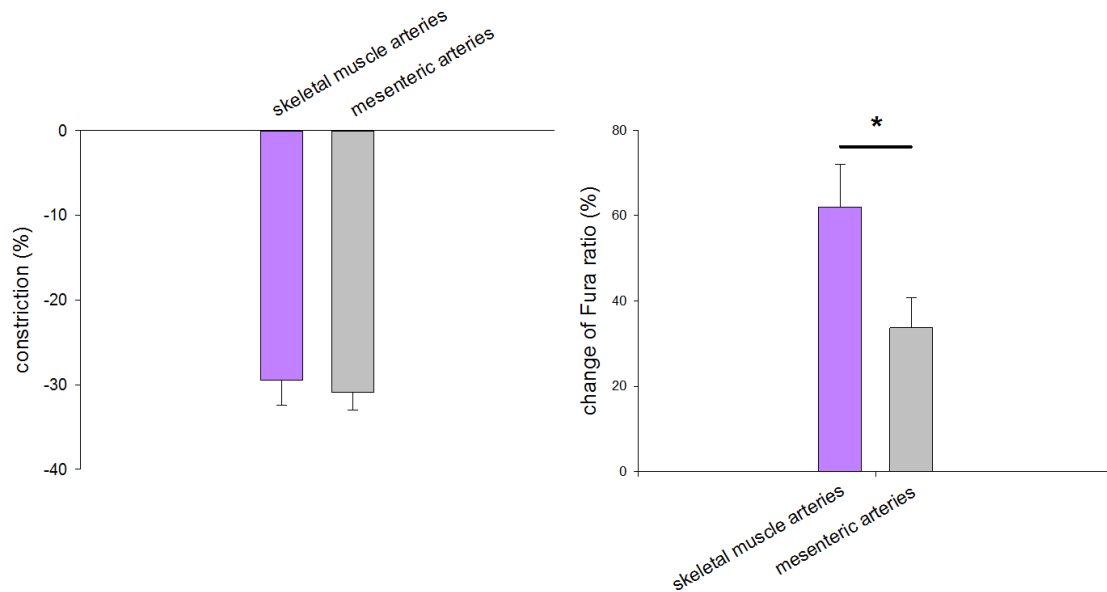


Figure 9: Effect of U46 on skeletal muscle arteries and mesenteric arteries

U46 (1 μ M) induced comparable constriction in both skeletal muscle (n=4) and mesenteric arteries (n=7), but a significantly higher Fura ratio in skeletal muscle arteries than in mesenteric arteries.

(* < 0.05) t-test

4.1.3. Relaxation

A single dose of acetylcholine (10 μ M), administered as part of a pre-test before the Fura-2 incubation, elicited an almost complete ($95.4 \pm 0.8\%$) dilation of the mesenteric arteries. As the test was done before the Fura-2 incubation, the Fura ratio could not be determined at this stage. The test was, however, not done in vessels that underwent further endothelial testing like the skeletal muscle arteries. As for the other experiments further analyzing the effects of the AMP-kinase on smooth muscle cells, it was also not performed on a continuous basis as an endothelial-independent effect was studied.

To test and compare the endothelial function of these different types of vessels however, the acetylcholine-induced dilation was studied in more detail by obtaining a dose-response curve (0.01 μ M – 1 μ M) after incubation with Fura-2.

In skeletal muscle arteries, increasing doses of acetylcholine induced dilations in a dose-dependent manner. These dilations were accompanied by respective decreases of the Fura ratio. In contrast, the mesenteric arteries, despite having responded well to the initial dose of acetylcholine subsequently only showed a small response to acetylcholine which was virtually independent of the applied dose (see Figure 10). While the skeletal muscle arteries dilated almost completely to an acetylcholine concentration of 0.3 μ M ($+97.5 \pm 1.1\%$), the mesenteric arteries reacted much less

and only presented with a small dilation even to the highest acetylcholine concentration of 30 μM ($+16.8 \pm 11.9\%$).

The Fura ratio of the mesenteric arteries also did not change significantly even at 30 μM acetylcholine ($-36.7 \pm 10.5\%$) while the ratio of the skeletal muscle arteries almost declined to the reference value that is obtained after adding acetylcholine 1 μM (see chapter 3.4.7.2 Analysis of Dose-Response Curves) at 0.3 μM acetylcholine ($-93.3 \pm 2.0\%$).

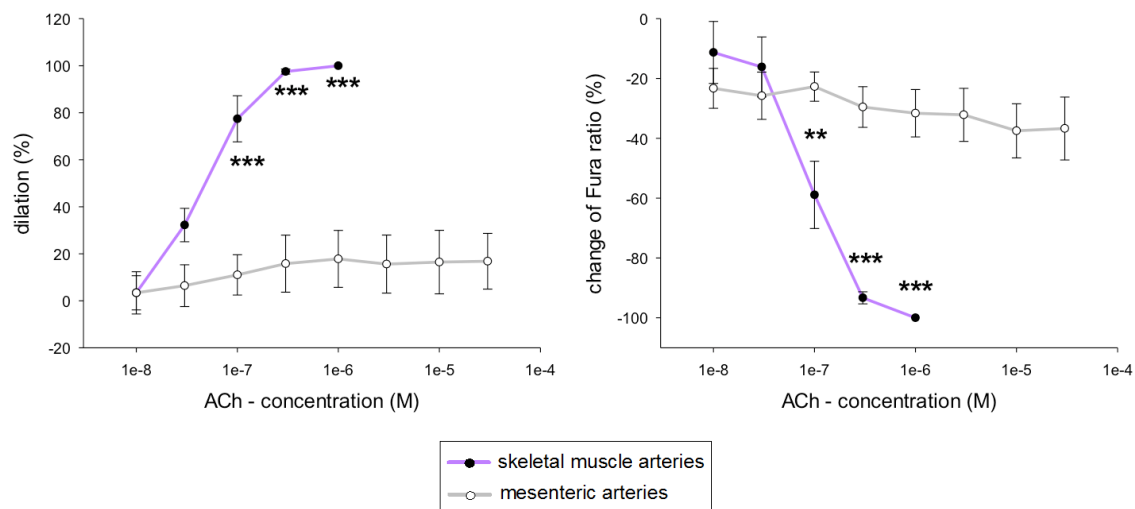


Figure 10: Dose-dependent effects of acetylcholine (ACh) in skeletal muscle arteries and mesenteric arteries

ACh induced a significant dilation and a decrease of the Fura ratio in skeletal muscle arteries ($n=4$), but hardly any dilation or decrease of the Fura ratio in mesenteric arteries ($n=7$).

(** < 0.01; *** < 0.001) Two-Way Anova

To further clarify the relative contribution of the endothelial component NO in the dilation of the skeletal muscle arteries, the eNOS was blocked by L-NAME (30 μM). The skeletal muscle arteries still dilated to comparable values (with L-NAME_{ACh 1 μM} : $+96.3 \pm 3.5\%$; without L-NAME_{ACh 1 μM} : 107.2 ± 7.5), but there was a significant decline of the drop in Fura ratio compared to vessels not treated with L-NAME (with L-NAME_{ACh 0.3 μM} : $-70.9 \pm 4.2\%$; without L-NAME_{ACh 1 μM} : $-118.6 \pm 22.7\%$).

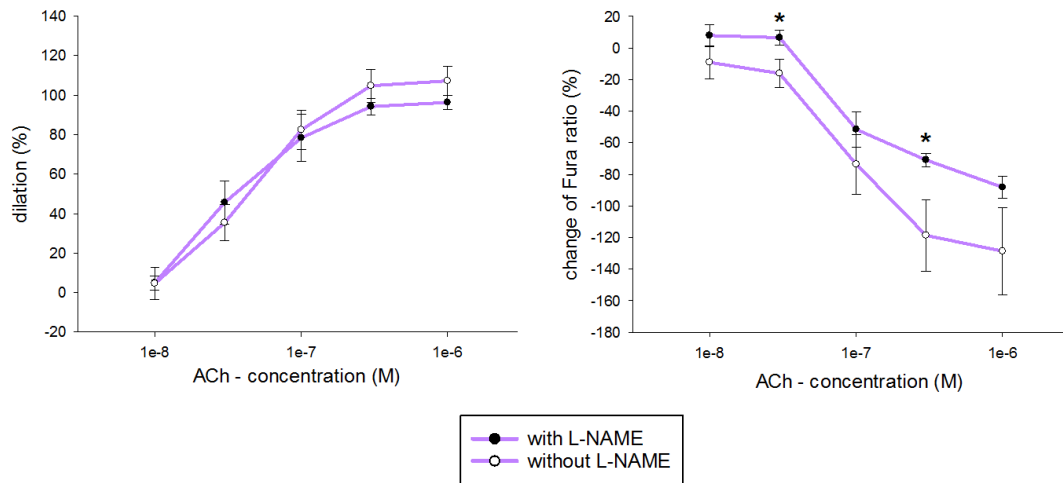


Figure 11: Influence of L-NAME on ACh-induced dilation in skeletal muscle arteries

The addition of L-NAME (30 μ M) did not significantly influence the dilation to increasing doses of A76 ($n=4$ for both groups), but did significantly reduce the decline of the Fura ratio. (* < 0,05) Two-Way Anova

The endothelium-independent vasodilator nifedipine (5 μ M), which was applied towards the end of the experiments, induced an almost maximal dilation in both, skeletal muscle and mesenteric arteries (skeletal muscle arteries: $+84.7 \pm 9.1\%$; mesenteric arteries: $+86.8 \pm 5.0\%$). The Fura ratio decreased similarly in both cases to or even below the basal values measured before the application of the vasoconstrictor (skeletal muscle arteries: $-140.5 \pm 52.6\%$; mesenteric arteries $-102.1 \pm 14.0\%$). Thus, there was no difference in the endothelium-independent vasodilation of skeletal muscle and mesenteric arteries.

The reasons for the differences between muscle and mesenteric arteries with regard to their response to acetylcholine were not studied further. The endothelium-independent smooth muscle cell responses were regarded as more important than the endothelium-dependent responses since, as shown before in hamster vessels, the AMP-kinase induces vasodilation in an endothelium-independent manner (Schneider, Schubert et al. (2015)).

All further experiments were performed in mesenteric arteries. Due to their multitude, these arteries were considered to allow simultaneous measurements of vascular reactions and harvesting for protein determination from the same animal.

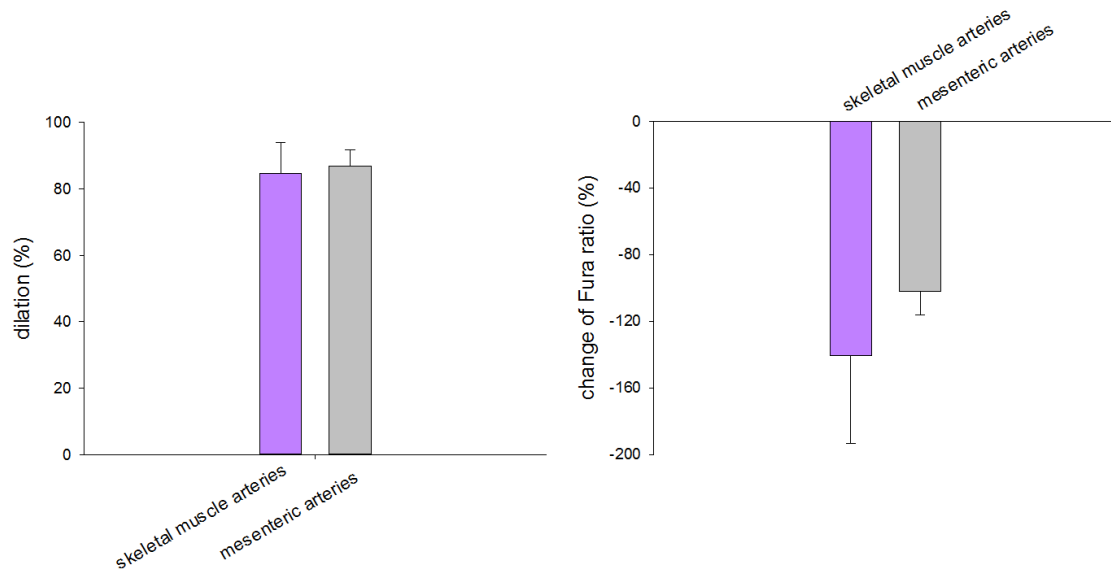


Figure 12: Effects of nifedipine on skeletal muscle arteries and mesenteric arteries

Nifedipine (5 μ M) induced dilation and a decrease of the Fura ratio to basal levels in both skeletal muscle arteries (n=4) and mesenteric arteries (n=7). t-test

4.2. AMP-Kinase in Mesenteric Arteries

4.2.1. Expression of AMP-Kinase's Subunits in Mesenteric Arteries

In order to confirm the expression of the AMP-kinase in small mesenteric arteries and to analyze which of its subunits were present, PCR was performed in vessels of C57Bl/6 mice.

Figure 13 shows that the Prkag2 gene encoding the regulatory γ_2 subunit was most expressed, followed by both the Prkaa1 and Prkaa2 genes, coding for the catalytic α_1 and α_2 subunits (γ_2 : 2.2 ± 0.8 ; α_1 : 1.6 ± 0.3 α_2 : 1.1 ± 0.2). All subunits were expressed in mesenteric arteries of C57Bl/6 mice except the γ_3 subunit, which was not found in these vessels.

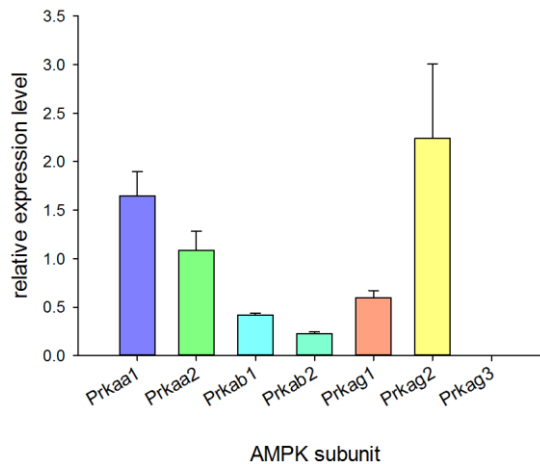


Figure 13: Relative expression levels of AMPK subunits in mesenteric arteries

All AMPK subunits were expressed in mesenteric arteries except the regulatory γ_3 subunit, with the regulatory γ_2 subunit most expressed, followed by the catalytic α_1 and α_2 subunits (n=3).

4.2.2. Influence of A76/PT1 on Mesenteric Arteries

Two different stimulators of the AMP-kinase, A76 and PT1, were used to analyze the effect of AMP-kinase activation concerning the vascular tone of mesenteric arteries. These two compounds are chemically not related and activate the AMP-kinase through different target mechanisms (see section 1.2.3 Regulation of the AMP-Kinase).

Both A76 and PT1 led to a dose-dependent dilation and in the case of A76 we also observed a concomitant dose-dependent decrease of the Fura ratio (as PT1 interacted with the Fura-2am signal the calcium values were not measured when PT1 was applied, as they were not representative). Typical original recordings are shown in Figure 14.

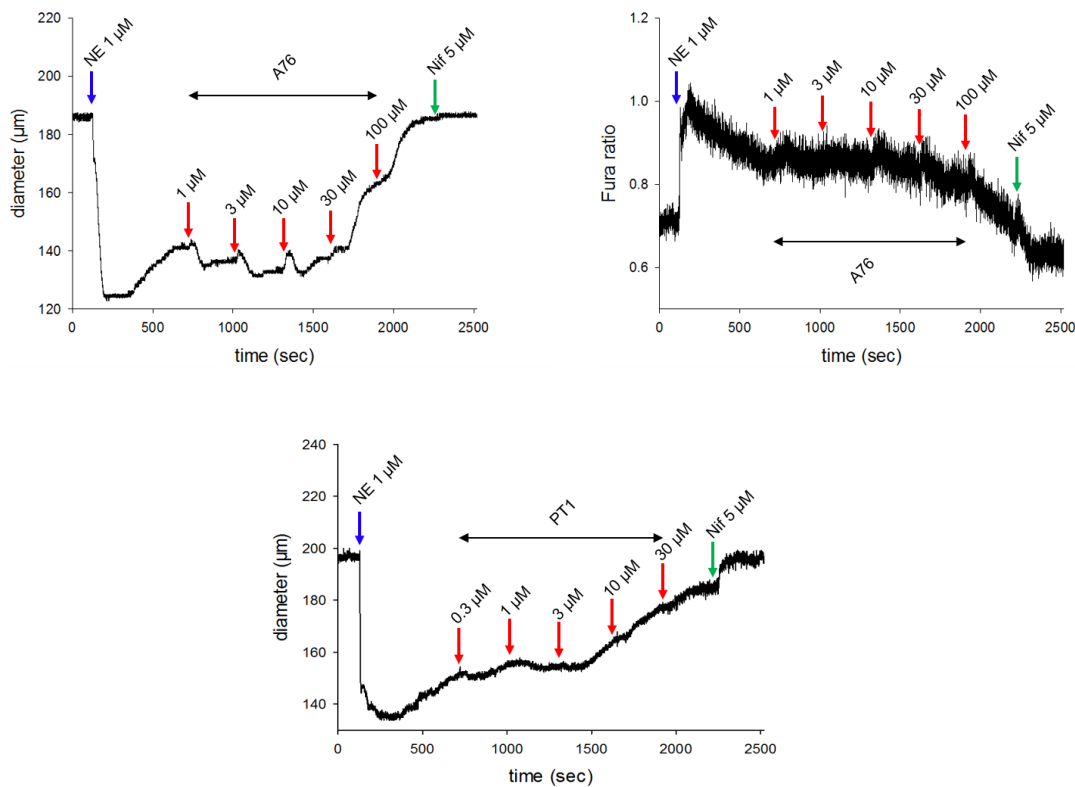


Figure 14: Dose-dependent dilation and Fura decrease on addition of A76 (red arrows) or PT1 (red arrows) in a mesenteric artery precontracted with norepinephrine (1 μM) (blue arrows) (green arrows symbolize addition of 5 μM nifedipine)

Vessels treated with either of the two presented with a dose dependent dilation (A76: 30 – 100 μM ; PT1: 10 – 30 μM). Maximal dilation and maximal decrease of the ratio was obtained at A76_{0.1%DMSO} 100 μM (dilation: $+93.4 \pm 3.2\%$; Fura ratio: $-79.9 \pm 6.7\%$) and PT1_{0.03%DMSO} 30 μM (dilation: $+72.1 \pm 12.1\%$). Concentrations of A76 above 10 μM or PT1 above 3 μM led to a significant dilation and a significant decrease of the Fura ratio when applying A76. As seen in Figure 15 and Figure 16 the control vessels treated with increasing doses of DMSO (0.001% – 0.1%), the solvent of A76 and PT1 did not dilate significantly. The observed decrease of the Fura ratio was due to time-dependent bleaching of Fura-2. The bleaching reduced the fluorescence signal obtained at 340 nm more than the signal obtained at 380 nm and did thus not represent a true Ca^{2+} decrease.

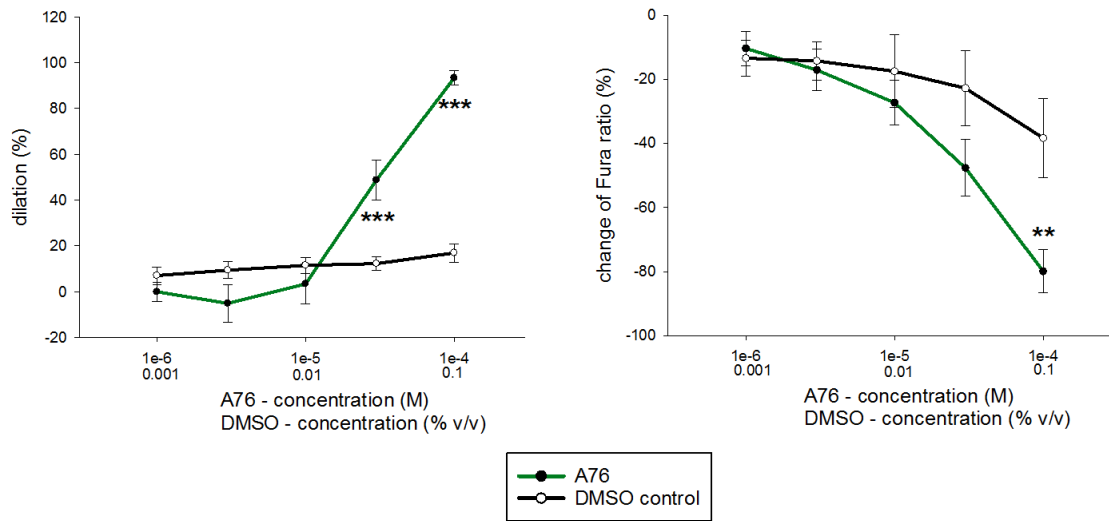


Figure 15: A76-induced dose-dependent dilation and decrease of the Fura ratio

A76 induced a significant dilation and a decrease of the Fura ratio in mesenteric arteries (n=4). In contrast to this, the sole use of the solvent (DMSO) did not elicit any significant dilation (n=4). (**<0.01; ***<0.001) Two-Way Anova

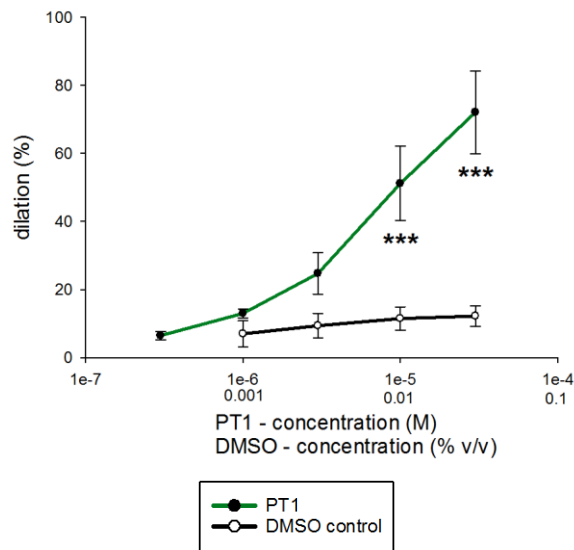


Figure 16: PT1-induced dose-dependent dilation

PT1 induced a significant dilation in mesenteric arteries (n=4) compared to DMSO-treated control vessels (n=4). (***)<0.001) Two-Way Anova

4.2.3. Calcium Sensitivity

Our group's previous experiments in hamster vessels have already shown that the AMP-kinase does not only dilate blood vessels by reducing the concentration of intracellular Ca^{2+} in smooth cells but also by reducing the smooth muscle cells' Ca^{2+} sensitivity. Here, we studied whether this was also the case in mouse vessels.

Due to the previously described interaction of PT1 and Fura-2am, experiments to test the effect of the AMP-kinase on Ca^{2+} sensitivity were only done with A76. Typical original recordings are shown in the following figure (see Figure 17).

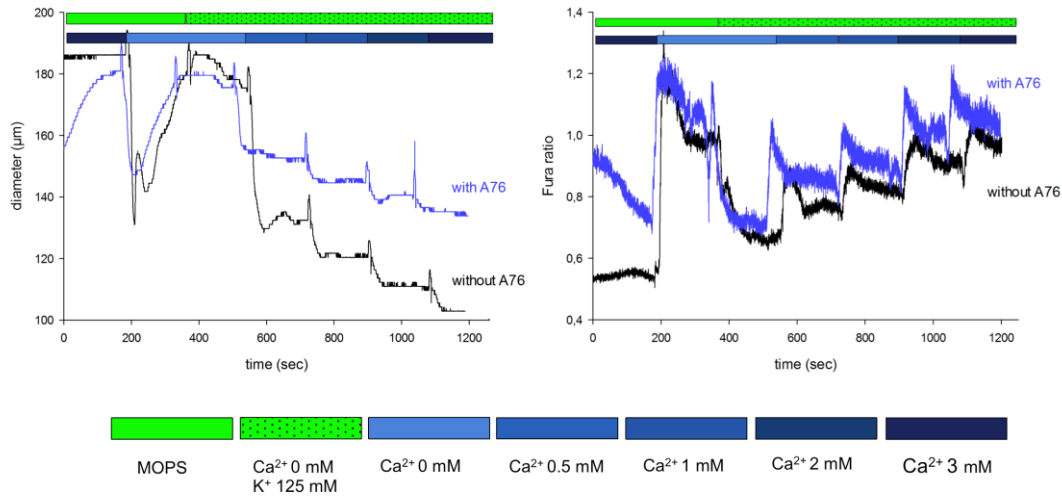


Figure 17: Dose-dependent constriction and Fura increase on addition of increasing doses of extracellular Ca^{2+} in a mesenteric artery with and without additional A76

A stepwise increase of extracellular Ca^{2+} (0.5 mM, 1 mM, 2 mM, 3 mM) led to an increase of the Fura ratio in a depolarized and Ca^{2+} -depleted vessel (MOPS used: Ca^{2+} free, 125 mM K^{+}) thus indicating a simultaneous increase in intracellular free Ca^{2+} (Fura ratio at Ca^{2+} 0 mM: 0.58 ± 0.03 , Fura ratio at Ca^{2+} 3 mM: 0.84 ± 0.07). This increase in intracellular free Ca^{2+} led to an increasing vasoconstriction (diameter at Ca^{2+} 0 mM: $150.8 \pm 10.6 \mu\text{m}$, diameter at Ca^{2+} 3 mM: $87.3 \pm 10.5 \mu\text{m}$). If the vessels were pretreated with A76 this constriction was significantly reduced ($p=0.04$) (diameter at Ca^{2+} 0 mM: $153.0 \pm 11.9 \mu\text{m}$, diameter at Ca^{2+} 3 mM: $111.8 \pm 11.4 \mu\text{m}$), though the increases of the Fura ratio were not altered (Fura ratio at Ca^{2+} 0 mM: 0.60 ± 0.03 , Fura ratio at Ca^{2+} 3 mM: 0.87 ± 0.08), indicating calcium desensitization of the contractile apparatus.

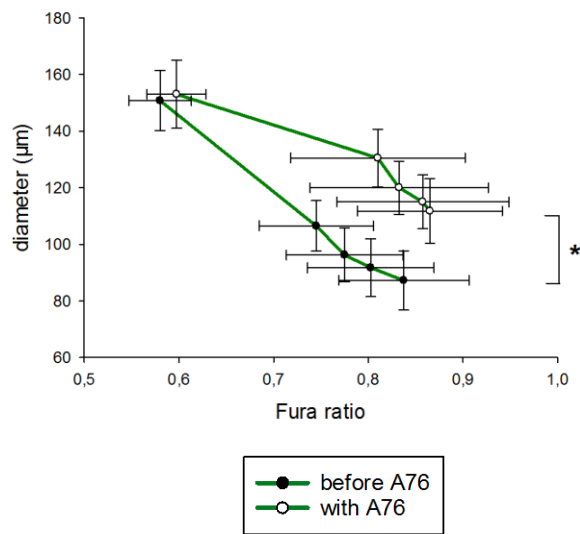


Figure 18: Effect of A76 on Ca^{2+} sensitivity

Vessels pre-treated with Ca^{2+} -free MOPS (K^+ 125 mM) were treated with increasing doses of extracellular Ca^{2+} (0.5 mM, 1 mM, 2 mM, 3 mM) with and without A76 (100 μM). There was a significantly reduced constrictor response when A76 was added. (***) <0.001) Non-linear regression analysis

4.2.4. The Relative Role of the Different AMP-Kinase's α Subunits as Studied in Knockout Mice

4.2.4.1. Basal Vascular Tone

At first, we studied whether the unstimulated vessels exhibited a basal tone i.e. without adding a vasoconstrictor. Under these conditions, it was expected that nifedipine would induce a vasodilation. In α_1 and the α_2 knockout vessels and vessels of the corresponding wild type animals no significant vasodilation on addition of nifedipine could be observed (data not shown), thus indicating the absence of a basal tone.

4.2.4.2. Reaction to Vasoconstrictors

In a further step, we studied whether knocking out one of the AMP-kinase's α subunits affected the vessels' response to the vasoconstrictor norepinephrine (1 μM).

There was no difference between the α_1 knockouts and their wild type controls for both constriction (KO: $-39.0 \pm 4.5\%$; WT: $-41.4 \pm 5.4\%$) and the accompanying increase of the Fura ratio (KO: $+25.9 \pm 3.7\%$; WT: $+47.8 \pm 11.6\%$).

In α_2 knockout vessels, however, constriction to norepinephrine was significantly stronger than in the corresponding wild type controls (KO: $-41.5 \pm 3.1\%$; WT: $-29.1 \pm 3.6\%$), while there was no difference regarding the change of the Fura ratio (KO: $+45.1 \pm 13$; WT: $+43.3 \pm 7.8$).

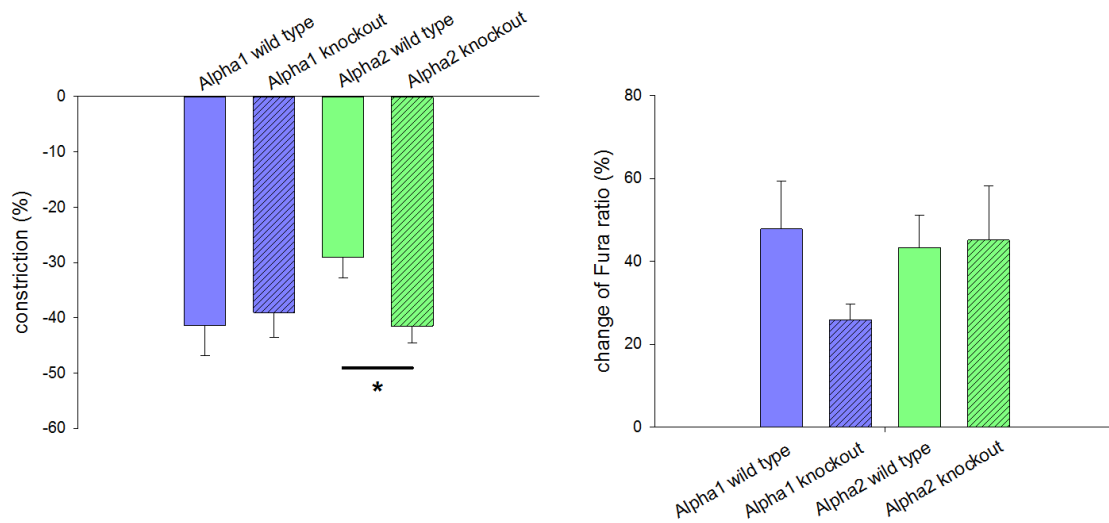


Figure 19: Effect of norepinephrine on α_1 and α_2 wild type and knockout vessels

Norepinephrine ($1 \mu\text{M}$) led to a comparable constriction and increase of the Fura ratio in α_1 knockout ($n=4$) and wild type vessels ($n=5$). In α_2 knockout vessels ($n=4$) constriction to norepinephrine ($1 \mu\text{M}$) was significantly higher than in the corresponding wild type vessels. ($n=4$), while there was no difference in the Fura ratio. ($* < 0.05$) t-test

Receptor-independent vasoconstriction for knockout and wild type vessels was then analyzed by comparing constriction to depolarization by K^+ (125 mM). Unlike norepinephrine-induced constriction, there was no difference between both knockouts and their respective wild type counterparts concerning both constriction and the Fura ratio on addition of K^+ (125 mM).

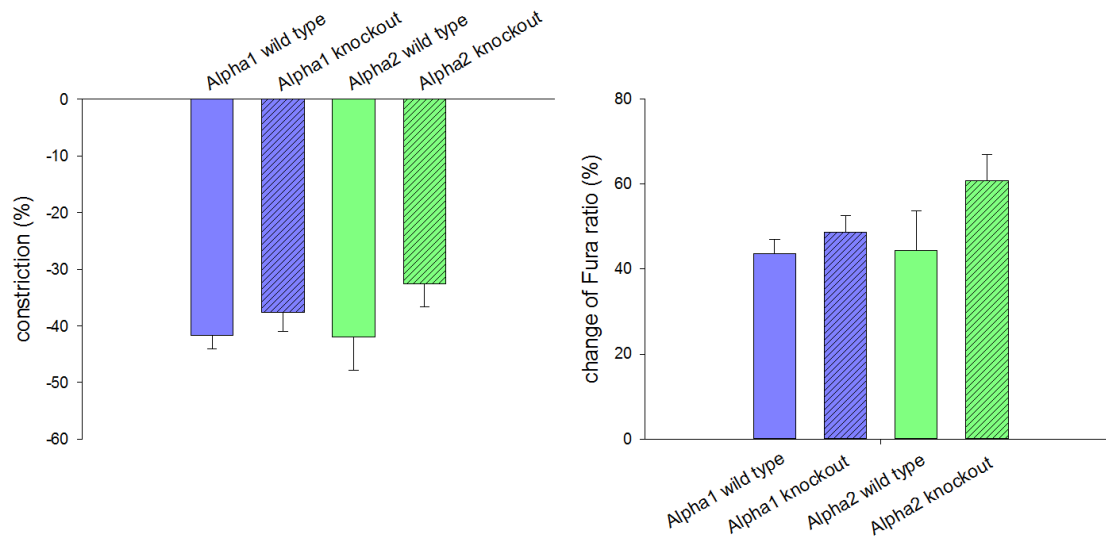


Figure 20: Effect of depolarization on α_1 and α_2 wild type and knockout vessels

Depolarization by K^+ (125 mM) induced equivalent constriction and a comparable increase of the Fura ratio in α_1 and α_2 wild type ($n_{\alpha_1}=6$; $n_{\alpha_2}=4$) and knockout ($n_{\alpha_1}=4$; $n_{\alpha_2}=4$) vessels. t-test

4.2.4.3. Response to Specific AMP-Kinase Activators

4.2.4.3.1. Response to PT1

The AMPK activator PT1 led to dose-dependent dilation in α_2 knockout vessels, which did not differ from the response of the respective wild type controls. Virtually identical maximal vasodilation was achieved by the highest concentration of PT1 (30 μ M) in both wild type (+72.1 \pm 12.1%) and knockout (+67.2 \pm 10.9%) vessels with their EC_{50} values not being significantly different either (WT: 5.7 \pm 1.1 μ M; KO: 9.1 \pm 1.3 μ M).

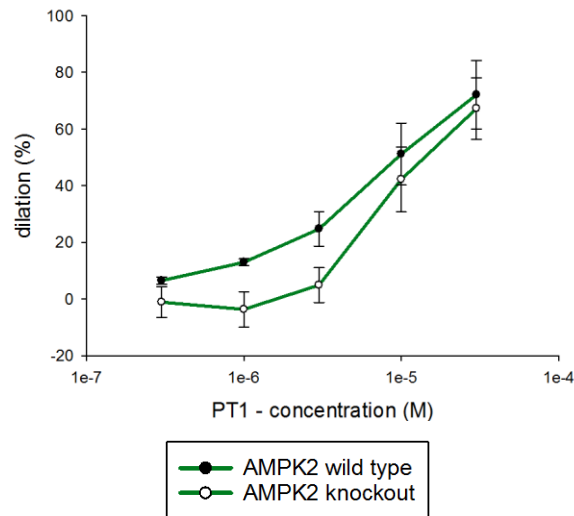


Figure 21: Effect of PT1 on α_2 wild type and knockout vessels

PT1 induced dose-dependent and almost maximal dilation in α_2 knockout vessels (n=6) that was comparable to wild type vessels (n=4). Two-Way Anova

In α_1 knockout vessels PT1 led to an increased maximal dilation compared to wild type vessels. There was already a tendency for stronger dilation in the knockout for lower PT1 concentrations (1–3 μM), but this was not significant ($p_{1\ \mu\text{M}}=0.203$; $p_{3\ \mu\text{M}}=0.131$). Dilation to higher concentrations of PT1 (10–30 μM) was, however, significantly enhanced compared to the wild type (KO_{30 μM} : +92.2 \pm 3.2%; WT_{30 μM} : +63.4 \pm 7.3). EC₅₀ values were, however, not changed, while the aforementioned maximum response was increased (KO: 5.3 \pm 0.004 μM ; WT: 7.4 \pm 1.5 μM).

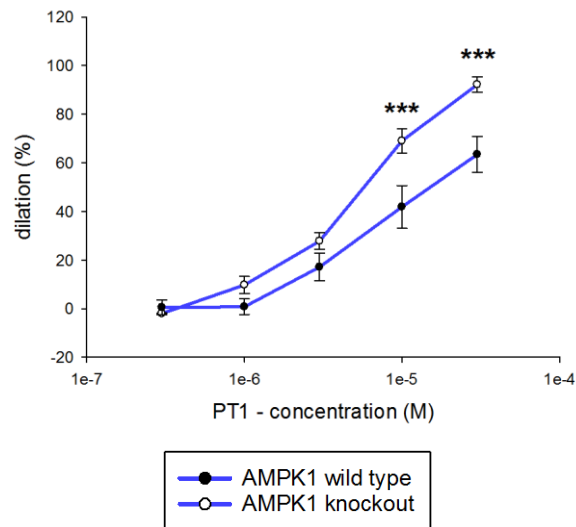


Figure 22: Effect of PT1 on α_1 wild type and knockout vessels

PT1-induced dilation was equally dose-dependent, but significantly enhanced in α_1 knockout vessels (n=5) compared to the wild type (n=5). (***) <math>P < 0.001</math> Two-Way Anova

4.2.4.3.2. Response to A76

A76, the other AMPK-activator that was tested also led to a concentration-dependent dilation and decrease of the Fura ratio in α_2 knockouts. As with PT1, there was no difference between the two groups concerning both dilation (KO_{A76} 100 μ M: +88.0 \pm 3.3%; WT_{A76} 100 μ M: +93.4 \pm 3.2%) and Fura ratio (KO_{A76} 100 μ M: -72.6 \pm 9.2%; WT_{A76} 100 μ M: -79.9 \pm 6.7%). EC₅₀ values also did not differ significantly (KO: 34.5 \pm 6.7 μ M; WT: 29.3 \pm 5.5 μ M).

4 Results

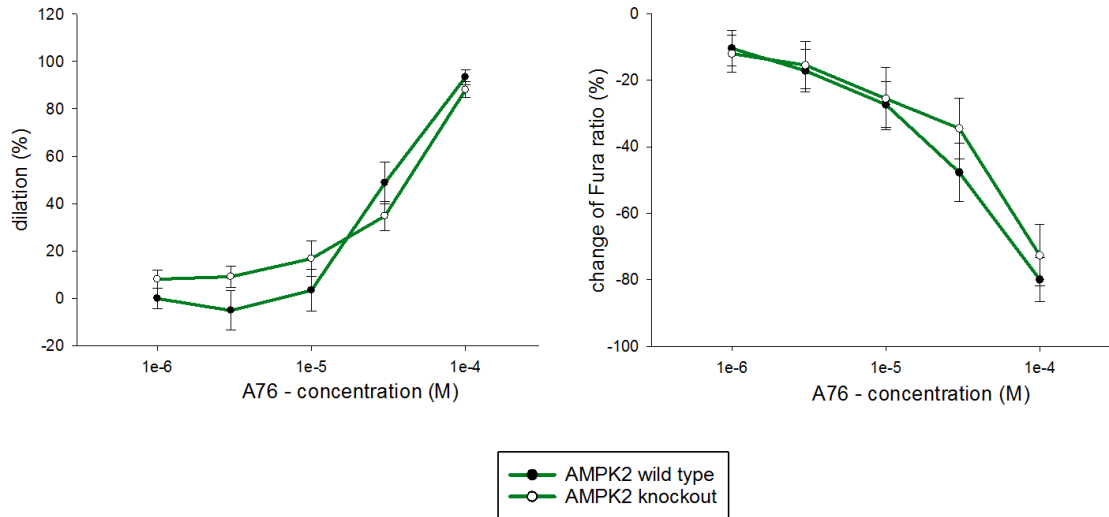


Figure 23: Effect of A76 on α_2 wild type and knockout vessels

A76-induced dilation and the decrease of the Fura ratio in α_2 knockout vessels (n=4) were not different from wild type vessels (n=4). Two-Way Anova

In α_1 knockout vessels, however, there was once again a tendency towards a stronger dilation than in the wild type vessels though the maximal response was not altered. Consequently, the EC_{50} values in α_1 knockout vessels were significantly lower than those in wild type vessels (KO: $23.3 \pm 1.6 \mu\text{M}$; WT: $39.8 \pm 4.9 \mu\text{M}$). Even if the vasodilation was enhanced in the α_1 knockout, there was no difference in the dose-dependent decrease of the Fura ratio at any point.

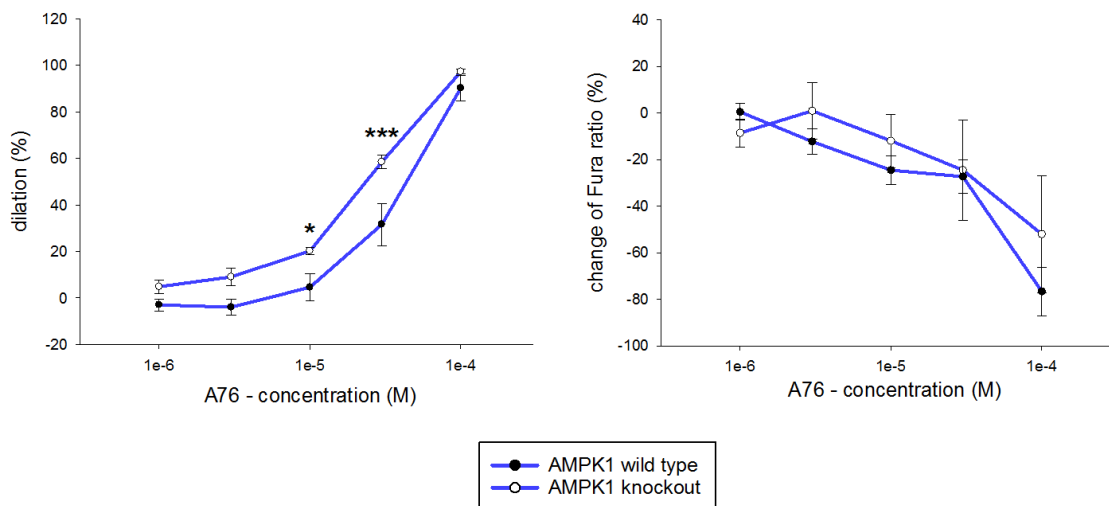


Figure 24: Effect of A76 on α_1 wild type and knockout vessels

A76 induced increased dilation, but no difference in the Fura ratio in α_1 knockout vessels (n=4) compared to wild type (n=5). (* < 0.05; *** < 0.001) Two-Way Anova

4.2.4.4. Differences in the Mechanisms of Calcium Decrease

4.2.4.4.1. Influence on BkCa-Channel-dependent Calcium Control

As other experiments in our lab indirectly suggested, the AMP-kinase's α_1 subunit might decrease intracellular Ca^{2+} in vascular smooth muscle cells by activating the BkCa-channel, while the α_2 subunit might do so by activating SERCA. The influence of A76 on these two calcium-decreasing mechanisms was consequently tested with the SERCA blocker thapsigargin (TG) and the BkCa-channel inhibitor iberiotoxin (IbTx) and compared in both types of AMP-kinase knockouts.

In α_2 knockout vessels pre-treated with IbTX (100 nM) there was less dilation specifically on higher concentrations of A76 (30 μM and 100 μM) than in equally treated wild type vessels ($\text{KO}_{\text{A76 } 100 \mu\text{M}}$: $+70.1 \pm 4.0\%$, $\text{WT}_{\text{A76 } 100 \mu\text{M}}$: $+91.4 \pm 2.5\%$). Surprisingly, despite there still being a substantial vasodilation there was an increase of the Fura ratio at 30 μM and 100 μM of A76 in α_2 knockout compared to wild type vessels ($\text{KO}_{\text{A76 } 100 \mu\text{M}}$: $+105.3 \pm 22.9\%$, $\text{WT}_{\text{A76 } 100 \mu\text{M}}$: $-55.3 \pm 19.6\%$). This increase could be blocked by adding the ORAI blocker YM 58483 (1 μM) (seen in pilot experiments).

EC_{50} values were, however, not significantly different between the two groups (KO : $37.6 \pm 1.9 \mu\text{M}$; WT : $33.8 \pm 5.6 \mu\text{M}$).

Further investigations revealed that the calcium signal producing this increase in the Fura ratio may have mainly originated from the outermost vessel layers, so that this calcium signal was considered to originate partly from adventitial non-muscle cells or, alternatively, to be due to an unspecific side effect of the treatment with iberiotoxin in α_2 knockout mice (as it was not seen in BkCa knockout mice). It is also conceivable that an increase of calcium occurred in a cellular compartment which did not lead to vasoconstriction. However, this was not further analyzed in the context of the present study.

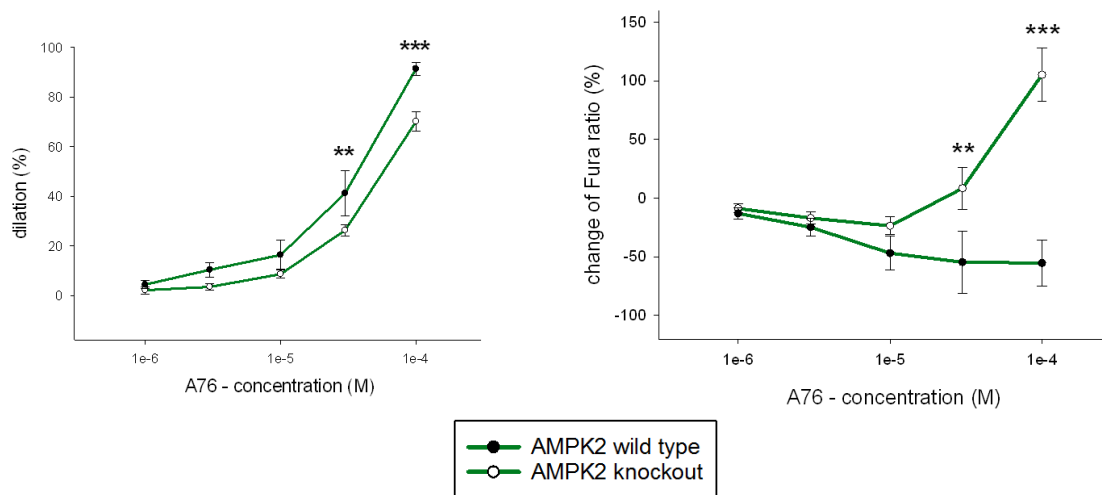


Figure 25: Effect of iberiotoxin (IbTx) on A76-related dilation and decrease of the Fura ratio in α_2 wild type and knockout vessels

In α_2 knockout vessels (n=10) pre-treated with IbTx (100 nM) A76 induced less dilation and even an increase of the Fura ratio compared to α_2 wild type vessels (n=6). The increase of the Fura ratio on 100 μ M A76 could be blocked by the ORAI blocker YM 58483 (1 μ M) (seen in pilot experiments). (**<0.01; ***<0.001) Two-Way Anova

When pre-treating α_1 wild type and knockout vessels with IbTx (100 nm) there was no essential difference between the two dose-response curves. The subanalysis showed that there was only a significantly increased dilation in the α_1 knockout vessels at 30 nm of A76 (WT_{30 μ M}: +21.3 \pm 5.5%, KO_{30 μ M}: +38.5 \pm 6.6%), while there was no difference at 100 nm of A76. There was, however, no change in the Fura ratio, where a comparable steady state could be seen until 30 nm of A76 followed by a similar drop to the highest concentration of A76. EC₅₀ values were similar between the two groups (KO: 32.8 \pm 4.2 μ M; WT: 43.4 \pm 3.1 μ M).

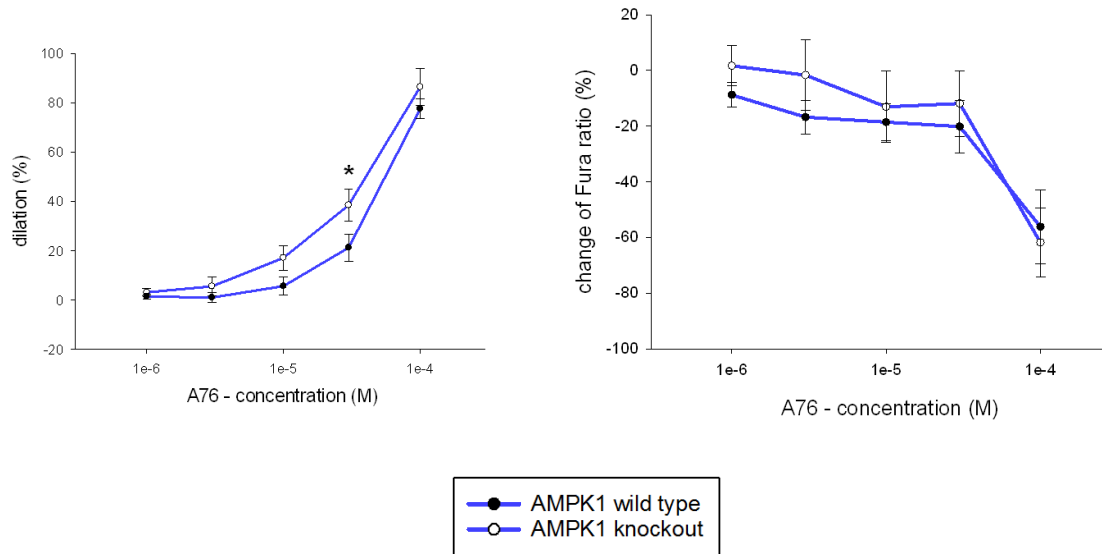


Figure 26: Effect of iberiotoxin (IbTX) on A76-related dilation and decrease of the Fura ratio in α_1 wild type and knockout vessels

In IbTX-pretreated vessels there was no essential difference in both vasodilation (with only a singular concentration of A76 leading to a significantly increased vasodilation) and change of the Fura ratio in α_1 knockout vessels (n=4) compared to wild type vessels (n=4), while there was no difference in the change of the Fura ratio. (*<0.05) Two-Way Anova

To assess for potential side effects of the pharmacological inhibition of BkCa-channels by IbTX, A76 induced dilations were studied in BkCa knockout mice in an additional series of experiments. As shown in Figure 27 and comparable to the α_1 knockouts, there was a tendency for stronger dilation at lower concentrations of A76 (1–10 μ M), but it was only significantly increased at a concentration of A76 30 μ M in BkCa knockouts (BkCa KO: $+68.1 \pm 6.1\%$; BkCa WT: $+45.6 \pm 3.7\%$). There was, however, no difference in the change of Fura ratio between the knockout and the wild type.

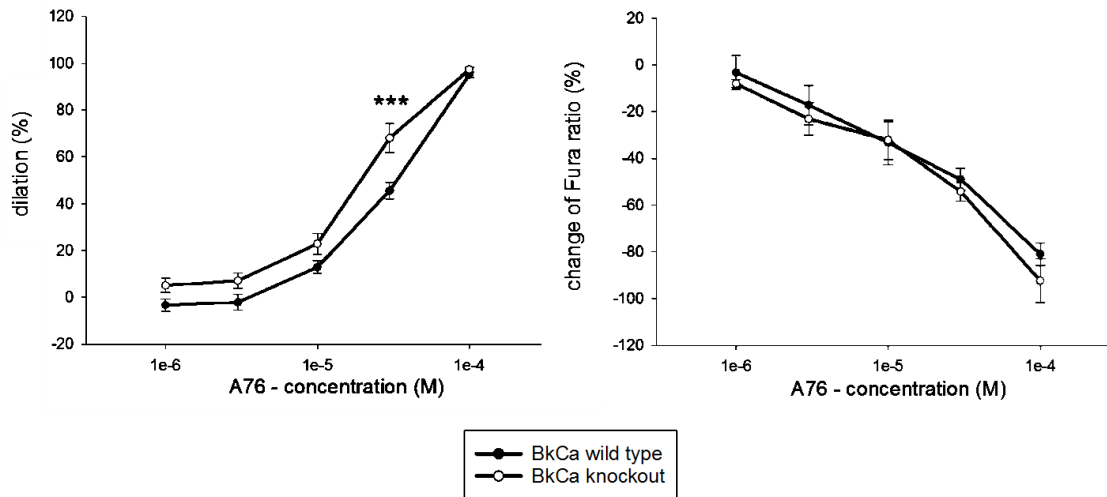


Figure 27: Dose-dependent dilation on addition of increasing doses of A76 in both BkCa wild type and knockout vessels

A76 induced a dose-dependent dilation and drop of Fura ratio in both BkCa wild type and knockout vessels. The dose-dependent dilation to A76 was significantly increased in the BkCa-knockouts (n=4) compared to the wild type (n=4), while there was no difference in the change of Fura ratio. (***) <math><0,001</math> Two-Way Anova

4.2.4.4.2. Influence on SERCA-dependent Calcium Control

In addition to the treatment with IbTx, both α_1 and α_2 vessels were pre-treated with TG (1 μ M).

In α_1 knockout vessels incubated with TG, there was less dilation but no difference in the decrease of the Fura ratio on addition of A76 at 100 μ M A76 (KO_{100 μ M}: +3.3 \pm 1.0%, Fura ratio: -16.8 \pm 1.2%) than in the equally treated wild type vessels (WT_{100 μ M}: +11.8 \pm 0.8%; Fura ratio: -18.6 \pm 2.3).

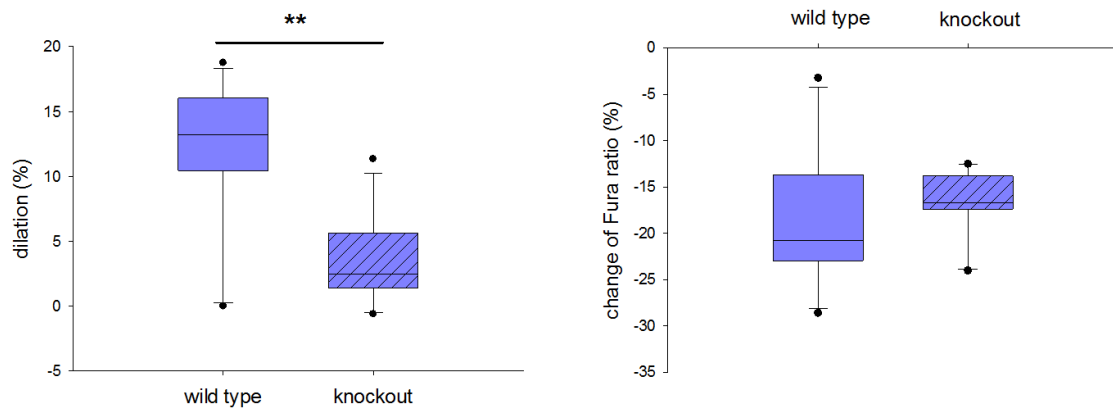


Figure 28: Effect of thapsigargin (TG) on A76 (100 μ M)-induced dilation and decrease of Fura ratio in α_1 knockout and wild type vessels

A76-induced dilation was significantly decreased in α_1 knockout vessels (n=11) compared to the wild type vessels (n=11) when the vessels were pre-treated with TG (1 μ M). There was, however, no change in the Fura ratio in the α_1 knockout vessels. (**<0,01) Two-Way Anova

There was, however, no difference when pre-treating α_2 wild type or knockout vessels with TG. Both wild type and knockout vessels dilated comparably (WT_{A76 100 μ M}: +11.0 \pm 5.6%, KO_{A76 100 μ M}: +18.5 \pm 7.1%), while there also was a similar decrease in the Fura ratio of both the α_2 wild type and the knockout vessels (WT_{A76 100 μ M}: -34.8 \pm 3.7%, KO_{A76 100 μ M}: -34.6 \pm 2.7%).

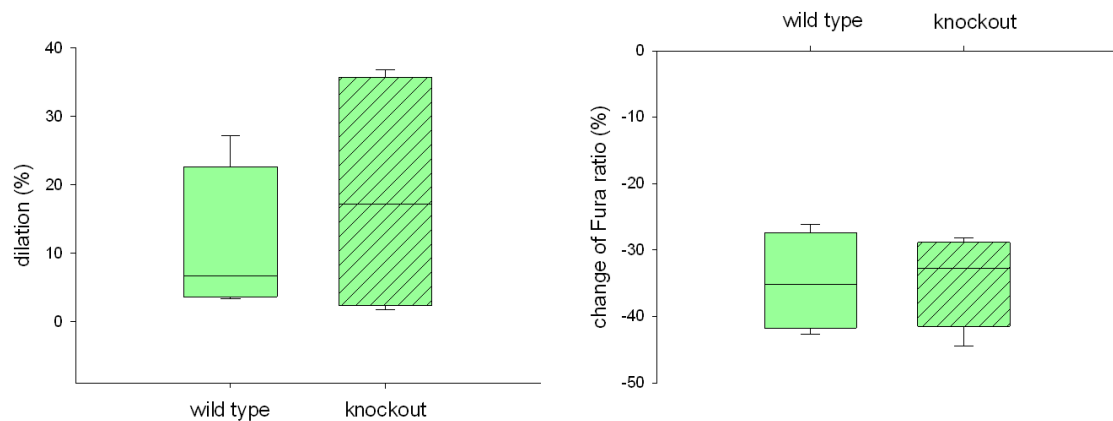


Figure 29: Effect of thapsigargin (TG) on A76 (100 μ M)-induced dilation and decrease of Fura ratio in α_2 knockout and wild type vessels

There was no difference in A76-induced dilation or decrease in the Fura ratio (100 μ M) in α_2 knockout (n=6) and wild type vessels (n=4) after incubation with TG (1 μ M). Two-Way Anova

4.2.4.5. Influence on Calcium Sensitivity

Ca²⁺ sensitivity in AMP-kinase's α_1 and α_2 knockout vessels was analyzed by comparing the calcium-constriction relation in knockout animals and their respective

wild type controls using the experimental protocol already described above (see paragraph 4.2.3 Calcium Sensitivity).

As in wild type vessels (see Figure 18 Effect of A76 on Ca^{2+} sensitivity), there was an upward shift, but no significant flattening of the graph in α_2 knockout vessels on addition of A76 (100 μM). On addition of A76 there was only slightly less constriction even on the highest concentration of extracellular calcium (constriction without A76: from Ca^{2+} 0 mM: $184.0 \pm 12.6 \mu\text{m}$ to Ca^{2+} 3 mM: $125.5 \pm 16.0 \mu\text{m}$; constriction with A76: from Ca^{2+} 0 mM: $184.3 \pm 12.9 \mu\text{m}$ to Ca^{2+} 3 mM: $147.8 \pm 16.8 \mu\text{m}$), while the Fura ratio did not change ($p=0.0533$). There was consequently no sign of calcium desensitization seen in α_2 knockout vessels.

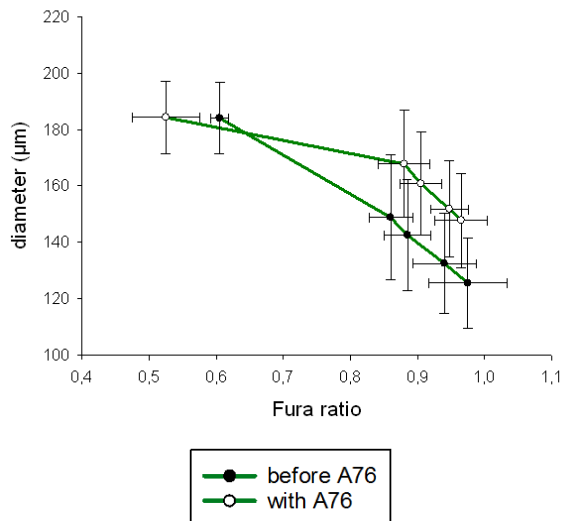


Figure 30: Effect of A76 on Ca^{2+} sensitivity in α_2 knockout vessels

A76-treated α_2 knockout ($n=4$) vessels showed no significant decrease in constriction and no significant increase in the Fura ratio when exposed to increasing doses of extracellular Ca^{2+} (0.5 mM, 1 mM, 2 mM, 3 mM) and A76 (100 μM). Non-linear regression analysis

A significant upward shift of the constriction values could, however, still be observed in both α_1 wild type and knockout vessels treated with A76 (100 μM). Whereby both wild type and knockout vessels presented with comparable Fura ratio levels before and after the addition of A76 (KO without A76: from Ca^{2+} 0 mM: 0.7 ± 0.02 to 3 mM Ca^{2+} : 1.1 ± 0.03 ; KO with A76: from Ca^{2+} 0 mM: 0.8 ± 0.07 to 3 mM Ca^{2+} : 1.1 ± 0.1 ; WT without A76: from 0 mM Ca^{2+} : 0.68 ± 0.04 to 3 mM Ca^{2+} : 0.98 ± 0.05 ; WT with A76: from 0 mM Ca^{2+} : 0.62 ± 0.06 to Ca^{2+} 3 mM: 0.9 ± 0.12), they both constricted significantly less ($p_{\text{KO/WT}}=0.0001$) to all levels of extracellular calcium (0.5–3 mM)

4 Results

when treated with A76 (KO without A76: from 0 mM Ca^{2+} : $185.0 \pm 8.4 \mu\text{m}$ to 3 mM Ca^{2+} : $116.3 \pm 11.8 \mu\text{m}$; KO with A76 0 mM Ca^{2+} : $187.8 \pm 8.1 \mu\text{m}$ to 3 mM Ca^{2+} : $164.5 \pm 15.3 \mu\text{m}$; WT without A76: from Ca^{2+} 0 mM: $185.0 \pm 8.4 \mu\text{m}$ to Ca^{2+} 3 mM: $116.3 \pm 11.8 \mu\text{m}$; WT with A76: from Ca^{2+} 0 mM: $187.8 \pm 8.1 \mu\text{m}$ to Ca^{2+} 3 mM: $164.5 \pm 15.3 \mu\text{m}$).

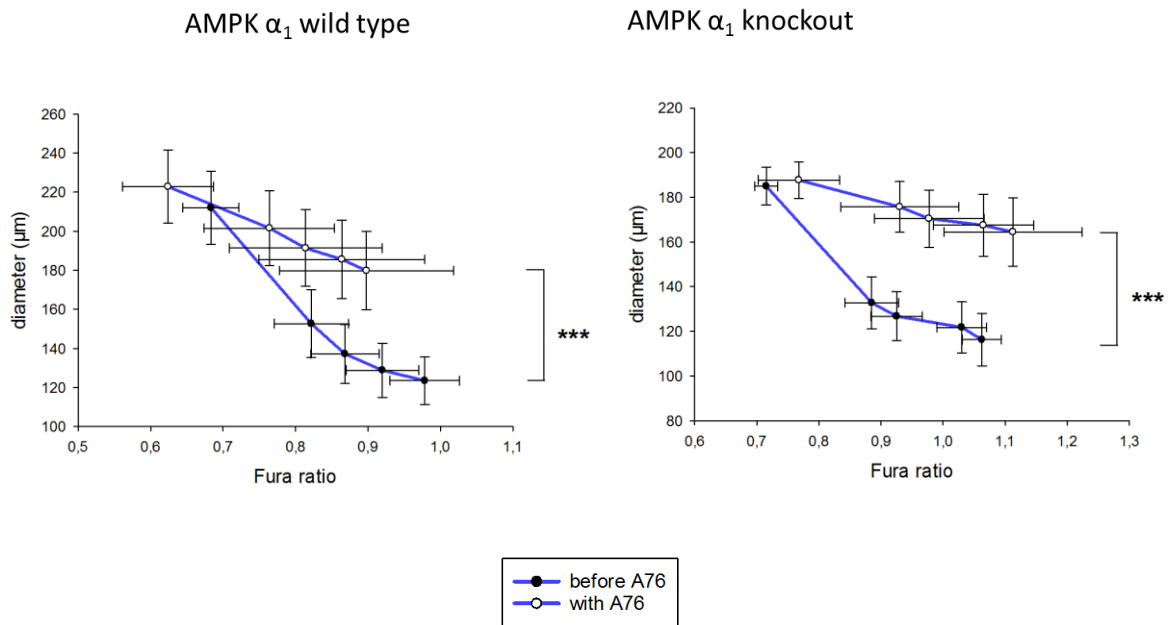


Figure 31: Effect of A76 on Ca^{2+} sensitivity in α_1 wild type and knockout vessels

Both A76-treated α_1 wild type (n=6) and knockout (n=4) vessels showed less constriction despite comparable levels of the Fura ratio, when treated with increasing doses of extracellular Ca^{2+} (0.5 mM, 1 mM, 2 mM, 3 mM) and A76 (100 μM). (***) <0.001) Non-linear regression analysis

5. Discussion

5.1. Findings

This thesis provides evidence that AMP-kinase activation induces a significant vasodilation in both mesenteric and skeletal muscle arteries of mice. The mechanisms leading to this vasodilation were shown to be the same ones that our group had already described in hamster vessels (Schneider, Schubert et al. 2015). As mesenteric arteries were shown to be well suited to analyze the effects of the AMP-kinase on basal vascular tone and simultaneously on the vessels' intracellular calcium levels, they could be used to further analyze the impact of the AMP-kinase's subunits using genetically modified mice. This thesis focused on the importance of the two catalytic α subunits (α_1 and α_2) for vasodilation. It could be shown that the two AMP-kinase activators A76 and PT1 dilate via the two α subunits, but predominantly via the α_2 subunit. Most importantly, it could also be shown that the α_2 subunit is essential for inducing calcium sensitivity.

5.2. Characterization of Mouse Arteries

Isolated arteries prove to be a good match to analyze the effect of the AMP-kinase as they contain in situ cells, which are important for vascular function but lack the biochemical complexity of a blood perfused living organ that would be present when studying small blood vessels in vivo. They thus facilitate the interpretation of the results, as there is less interference with the vascular pathway that is studied. It should be noted that to determine physiological relevance, in vivo experiments are to be carried out at a later stage. (Kreutz (2013))

All of our group's former experiments addressed hamster femoral skeletal muscle arteries, where it could be shown that AMP-kinase's activation induces substantial vasodilation in a calcium-dependent and calcium-independent manner. However, due to the lack of specific activators, it was hardly possible to study the contribution of the single subunits of the heterotrimeric AMPK enzyme. To further evaluate the importance of the AMP-kinase's subunits in this thesis, it was necessary to switch to mouse arteries, as gene targeting tools for hamsters are much rarer and less established than mouse knockout models (Fan, Li et al. (2014)). The AMP-kinase's impact on mouse vessels had, until our studies were performed, mainly been analyzed in larger arteries including the aorta, where AMP-kinase's activation can induce vasodilation in an endothelium-dependent way by activating the eNOS and in

an endothelium-independent way (Cacicedo, Gauthier et al. (2011); Goirand, Solar et al. (2007)). Analyses of small resistance arteries, however, were missing.

Our experiments with mouse femoral skeletal muscle arteries showed no differences to the previously analyzed hamster vessels. Due to skeletal muscle arteries only delivering very little material for future Western Blot analysis, another vessel type was sought. Mouse mesenteric arteries had long been used for vascular studies and because they presented much more material for the aforementioned Western Blots, it was decided to switch from hamster skeletal muscle arteries to mouse mesenteric arteries.

Due to this change in vessel type, the differences and commonalities of these two vessel types concerning their vasoconstrictive and vasodilative reactivity had to be evaluated. While my experiments showed that there is no relevant difference in vessel constriction to U46, there appears to be less change in the Fura ratio (reflecting smooth muscle intracellular free calcium) in mesenteric arteries. As there is no significant difference in the raw Fura signal data, which could explain the increased ratio of the skeletal muscle arteries, the mesenteric arteries seem to be more calcium sensitive than skeletal muscle arteries. This would have to be investigated further.

Acetylcholine seems to disappear more quickly in mesenteric as compared to skeletal muscle arteries, leading to a decreased endothelial reactivity to increasing doses of acetylcholine in mesenteric arteries, despite there being a good dilation induced by a single dose of acetylcholine (15 μ M). The reason for this remains unclear. There are several possible explanations for this phenomenon that are further explained below.

Mesenteric arteries might present with fewer M3 receptors compared to skeletal muscle arteries, but this would not explain the comparable dilation to a single dose of acetylcholine. The M3 receptors in mesenteric arteries could, however, also be desensitized when adding increasing doses of ACh, a phenomenon that has already been described in various other cell types (Tobin, Lambert et al. (1992); Willets, Challiss et al. (2001)).

Interference with adipokines from mesenteric fatty tissue might also explain the better dilation of skeletal muscle arteries, which are not surrounded by fatty tissue. While there seems to be an interaction between perivascular adipose tissue (PVAT) and the eNOs via Cav-1, which blocks the eNOS and has been described in larger conductance vessels, PVAT is said to not influence acetylcholine-induced dilation of resistance arteries (Lee, Chen et al. (2014); Marchesi, Ebrahimian et al. (2009)).

Additionally, resistance arteries are small arteries where vasodilation is also more regulated via EDHF than eNOS (Bolz, de Wit et al. (1999); Shimokawa, Yasutake et al. (1996)). The PVAT's influence on the eNOS consequently seems to be of minor importance for the vessels that were analyzed in this thesis.

As mentioned by Li, Andersen et al. (2013), there can also be less dilation to increasing doses of acetylcholine in rat mesenteric arteries when PVAT is still attached to these arteries. In my setup, however, PVAT was completely removed, so that mechanically impaired diffusion of the vasodilators cannot explain the findings.

The difference might also result from an augmented mesenteric endothelial death during the Fura incubation period of two hours. If the mesenteric endothelium is more susceptible to cellular death than its skeletal muscle counterpart, it would also explain the comparable reaction to the single dose of acetylcholine, as this was administered before the vessels were incubated with Fura-2. This is, however, also rather unlikely, as other experiments show that ACh is a very potent vasodilator, which only needs a relatively small number of endothelial cells to induce vasodilation.

While there was a huge difference in endothelial reactivity, endothelial-independent relaxation induced by the L-type Ca^{2+} channel blocker nifedipine was comparable between skeletal muscle and mesenteric arteries. As nifedipine was added at the very end of the experiment and as the analysis had to be made comparing the effect of nifedipine to the initial constriction induced by norepinephrine, the reaction to nifedipine might have been contaminated by the reactions to the increasing doses of acetylcholine, which were added initially.

As this thesis aimed to analyze the endothelium-independent mechanisms of AMP-kinase's activation and due to them presenting more material for further molecular studies, all AMP-kinase experiments were performed on mesenteric arteries.

5.3. The AMP-Kinase in Mouse Mesenteric Arteries

As already described in Section 1.2.2.2 Pathophysiological Relevance of the AMP-Kinase, both catalytic AMPK α subunits have been described to have different effects on the AMP-kinase's metabolic importance. While the lack of the α_2 subunit severely influences glucose homeostasis, leading to glucose intolerance and insulin resistance and resulting in an elevated blood pressure, the knockout of the α_1 subunit impairs the cell's reactivity to oxidative stress leading to a shortened erythrocyte life span, anemia and splenomegaly (Wang, Liang et al. (2011); Viollet, Andreelli et al. (2003); Foretz, Hebrard et al. (2011); Wang, Dale et al. (2010)).

As described by Rubin, Magliola et al. (2005) the AMP-kinase's α_1 subunit is predominant in vascular smooth muscle cells of large arteries like the aorta. There was, however, not yet any indication about which catalytic α subunit and consequently which of the AMPK isomers would be of more dilatory importance in resistance arteries. The knockout experiments performed in this thesis aimed to further analyze this aspect. However, it is important to know that knockout animals can potentially adapt to the knockout of the respective gene. The result might thus not always be equivalent to the one gene being knocked out, but it could also reflect the organism's adaptive reaction. It is also important to note that the AMP-kinase's global double knockout, the knockout of both the α_1 and the α_2 gene, is not viable, so that only global single knockouts were analyzed (Viollet, Athesa et al. (2009); Fu, Zhao et al. (2013)).

It could be shown that all underlying genes for the AMP-kinases subunits except the Prkag3 gene, expressing the γ_3 subunit, were present in the mouse mesenteric arteries used in this thesis.

Both AMP-kinase activators that were used in this thesis, A76 and PT1, dilate blood vessels via an endothelial-independent way by activating the smooth muscle cell's AMP-kinase (Schneider, Schubert et al. (2015)). These studies did not reveal any major endothelium-dependent vasodilatory component in the small vessels that were studied. Nevertheless, as several studies have described an endothelial AMP-kinase component that phosphorylates and thus activates the eNOS, L-NAME was used to inhibit a potential endothelial effect (Chen, Peng et al. (2009); Chen, Montagnani et al. (2003); Ford, Teschke et al. (2012)). The AMP-kinase activator A76 is reported to activate the AMP-kinase by binding to the β_1 subunit, while PT1 is reported to activate the AMP-kinase by binding to the α_1 subunit (Scott, van Denderen et al. (2008); Pang, Zhang et al. (2008)). The well-known AMPK activator AICAR for example is also reported to activate the AMP-kinase via the α_1 subunit (Goirand, Solar et al. (2007)).

Especially with PT1, which is considered to bind to the α_1 subunit, one would expect this subunit to be of major importance for the dilation induced by the AMP-kinase. It was thus surprising that the vasodilation was not impaired in α_1 knockout vessels. In α_2 knockout vessels no difference between the knockout and the wild type vessels could be seen on addition of PT1. This second effect can be explained more easily as the α_1 subunit, to which PT1 binds, would be able to take over for the knocked out α_2 subunit. The results from the α_1 knockouts indicate a major importance for the

activation of PT1 via the α_2 subunit. This implies that PT1 presumably influences the AMP-kinase via further binding sites in addition to its known binding site at the α_1 subunit. This has also been demonstrated by Pang, Zhang et al. (2008).

There may also be a compensatory upregulation of the AMP-kinase's α_2 subunit and/or its respective dilatory mechanism covering for the loss of the AMP-kinase's α_1 subunit. This also seems to be the case in the α_2 knockout vessels, as one would expect at least a slight decrease in vasodilation when the α_1 subunit, which is the main subunit in smooth muscle cells, is the only subunit inducing vasodilation (Rubin, Magliola et al. (2005)).

As seen with PT1, the experiments with the other AMP-kinase activator A76 show similar results. The vasodilation elicited by them is not negatively influenced by the knockout of one of the subunits and there even is an increased dilation in the α_1 knockout vessels when adding A76. This implies that A76, just like PT1, appears to have different AMP-kinase target sites. A76 seemed to preferably activate the AMP-kinase via its α_2 subunit. However, it could also activate the AMP-kinase via the α_1 subunit even if less effectively. This was also observed by Xiao, Sanders et al. (2013). However, as with PT1, there seemed to be an efficient compensatory upregulation of the existing α subunit or its vasodilating mechanism, when the significant other subunit was knocked out.

A compensatory upregulation of the still existent α subunit has until now also been described in the gastrocnemius and soleus muscle (Jorgensen, Treebak et al. (2007); Jorgensen, Viollet et al. (2004)).

Both A76 and PT1 could also activate some other AMPK-independent vasodilative mechanism in a non-specific way. However, both activators, which are structurally unrelated, showed the same kind of reaction and as many studies have proven a direct AMP-kinase activation without presenting any relevant alternative dilatory mechanisms (except A76's AMP-kinase-independent inhibitory influence on the Na^+/K^+ -ATPase) this seems highly unlikely (Benziane, Bjornholm et al. (2009); Pang, Zhang et al. (2008); Scott, van Denderen et al. (2008)).

5.3.1. The Effect of the AMP-Kinase's α Subunits on Decreasing Intracellular Calcium Levels

As mentioned in Section 1.1.2 Regulation of Vascular Tone, there are two mechanisms to induce vasodilation, the calcium-dependent and the calcium-independent mechanism, also called calcium desensitization. Both of these mechanisms are influenced by the AMP-kinase activity with calcium desensitization being discussed later in this chapter (Wang, Liang et al. (2011)). Vasodilation via the calcium-dependent mechanism has in other vessels been shown to involve calcium-decreasing mechanisms, one of which is SERCA activation, which induces a calcium uptake from the cytoplasm into its stores. Calcium that is removed by SERCA can consequently no longer be used to augment calmodulin-mediated MLCK activity and induce vasoconstriction (Brini and Carafoli (2009)). As shown by Schneider, Schubert et al. (2015), the AMP-kinase decreases intracellular calcium levels by activating SERCA via phosphorylation of phospholamban. While non phosphorylated phospholamban inhibits SERCA activity, the phosphorylated version allows for an enhanced SERCA activity (Jackson and Colyer (1996)).

Another possibility to decrease the level of intracellular calcium and thus induce dilation in smooth muscle is by blocking the influx through voltage gated calcium channels via hyperpolarization. The BkCa-channel is a calcium-dependent potassium channel that induces hyperpolarization and consequently vasodilation on activation. It has been shown that the AMP-kinase could activate these channels in both mice and hamsters (Foller, Jaumann et al. (2012); Schneider, Schubert et al. (2015)).

As these experiments showed a tendency that the two calcium-dependent vasodilative mechanisms might be attributed to one of the two AMPK α subunits, further experiments were conducted to verify this assumption. Only vessels from α_1 knockout animals were sensitive to a SERCA blockade by its specific inhibitor thapsigargin. α_1 knockout vessels that were treated according to this protocol showed less dilation and a tendency towards a decrease of the Fura ratio at least when applying the highest dose of A76 (100 μ M). This is consistent with the interpretation that the (remaining) α_2 subunit is interfering with the intracellular calcium levels via SERCA activation. In contrast α_2 knockout vessels did not present with any differences compared to the wild type vessels when treated the same way. It must be noted that thapsigargin itself induced an almost complete vasodilation after 8-10 minutes. As this would interfere over time with obtaining a concentration response curve, only one concentration of

A76 could be used. In order to analyze the biggest effect, the highest dose of A76 that was used in the dose-response curves of 100 μ M was chosen for these experiments. The other calcium decreasing mechanism was tested by pre-treating vessels with the BkCa-channel blocker iberiotoxin. There was slightly less dilation in the α_2 knockout vessels when blocking the BkCa-channels. As this decrease in dilation could not be seen in the α_1 knockouts, it is tempting to speculate that the AMPK α_1 subunit predominantly induced vasodilation via BkCa-channel activation.

However, since there were only slight differences with respect to the dose-response curves, one has to assume that strong compensatory mechanisms hid clearer knockout effects of either subunit. Other experiments performed in our laboratory have indeed shown that only the combined inhibition of SERCA and the BkCa-channels could severely reduce the AMPK-induced dilation (Schneider, Schubert et al. (2015)). Another possibility is a potential compensatory increase of the remaining α subunit after the knockout of either the α_1 or the α_2 subunit. It has been shown in skeletal muscle that the expression of the remaining subunit can be upregulated (Jorgensen, Viollet et al. (2004); Jorgensen, Treebak et al. (2007)). We did not test this possibility in more detail.

For further analysis, BkCa knockout vessels should be tested with thapsigargin to verify that there is no longer an effect on A76 induced dilation, as both dilatory mechanisms would not be functional in this setting and a complete knockout would have been generated.

5.3.2. The Effect of the AMP-Kinase's α Subunits on Calcium Sensitivity

Calcium sensitivity is the other important mechanism in addition to the receptor-mediated increase or decrease of intracellular calcium for regulating vascular tone. Compared to the receptor-mediated regulatory mechanism, which affects vascular tone instantly, calcium desensitization takes effect with a delay of approximately five minutes.

Calcium sensitivity is regulated by both the MLCP and the MLCK and their respective activation or inhibition. The AMP-kinase does not influence the MLC directly, but is reported to influence both the MLCP, the MLCK and actin to induce calcium desensitization and consequently vasodilation in larger conductance and small resistance arteries (Bultot, Horman et al. (2009); Horman, Morel et al. (2008); Wang, Liang et al. (2011); Schubert, Qiu et al. (2017)).

In mouse vessels it could be shown that the AMP-kinase activates the MLCP by blocking the RhoA/ROCK/MYPT1 pathway, which would otherwise block the MLCP, via p190-GAP (Wang, Liang et al. (2011)).

The AMP-kinase has, however, not only been described to take part in calcium desensitization via blocking the inhibition of the MLCP but it has also been reported to block the MLCK directly via phosphorylation at Ser⁸¹⁵ (Horman, Morel et al. (2008)). There is only scarce evidence concerning which AMPK α subunit is responsible for inducing this delayed dilation, with Wang, Liang et al. (2011) describing an influence of the α_2 subunit for this in the aorta. To date there is no evidence for the influence of both AMPK subunits on calcium sensitivity in resistance arteries.

These mechanisms were not found to play a role in other experiments performed in our lab. Rather, the AMP-kinase influenced vascular tone in a calcium independent manner by actin-depolymerization. It could be shown by Schubert, Qiu et al. (2017) that the AMP-kinase dephosphorylates cofilin, which influences actin thickness and ramification and induces depolymerization of F-actin, thus leading to vasodilation.

My experiments were not meant to further analyze the influence of the AMP-kinase on the different mechanisms influencing calcium sensitivity but focused on the relative roles of the AMP-kinase's α subunits.

I could show that A76 induced calcium desensitization in ordinary mesenteric arteries. By firstly pre-treating the vessels with calcium-free MOPS and then with a calcium-free MOPS with an elevated potassium (K^+ 125 mM), it was ensured that both the vessels' intracellular calcium stores and the extracellular calcium level was down to zero and the voltage-dependent calcium channels (VDCCs) were opened. By opening the voltage-dependent calcium channels a change in the extracellular calcium levels led to a corresponding change in intracellular calcium levels. A76 reduced vasoconstriction to the increasing calcium concentrations compared to a pre-test that presented with the same intracellular calcium levels but without the AMP-kinase activator. These experiments could not be performed with PT1 as it interfered with the calcium measurement.

To further evaluate which α subunit has a major influence on calcium sensitivity, experiments were consequently conducted in the respective AMP-kinase's subunit knockout mice. Due to bleaching artefacts of Fura, which can occur in long term experiments such as these, absolute as opposed to relative values were analyzed. Using these absolute values, however, usually makes the resulting evaluation more

susceptible to vessel-related characteristics such as different original Fura loading, but as vessel characteristics were comparable to the baseline in each experiment and due to heavy bleaching artefacts that interfered with the analysis, absolute values still provided the more reliable data. As in wild type vessels, A76 impaired the vasoconstriction induced by increasing doses of extracellular Ca^{2+} , thus inducing calcium desensitization in α_1 knockout vessels. Adding A76 did, however, not lead to decreased vasoconstriction and thus calcium desensitization in α_2 knockout vessels. Due to these experiments, the AMP-kinase's α_2 subunit seems to control calcium sensitivity. This is an important new function of the α_2 subunit and potentially offers a new specific target for vasoactive medication, especially when Ca^{2+} -entry blockers are not effective.

This study, however, has not yet analyzed whether this α_2 subunit-mediated effect works through actin depolymerization.

5.4. Consequences of these Findings for Vascular Control

Basal vascular tone is of major importance in regulating tissue perfusion by adapting vascular resistance (Jackson (2000)). Basal vascular tone in resistance arteries is mainly defined by myogenic tone, which provides a baseline constriction, upon which further stimuli including vasoconstrictors or endothelium dependent factors like eNOS and EDHF can influence the basal vascular tone (Vallance (1992); Shimokawa, Yasutake et al. (1996); Tykocki, Boerman et al. (2017)). Numerous ion channels influencing the membrane potential play an important role in setting the myogenic tone (Tykocki, Boerman et al. (2017)).

Regarding literature findings, the activated AMP-kinase is considered to decrease basal vascular tone by phosphorylating the eNOS, consequently inhibiting the phosphorylation of the MLC via the RhoA/ROCK/MYPT1 pathway (Chen, Peng et al. (2009); Chen, Montagnani et al. (2003); Ford, Teschke et al. (2012); Wang et al. (2011)). In my experiments both the α_1 and the α_2 knockouts present with no significant basal tone, but appear to be completely relaxed, which agrees with our earlier findings of a lack of endothelial AMP-kinase induced dilation.

On the other hand, the AMP-kinase and its two catalytic subunits are said to influence vascular tone by inhibiting vasoconstriction (Wang, Liang et al. (2011); Horman, Morel et al. (2008); Gayard, Guilluy et al. (2011)). Wang, Liang et al. (2011) and Gayard, Guilluy et al. (2011) showed that the AMP-kinase inhibits the RhoA/ROCK/MYPT1

pathway via phosphorylation of serine of p190-GAP or Ser¹⁸⁸ and thus activates the MLCP, leading to a vasodilation.

In my experiments, the AMPK α_2 subunit significantly decreased vasoconstriction to norepinephrine (also seen in Wang, Liang et al. (2011)), while at the same time not significantly influencing the Fura ratio, which thus further implies that the AMPK α_2 subunit decreases calcium sensitivity (as already pointed out in Chapter 5.3.2). As vasoconstriction and vasodilation lead to changes in blood pressure, the increased constriction observed in α_2 knockout mice compared to the control mice can also explain the increased blood pressure observed in α_2 knockout mice by Wang, Liang et al. (2011). Reducing blood pressure by activating the AMP-kinase would thus be an interesting mechanism for hypertensive patients. Due to the AMP-kinase's metabolic effects it would be of even greater importance for patients suffering from the metabolic syndrome. The well-known antidiabetic drug Metformin, which has been described to lower blood glucose via AMP-kinase activation, could thus be seen as a potential antihypertensive drug (Zhou, Myers et al. (2001)). It has, however, been described to have no significant effect on blood pressure in diabetic and non-diabetic humans (Snorgaard, Kober et al. (1997); Wulffele, Kooy et al. (2004)). In recent years Metformin has also been described to lower blood glucose in an AMP-kinase independent manner (Rena, Hardie et al. (2017)). This and the lack of influence on vascular tone show that the effect mechanisms of Metformin have not yet been completely understood.

In contrast to what would be expected from literature and from the α_2 experiments, there was no difference in constriction to norepinephrine in α_1 wild type and knockout vessels (Wang, Liang et al. (2011); Horman, Morel et al. (2008)). In addition to this non-existent difference in constriction to norepinephrine in the α_1 knockout, there was no difference for both α_1 and α_2 wild type and knockout vessels concerning constriction to K⁺ 125 mM. Horman, Morel et al. (2008) reported less constriction in wild type than in α_1 knockout mice on addition of K⁺ 100 mM, which is an indication that the AMP-kinase might not only influence the MLCP but also block the MLCK. As mentioned earlier Horman, Morel et al. (2008) used aortic rings and thus conductance vessels, where the AMP-kinase could influence vascular tone in a subunit independent fashion and where it might present with this additional effect on the MLCK. This has until now not been further evaluated in additional studies.

This study focused on the pharmacological stimuli of the AMP-kinase. The AMP-kinase is, however, also activated by physiological stimuli like hypoxia, fasting or physical exercise that increase ATP consumption inducing an increase in the AMP/ATP ratio (Hardie, Carling et al. 1998); Hardie and Lin (2017)). As these stimuli are, however, more difficult to quantitatively measure, it was decided to focus on a pharmacological stimulation.

To further analyze the importance and the effects of the AMP-kinase pharmacologically blocking the AMP-kinase would also be an option as the double knockout is not viable. Unfortunately, the most potent inhibitor of the AMP-kinase, compound C, has been described as unselective, so that this method was not used in this study (Bain, Plater et al. (2007).

A good alternative would have been inducible, smooth muscle specific AMPK knockout mice for both α subunits, but these mice were not yet available at the time of my experiments.

6. Summary

The heterotrimeric AMP-kinase is an enzyme which is nearly ubiquitously expressed. It was originally considered to play a role in the liver and muscle metabolism but there is increasing evidence that it also plays a role in the control of vascular functions. To further examine the effects of the AMP-kinase and its subunits on vascular tone, it was important to switch from a hamster model to a mouse model, as a hamster knockout model was not available. In this thesis, it was therefore determined whether mouse arteries present with a similar AMP-kinase induced regulation of the vascular tone compared to the hamster skeletal muscle arteries previously used in our group. It was further analyzed whether this influence on the vascular tone can be seen in different vascular beds, such as the vascular beds of mesenteric and skeletal muscle arteries. Studies of knockout animals were subsequently conducted to determine whether the two alternative AMP-kinase α subunits played any specific role in the regulation of the vascular tone of small murine arteries.

All experiments were carried out using freshly isolated vessels that were kept under constant pressure. Changes in vascular diameter were studied by a video-based approach, whereas the intracellular free calcium in the vascular smooth muscle was measured using the Fura-2 technique. The AMP-kinase, which is stimulated by hypoxia, fasting or physical exercise in vivo, was studied here using two structurally different pharmacologic stimulators, A769662 and PT1.

Western Blot analyses to analyze the signaling processes, which are beyond the scope of this thesis, require sufficient quantities of vessel-derived protein. It was therefore decided to focus mainly on mesenteric arteries as the mesenteric vascular bed provides ample material compared to the limited number of accessible skeletal muscle arteries in the mouse. Our analysis of the two different vascular beds showed that both exhibited a marked endothelium-dependent dilation in response to acetylcholine after precontraction with the thromboxane analogue U46619. The acetylcholine-induced response, however, faded quickly in mesenteric arteries but not in skeletal muscle arteries. This was probably due to M3 receptor desensitization or a potential adipokine interference.

As the AMP-kinase's effects were studied with reference to the vascular smooth muscle, this aspect was not studied further. It could be shown that all isoforms of the three AMP-kinase subunits (α , β , γ) were expressed in the mesenteric arteries, except the γ_3 subunit. In mesenteric arteries both catalytic subunits (α_1 and α_2) were present

but the α_1 subunit was expressed at a higher level than the α_2 subunit. Both AMP-kinase activators (A76 and PT1) led to a dose-dependent dilation and A76 also resulted in a concentration-dependent decrease of the smooth muscles' free calcium concentration (as measured by the Fura ratio) in mesenteric arteries. Earlier studies with hamster vessels by our lab revealed that the decrease in calcium is due to SERCA and BkCa-channel activation. The silencing of one of the α subunits only exerted minor effects on the overall dilatory response of the vessels to the AMP-kinase stimulation. This surprisingly little influence of either the α_1 or the α_2 knockout on the overall dilation suggests that even if a specific effect of the subunits for one of these calcium-decreasing mechanisms existed, it was probably hidden by a mutual compensation of the calcium decreasing effects of BkCa channel and SERCA activation. However, further experiments with the SERCA blocker thapsigargin showed that only vessels from α_1 knockout mice were sensitive to SERCA inhibition, suggesting that the AMPK α_2 subunit induces vasodilation and a decrease in the intracellular calcium levels by mainly activating SERCA, which in turn would be consistent with the predominant activation of BkCa-channels by the AMPK α_1 subunit. In functionally calcium-permeabilized vessels, stimulation of the AMP-kinase reduced the contractile response of the arteries to increasing calcium concentrations, which is defined as calcium desensitization of the smooth muscle. This mechanism could also be observed in intact vessels since murine mesenteric arteries could in appropriate conditions dilate without changes in intracellular calcium levels. This calcium-independent dilatory mechanism, was also analyzed for the influence of the AMP-kinase and its subunits. We could demonstrate that the calcium-independent vasodilation is primarily regulated by the AMP-kinase's α_2 subunit, without evident compensation by the α_1 subunit, thus offering a potential new target for vasoactive medication. This study has, however, not further analyzed the mechanisms underlying this calcium desensitization.

Due to the AMP-kinase's metabolic and vasoregulating effects for patients presenting with the metabolic syndrome for instance, these findings can offer further understanding for potential medication that targets metabolic and vascular effects at the same time. To further investigate the physiological impact of these findings, experiments with in vivo models and inducible, smooth muscle specific AMPK double knockout mice, which were not yet available at the time of my experiments, should be conducted.

7. Zusammenfassung

Die heterotrimere AMP-Kinase ist ein beinahe ubiquitär exprimiertes Enzym, von dem ursprünglich ausgegangen war, dass es eine wichtige Rolle im Leber- und Muskelstoffwechsel spielt. Es gibt jedoch zunehmend Hinweise darauf, dass die AMP-Kinase auch in der Kontrolle der Gefäßfunktion eine Rolle spielt. Um die Effekte der AMP-Kinase und ihrer Untereinheiten weiter zu untersuchen, war es wichtig von einem Hamster- auf ein Mausmodell zu wechseln, da Hamsterknockoutmodelle nicht existierten. In dieser Doktorarbeit wurde daher zuerst untersucht, ob Mausexperimente, im Vergleich zu den zuvor in unserer Arbeitsgruppe verwendeten Hamsterskelettmuskelarterien, eine ähnliche AMP-Kinase-induzierte Regulation des Gefäßtonus zeigten. Weiterhin wurde untersucht, ob dieser Einfluss auf den Gefäßtonus in verschiedenen Gefäßbetten, wie zum Beispiel den Gefäßbetten der Mesenterial- und der Skelettmuskelarterien, gesehen werden kann. Im Anschluss daran wurden Versuche an Knockouttieren durchgeführt, um festzustellen, ob die zwei alternativen AMPK α Untereinheiten eine spezifische Rolle in der Regulation des Gefäßtonus der kleinen Mausexperimente spielen.

Alle Experimente wurden an frisch isolierten Gefäßen durchgeführt, die unter einem konstanten Druck gehalten wurden. Änderungen des Gefäßdurchmessers wurden videographisch registriert, während das freie intrazelluläre Calcium in den glatten Gefäßmuskelzellen mit Hilfe der Fura-2 Technik gemessen wurde.

Die AMP-Kinase, die unter anderem durch Hypoxie, Fasten oder sportliche Aktivität in vivo stimuliert wird, wurde hier mit Hilfe von zwei strukturell unterschiedlichen pharmakologischen Stimulatoren, A769662 and PT1, untersucht.

Da die Western Blotanalysen, als Mittel zur über diese Doktorarbeit hinausgehenden Analyse zellulärer Signalwege, ausreichende Mengen an Protein aus den Gefäßen benötigen, wurde beschlossen den Fokus auf die Mesenterialgefäße zu legen, da das mesenteriale Gefäßbett, verglichen mit der begrenzten Anzahl zugänglicher Skelettmuskelarterien in der Maus, ausreichend Gefäßmaterial liefern kann.

Unsere Analyse der beiden verschiedenen Gefäßbetten zeigte, dass die Gefäße dieser beiden Gefäßbetten nach einer Vorkontraktion mit dem Thromboxananalogen U46619 eine starke Endothel-abhängige Dilatation auf Acetylcholin zeigten. Die durch Acetylcholin induzierte Vasodilatation ließ jedoch in den Mesenterialarterien, nicht aber in den Skelettmuskelarterien, schnell nach. Dies lag wahrscheinlich an einer Desensitivierung der M3-Rezeptoren oder einer potentiellen Interferenz durch

Adipokine. Da die Effekte der AMP-Kinase in Bezug auf den glatten Gefäßmuskel untersucht wurden, wurde dieser Aspekt jedoch nicht weiter untersucht.

Es konnte gezeigt werden, dass alle Isoformen der drei AMP-Kinase Untereinheiten (α , β , γ) bis auf die γ_3 Untereinheit in den Mesenterialarterien exprimiert waren. In den Mesenterialarterien waren beide katalytischen Untereinheiten (α_1 und α_2) vorhanden, die α_1 Untereinheit war jedoch stärker exprimiert als die α_2 Untereinheit. Beide AMPK-Aktivatoren (A76 und PT1) induzierten eine dosisabhängige Vasodilatation, wobei A76 auch einen konzentrationsabhängigen Abfall der intrazellulären freien Calciumkonzentration in den glatten Muskelzellen der Mesenterialgefäße induzierte. Unsere früheren Versuche an Hamstergefäßen hatten gezeigt, dass dieser Calciumabfall durch Aktivierung der SERCA und der BkCa-Kanäle entsteht. Der Knockout einer der zwei α Untereinheiten hatte nur einen geringen Effekt auf die durch die AMPK-Stimulation ausgelöste, gesamte vasodilatatorische Gefäßantwort. Dieser überraschend geringe Einfluss sowohl der α_1 als auch der α_2 Untereinheit auf die Gesamtdilatation suggeriert eine gegenseitige Kompensation der Calcium-reduzierenden Effekte (der BkCa-Kanal und der SERCA Aktivierung), die einen eventuell existierenden spezifischen Effekt der α Untereinheiten auf einen dieser Calcium-reduzierenden Mechanismen maskiert.

Weitere Experimente mit dem SERCA-Blocker Thapsigargin haben gezeigt, dass nur Gefäße von α_1 Knockoutmäusen empfindlich für eine Hemmung der SERCA waren, was darauf hindeutet, dass die AMPK α_2 Untereinheit hauptsächlich durch eine Aktivierung der SERCA eine Vasodilatation und einen Abfall der intrazellulären Calciumspiegel induziert. Dies wäre wiederum vereinbar mit der vorrangigen Aktivierung der BkCa-Kanäle durch die AMPK α_1 Untereinheit.

In funktionell Calcium-durchlässigen Gefäßen führte die Stimulation der AMP-Kinase zu einer reduzierten Gefäßkontraktion auf ansteigende Calciumkonzentrationen. Dies bezeichnet man als Calciumdesensitivierung des glatten Gefäßmuskels. Dieser Mechanismus konnte auch in intakten Mausgefäßen beobachtet werden, da die Mesenterialgefäße unter den richtigen Bedingungen ohne Änderung der intrazellulären Calciumspiegel dilatieren konnten. Dieser Calcium-unabhängige Dilatationsmechanismus wurde ebenfalls auf den Einfluss der AMP-Kinase und ihrer Untereinheiten analysiert. Wir konnten zeigen, dass die Calcium-unabhängige Vasodilatation vorrangig durch die AMPK α_2 Untereinheit reguliert wird. Es zeigten sich keine Hinweise auf eine offensichtliche Kompensation durch die α_1 Untereinheit,

sodass diese Regulation der Calciumdesensitivierung durch die α_2 Untereinheit einen potentiellen neuen Angriffspunkt für vasoaktive Medikamente darstellt. Diese Arbeit beschäftigte sich jedoch nicht genauer mit den dieser Calciumdesensitivierung zugrunde liegenden Mechanismen.

Aufgrund der metabolischen und gefäßregulierenden Effekte der AMP-Kinase für Patienten mit zum Beispiel dem metabolischen Syndrom können diese Erkenntnisse zu einem besseren Verständnis für potentielle neue Medikamente, die an metabolischen und vaskulären Effekten gleichzeitig angreifen, führen. Um die physiologische Bedeutung dieser Erkenntnisse weiter zu untersuchen, sollten Versuche an in vivo Modellen und induzierbaren glattmuskulären AMPK Doppelknockoutmäusen, die zur Zeit der Durchführung dieser Experimente noch nicht verfügbar waren, durchgeführt werden.

8. References

8.1. Books

Hick, A. and C. Hick (2013). Kurzlehrbuch Physiologie. Munich, Urban & Fischer.

Pape, H.-C., A. Kurtz and S. Silbernagl (2014). Physiologie. Stuttgart, Thieme.

8.2. Articles

Adelstein, R. S. and E. Eisenberg (1980). "Regulation and kinetics of the actin-myosin-ATP interaction." Annu Rev Biochem **49**: 921-956.

Bain, J., L. Plater, M. Elliott, N. Shpiro, C. J. Hastie, H. McLauchlan, I. Klevernic, J. S. Arthur, D. R. Alessi and P. Cohen (2007). "The selectivity of protein kinase inhibitors: a further update." Biochem J **408**(3): 297-315.

Benham, C. D. (1989). "Voltage-gated and agonist-mediated rises in intracellular Ca²⁺ in rat clonal pituitary cells (GH3) held under voltage clamp." J Physiol **415**: 143-158.

Benziane, B., M. Bjornholm, L. Lantier, B. Viollet, J. R. Zierath and A. V. Chibalin (2009). "AMP-activated protein kinase activator A-769662 is an inhibitor of the Na(+)-K(+)-ATPase." Am J Physiol Cell Physiol **297**(6): C1554-1566.

Blodow, S., H. Schneider, U. Storch, R. Wizemann, A. L. Forst, T. Gudermann and M. Mederos y Schnitzler (2013). "Novel role of mechanosensitive AT1B receptors in myogenic vasoconstriction." Pflugers Arch **466**(7): 1343-1353.

Bolz, S. S., C. de Wit and U. Pohl (1999). "Endothelium-derived hyperpolarizing factor but not NO reduces smooth muscle Ca²⁺ during acetylcholine-induced dilation of microvessels." Br J Pharmacol **128**(1): 124-134.

Bolz, S. S., J. Galle, R. Derwand, C. de Wit and U. Pohl (2000). "Oxidized LDL increases the sensitivity of the contractile apparatus in isolated resistance arteries for Ca(2+) via a rho- and rho kinase-dependent mechanism." Circulation **102**(19): 2402-2410.

Bolz, S. S., L. Vogel, D. Sollinger, R. Derwand, C. de Wit, G. Loirand and U. Pohl (2003). "Nitric oxide-induced decrease in calcium sensitivity of resistance arteries is

attributable to activation of the myosin light chain phosphatase and antagonized by the RhoA/Rho kinase pathway." Circulation **107**(24): 3081-3087.

Brini, M. and E. Carafoli (2009). "Calcium pumps in health and disease." Physiol Rev **89**(4): 1341-1378.

Bultot, L., S. Horman, D. Neumann, M. P. Walsh, L. Hue and M. H. Rider (2009). "Myosin light chains are not a physiological substrate of AMPK in the control of cell structure changes." FEBS Lett **583**(1): 25-28.

Cacicedo, J. M., M. S. Gauthier, N. K. Lebrasseur, R. Jasuja, N. B. Ruderman and Y. Ido (2011). "Acute exercise activates AMPK and eNOS in the mouse aorta." Am J Physiol Heart Circ Physiol **301**(4): H1255-1265.

Cao, X., T. Luo, X. Luo and Z. Tang (2014). "Resveratrol prevents AngII-induced hypertension via AMPK activation and RhoA/ROCK suppression in mice." Hypertens Res **37**(9): 803-810.

Carling, D., V. A. Zammit and D. G. Hardie (1987). "A common bicyclic protein kinase cascade inactivates the regulatory enzymes of fatty acid and cholesterol biosynthesis." FEBS Lett **223**(2): 217-222.

Chang, C. C., S. S. Wang, H. C. Huang, C. Y. Chan, F. Y. Lee, H. C. Lin, J. Y. Nong, C. L. Chuang and S. D. Lee (2011). "Selective cyclooxygenase inhibition improves hepatic encephalopathy in fulminant hepatic failure of rat." Eur J Pharmacol **666**(1-3): 226-232.

Chen, H., M. Montagnani, T. Funahashi, I. Shimomura and M. J. Quon (2003). "Adiponectin stimulates production of nitric oxide in vascular endothelial cells." J Biol Chem **278**(45): 45021-45026.

Chen, Z., I. C. Peng, W. Sun, M. I. Su, P. H. Hsu, Y. Fu, Y. Zhu, K. DeFea, S. Pan, M. D. Tsai and J. Y. Shyy (2009). "AMP-activated protein kinase functionally phosphorylates endothelial nitric oxide synthase Ser633." Circ Res **104**(4): 496-505.

Chen, Z. P., K. I. Mitchelhill, B. J. Michell, D. Stapleton, I. Rodriguez-Crespo, L. A. Witters, D. A. Power, P. R. Ortiz de Montellano and B. E. Kemp (1999). "AMP-

activated protein kinase phosphorylation of endothelial NO synthase." FEBS Lett **443**(3): 285-289.

Cheung, P. C., I. P. Salt, S. P. Davies, D. G. Hardie and D. Carling (2000). "Characterization of AMP-activated protein kinase gamma-subunit isoforms and their role in AMP binding." Biochem J **346 Pt 3**: 659-669.

Cool, B., B. Zinker, W. Chiou, L. Kifle, N. Cao, M. Perham, R. Dickinson, A. Adler, G. Gagne, R. Iyengar, G. Zhao, K. Marsh, P. Kym, P. Jung, H. S. Camp and E. Frevert (2006). "Identification and characterization of a small molecule AMPK activator that treats key components of type 2 diabetes and the metabolic syndrome." Cell Metab **3**(6): 403-416.

Dabrowska, R., D. Aromatorio, J. M. Sherry and D. J. Hartshorne (1977). "Composition of the myosin light chain kinase from chicken gizzard." Biochem Biophys Res Commun **78**(4): 1263-1272.

Dabrowska, R., J. M. Sherry, D. K. Aromatorio and D. J. Hartshorne (1978). "Modulator protein as a component of the myosin light chain kinase from chicken gizzard." Biochemistry **17**(2): 253-258.

Dong, Y., M. Zhang, B. Liang, Z. Xie, Z. Zhao, S. Asfa, H. C. Choi and M. H. Zou (2010). "Reduction of AMP-activated protein kinase alpha2 increases endoplasmic reticulum stress and atherosclerosis in vivo." Circulation **121**(6): 792-803.

Enkhjargal, B., S. Godo, A. Sawada, N. Suvd, H. Saito, K. Noda, K. Satoh and H. Shimokawa (2014). "Endothelial AMP-activated protein kinase regulates blood pressure and coronary flow responses through hyperpolarization mechanism in mice." Arterioscler Thromb Vasc Biol **34**(7): 1505-1513.

Eto, M., T. Kitazawa, M. Yazawa, H. Mukai, Y. Ono and D. L. Brautigan (2001). "Histamine-induced vasoconstriction involves phosphorylation of a specific inhibitor protein for myosin phosphatase by protein kinase C alpha and delta isoforms." J Biol Chem **276**(31): 29072-29078.

Fan, Z., W. Li, S. R. Lee, Q. Meng, B. Shi, T. D. Bunch, K. L. White, I. K. Kong and Z. Wang (2014). "Efficient gene targeting in golden Syrian hamsters by the CRISPR/Cas9 system." PLoS One **9**(10): e109755.

Ferrer, A., C. Caelles, N. Massot and F. G. Hegardt (1985). "Activation of rat liver cytosolic 3-hydroxy-3-methylglutaryl coenzyme A reductase kinase by adenosine 5'-monophosphate." Biochem Biophys Res Commun **132**(2): 497-504.

Fogarty, S. and D. G. Hardie (2009). "Development of protein kinase activators: AMPK as a target in metabolic disorders and cancer." Biochim Biophys Acta **1804**(3): 581-591.

Foller, M., M. Jaumann, J. Dettling, A. Saxena, T. Pakladok, C. Munoz, P. Ruth, M. Sopjani, G. Seeböhm, L. Ruttiger, M. Knipper and F. Lang (2012). "AMP-activated protein kinase in BK-channel regulation and protection against hearing loss following acoustic overstimulation." FASEB J **26**(10): 4243-4253.

Ford, R. J., S. R. Teschke, E. B. Reid, K. K. Durham, J. T. Kroetsch and J. W. Rush (2012). "AMP-activated protein kinase activator AICAR acutely lowers blood pressure and relaxes isolated resistance arteries of hypertensive rats." J Hypertens **30**(4): 725-733.

Foretz, M., S. Hebrard, S. Guihard, J. Leclerc, M. Do Cruzeiro, G. Hamard, F. Niedergang, M. Gaudry and B. Viollet (2011). "The AMPK γ 1 subunit plays an essential role in erythrocyte membrane elasticity, and its genetic inactivation induces splenomegaly and anemia." FASEB J **25**(1): 337-347.

Fu, X., J. X. Zhao, M. J. Zhu, M. Foretz, B. Viollet, M. V. Dodson and M. Du (2013). "AMP-activated protein kinase α 1 but not α 2 catalytic subunit potentiates myogenin expression and myogenesis." Mol Cell Biol **33**(22): 4517-4525.

Gayard, M., C. Guilluy, A. Rousselle, B. Viollet, D. Henrion, P. Pacaud, G. Loirand and M. Rolli-Derkinderen (2011). "AMPK α 1-induced RhoA phosphorylation mediates vasoprotective effect of estradiol." Arterioscler Thromb Vasc Biol **31**(11): 2634-2642.

Goirand, F., M. Solar, Y. Athes, B. Viollet, P. Mateo, D. Fortin, J. Leclerc, J. Hoerter, R. Ventura-Clapier and A. Garnier (2007). "Activation of AMP kinase α 1 subunit induces aortic vasorelaxation in mice." J Physiol **581**(Pt 3): 1163-1171.

Goransson, O., A. McBride, S. A. Hawley, F. A. Ross, N. Shpiro, M. Foretz, B. Viollet, D. G. Hardie and K. Sakamoto (2007). "Mechanism of action of A-769662, a valuable

- tool for activation of AMP-activated protein kinase." J Biol Chem **282**(45): 32549-32560.
- Grynkiewicz, G., M. Poenie and R. Y. Tsien (1985). "A new generation of Ca²⁺ indicators with greatly improved fluorescence properties." J Biol Chem **260**(6): 3440-3450.
- Hardie, D. G. (2007). "AMP-activated/SNF1 protein kinases: conserved guardians of cellular energy." Nat Rev Mol Cell Biol **8**(10): 774-785.
- Hardie, D. G. (2018). "Keeping the home fires burning: AMP-activated protein kinase." J R Soc Interface **15**(138).
- Hardie, D. G. and D. Carling (1997). "The AMP-activated protein kinase--fuel gauge of the mammalian cell?" Eur J Biochem **246**(2): 259-273.
- Hardie, D. G., D. Carling and M. Carlson (1998). "The AMP-activated/SNF1 protein kinase subfamily: metabolic sensors of the eukaryotic cell?" Annu Rev Biochem **67**: 821-855.
- Hardie, D. G. and S. C. Lin (2017). "AMP-activated protein kinase - not just an energy sensor." F1000Res **6**: 1724.
- Hawley, S. A., M. Davison, A. Woods, S. P. Davies, R. K. Beri, D. Carling and D. G. Hardie (1996). "Characterization of the AMP-activated protein kinase kinase from rat liver and identification of threonine 172 as the major site at which it phosphorylates AMP-activated protein kinase." J Biol Chem **271**(44): 27879-27887.
- Hick, A. and C. Hick (2013). Kurzlehrbuch Physiologie. Munich, Urban & Fischer.
- Horman, S., N. Morel, D. Vertommen, N. Hussain, D. Neumann, C. Beauloye, N. El Najjar, C. Forcet, B. Viollet, M. P. Walsh, L. Hue and M. H. Rider (2008). "AMP-activated protein kinase phosphorylates and desensitizes smooth muscle myosin light chain kinase." J Biol Chem **283**(27): 18505-18512.
- Huang, Y., C. A. Smith, G. Chen, B. Sharma, A. S. Miner, R. W. Barbee and P. H. Ratz (2017). "The AMP-Dependent Protein Kinase (AMPK) Activator A-769662 Causes Arterial Relaxation by Reducing Cytosolic Free Calcium Independently of an Increase in AMPK Phosphorylation." Front Pharmacol **8**: 756.

-
- Intengan, H. D. and E. L. Schiffrin (2000). "Structure and mechanical properties of resistance arteries in hypertension: role of adhesion molecules and extracellular matrix determinants." Hypertension **36**(3): 312-318.
- Jackson, W. A. and J. Colyer (1996). "Translation of Ser16 and Thr17 phosphorylation of phospholamban into Ca²⁺-pump stimulation." Biochem J **316** (Pt 1): 201-207.
- Jackson, W. F. (2000). "Ion channels and vascular tone." Hypertension **35**(1 Pt 2): 173-178.
- Jorgensen, S. B., J. T. Treebak, B. Viollet, P. Schjerling, S. Vaulont, J. F. Wojtaszewski and E. A. Richter (2007). "Role of AMPK α 2 in basal, training-, and AICAR-induced GLUT4, hexokinase II, and mitochondrial protein expression in mouse muscle." Am J Physiol Endocrinol Metab **292**(1): E331-339.
- Jorgensen, S. B., B. Viollet, F. Andreelli, C. Frosig, J. B. Birk, P. Schjerling, S. Vaulont, E. A. Richter and J. F. Wojtaszewski (2004). "Knockout of the α 2 but not α 1 5'-AMP-activated protein kinase isoform abolishes 5-aminoimidazole-4-carboxamide-1- β -D-ribofuranoside but not contraction-induced glucose uptake in skeletal muscle." J Biol Chem **279**(2): 1070-1079.
- Kimura, K., M. Ito, M. Amano, K. Chihara, Y. Fukata, M. Nakafuku, B. Yamamori, J. Feng, T. Nakano, K. Okawa, A. Iwamatsu and K. Kaibuchi (1996). "Regulation of myosin phosphatase by Rho and Rho-associated kinase (Rho-kinase)." Science **273**(5272): 245-248.
- Kitazawa, T., M. Eto, T. P. Woodsome and D. L. Brautigan (2000). "Agonists trigger G protein-mediated activation of the CPI-17 inhibitor phosphoprotein of myosin light chain phosphatase to enhance vascular smooth muscle contractility." J Biol Chem **275**(14): 9897-9900.
- Kreutz, C.-P. (2013). Die Rolle der AMP-Kinase bei der Regulation des Vasotonus Dissertation, LMU München.
- Lee, M. H., S. J. Chen, C. M. Tsao and C. C. Wu (2014). "Perivascular adipose tissue inhibits endothelial function of rat aortas via caveolin-1." PLoS One **9**(6): e99947.

- Li, R., I. Andersen, J. Aleke, V. Golubinskaya, H. Gustafsson and H. Nilsson (2013). "Reduced anti-contractile effect of perivascular adipose tissue on mesenteric small arteries from spontaneously hypertensive rats: Role of Kv7 channels." Eur J Pharmacol **698**(1-3): 310-315.
- Marchesi, C., T. Ebrahimian, O. Angulo, P. Paradis and E. L. Schiffrin (2009). "Endothelial nitric oxide synthase uncoupling and perivascular adipose oxidative stress and inflammation contribute to vascular dysfunction in a rodent model of metabolic syndrome." Hypertension **54**(6): 1384-1392.
- Meininger, G. A., D. C. Zawieja, J. C. Falcone, M. A. Hill and J. P. Davey (1991). "Calcium measurement in isolated arterioles during myogenic and agonist stimulation." Am J Physiol **261**(3 Pt 2): H950-959.
- Mitchelhill, K. I., D. Stapleton, G. Gao, C. House, B. Michell, F. Katsis, L. A. Witters and B. E. Kemp (1994). "Mammalian AMP-activated protein kinase shares structural and functional homology with the catalytic domain of yeast Snf1 protein kinase." J Biol Chem **269**(4): 2361-2364.
- Mizuno, Y., E. Isotani, J. Huang, H. Ding, J. T. Stull and K. E. Kamm (2008). "Myosin light chain kinase activation and calcium sensitization in smooth muscle in vivo." Am J Physiol Cell Physiol **295**(2): C358-364.
- Momcilovic, M., S. P. Hong and M. Carlson (2006). "Mammalian TAK1 activates Snf1 protein kinase in yeast and phosphorylates AMP-activated protein kinase in vitro." J Biol Chem **281**(35): 25336-25343.
- Motulsky, H. J. and L. A. Ransnas (1987). "Fitting curves to data using nonlinear regression: a practical and nonmathematical review." FASEB J **1**(5): 365-374.
- Munday, M. R., D. G. Campbell, D. Carling and D. G. Hardie (1988). "Identification by amino acid sequencing of three major regulatory phosphorylation sites on rat acetyl-CoA carboxylase." Eur J Biochem **175**(2): 331-338.
- Pang, T., Z. S. Zhang, M. Gu, B. Y. Qiu, L. F. Yu, P. R. Cao, W. Shao, M. B. Su, J. Y. Li, F. J. Nan and J. Li (2008). "Small molecule antagonizes autoinhibition and activates AMP-activated protein kinase in cells." J Biol Chem **283**(23): 16051-16060.

-
- Pape, H.-C., A. Kurtz and S. Silbernagl (2014). Physiologie. Stuttgart, Thieme.
- Rena, G., D. G. Hardie and E. R. Pearson (2017). "The mechanisms of action of metformin." Diabetologia **60**(9): 1577-1585.
- Roe, M. W., J. J. Lemasters and B. Herman (1990). "Assessment of Fura-2 for measurements of cytosolic free calcium." Cell Calcium **11**(2-3): 63-73.
- Rubin, L. J., L. Magliola, X. Feng, A. W. Jones and C. C. Hale (2005). "Metabolic activation of AMP kinase in vascular smooth muscle." J Appl Physiol (1985) **98**(1): 296-306.
- Sanders, M. J., Z. S. Ali, B. D. Hegarty, R. Heath, M. A. Snowden and D. Carling (2007). "Defining the mechanism of activation of AMP-activated protein kinase by the small molecule A-769662, a member of the thienopyridone family." J Biol Chem **282**(45): 32539-32548.
- Sanders, M. J., P. O. Grondin, B. D. Hegarty, M. A. Snowden and D. Carling (2007). "Investigating the mechanism for AMP activation of the AMP-activated protein kinase cascade." Biochem J **403**(1): 139-148.
- Schneider, H., K. M. Schubert, S. Blodow, C. P. Kreutz, S. Erdogmus, M. Wiedenmann, J. Qiu, T. Fey, P. Ruth, L. T. Lubomirov, G. Pfitzer, Y. S. M. Mederos, D. G. Hardie, T. Gudermann and U. Pohl (2015). "AMPK Dilates Resistance Arteries via Activation of SERCA and BKCa Channels in Smooth Muscle." Hypertension **66**(1): 108-116.
- Schubert, K. M., J. Qiu, S. Blodow, M. Wiedenmann, L. T. Lubomirov, G. Pfitzer, U. Pohl and H. Schneider (2017). "The AMP-Related Kinase (AMPK) Induces Ca(2+)-Independent Dilation of Resistance Arteries by Interfering With Actin Filament Formation." Circ Res **121**(2): 149-161.
- Scott, J. W., N. Ling, S. M. Issa, T. A. Dite, M. T. O'Brien, Z. P. Chen, S. Galic, C. G. Langendorf, G. R. Steinberg, B. E. Kemp and J. S. Oakhill (2014). "Small molecule drug A-769662 and AMP synergistically activate naive AMPK independent of upstream kinase signaling." Chem Biol **21**(5): 619-627.

Scott, J. W., B. J. van Denderen, S. B. Jorgensen, J. E. Honeyman, G. R. Steinberg, J. S. Oakhill, T. J. Iseli, A. Koay, P. R. Gooley, D. Stapleton and B. E. Kemp (2008). "Thienopyridone drugs are selective activators of AMP-activated protein kinase beta1-containing complexes." Chem Biol **15**(11): 1220-1230.

Shaw, R. J., M. Kosmatka, N. Bardeesy, R. L. Hurley, L. A. Witters, R. A. DePinho and L. C. Cantley (2004). "The tumor suppressor LKB1 kinase directly activates AMP-activated kinase and regulates apoptosis in response to energy stress." Proc Natl Acad Sci U S A **101**(10): 3329-3335.

Shimokawa, H., H. Yasutake, K. Fujii, M. K. Owada, R. Nakaike, Y. Fukumoto, T. Takayanagi, T. Nagao, K. Egashira, M. Fujishima and A. Takeshita (1996). "The importance of the hyperpolarizing mechanism increases as the vessel size decreases in endothelium-dependent relaxations in rat mesenteric circulation." J Cardiovasc Pharmacol **28**(5): 703-711.

Sim, A. T. and D. G. Hardie (1988). "The low activity of acetyl-CoA carboxylase in basal and glucagon-stimulated hepatocytes is due to phosphorylation by the AMP-activated protein kinase and not cyclic AMP-dependent protein kinase." FEBS Lett **233**(2): 294-298.

Snorgaard, O., L. Kober and J. Carlsen (1997). "The effect of metformin on blood pressure and metabolism in nondiabetic hypertensive patients." J Intern Med **242**(5): 407-412.

Stapleton, D., G. Gao, B. J. Michell, J. Widmer, K. Mitchelhill, T. Teh, C. M. House, L. A. Witters and B. E. Kemp (1994). "Mammalian 5'-AMP-activated protein kinase non-catalytic subunits are homologs of proteins that interact with yeast Snf1 protein kinase." J Biol Chem **269**(47): 29343-29346.

Stapleton, D., K. I. Mitchelhill, G. Gao, J. Widmer, B. J. Michell, T. Teh, C. M. House, C. S. Fernandez, T. Cox, L. A. Witters and B. E. Kemp (1996). "Mammalian AMP-activated protein kinase subfamily." J Biol Chem **271**(2): 611-614.

Suter, M., U. Riek, R. Tuerk, U. Schlattner, T. Wallimann and D. Neumann (2006). "Dissecting the role of 5'-AMP for allosteric stimulation, activation, and deactivation of AMP-activated protein kinase." J Biol Chem **281**(43): 32207-32216.

- Teo, T. S. and J. H. Wang (1973). "Mechanism of activation of a cyclic adenosine 3':5'-monophosphate phosphodiesterase from bovine heart by calcium ions. Identification of the protein activator as a Ca²⁺ binding protein." J Biol Chem **248**(17): 5950-5955.
- Thornton, C., M. A. Snowden and D. Carling (1998). "Identification of a novel AMP-activated protein kinase beta subunit isoform that is highly expressed in skeletal muscle." J Biol Chem **273**(20): 12443-12450.
- Timmermans, A. D., M. Balteau, R. Gelinas, E. Renguet, A. Ginion, C. de Meester, K. Sakamoto, J. L. Balligand, F. Bontemps, J. L. Vanoverschelde, S. Horman, C. Beauloye and L. Bertrand (2014). "A-769662 potentiates the effect of other AMP-activated protein kinase activators on cardiac glucose uptake." Am J Physiol Heart Circ Physiol **306**(12): H1619-1630.
- Tobin, A. B., D. G. Lambert and S. R. Nahorski (1992). "Rapid desensitization of muscarinic m3 receptor-stimulated polyphosphoinositide responses." Mol Pharmacol **42**(6): 1042-1048.
- Tsien, R. Y., T. J. Rink and M. Poenie (1985). "Measurement of cytosolic free Ca²⁺ in individual small cells using fluorescence microscopy with dual excitation wavelengths." Cell Calcium **6**(1-2): 145-157.
- Tykocki, N. R., E. M. Boerman and W. F. Jackson (2017). "Smooth Muscle Ion Channels and Regulation of Vascular Tone in Resistance Arteries and Arterioles." Compr Physiol **7**(2): 485-581.
- Uto, A., H. Arai and Y. Ogawa (1991). "Reassessment of Fura-2 and the ratio method for determination of intracellular Ca²⁺ concentrations." Cell Calcium **12**(1): 29-37.
- Vallance, P. (1992). "Endothelial regulation of vascular tone." Postgrad Med J **68**(803): 697-701.
- Viollet, B., F. Andreelli, S. B. Jorgensen, C. Perrin, D. Flamez, J. Mu, J. F. Wojtaszewski, F. C. Schuit, M. Birnbaum, E. Richter, R. Burcelin and S. Vaulont (2003). "Physiological role of AMP-activated protein kinase (AMPK): insights from knockout mouse models." Biochem Soc Trans **31**(Pt 1): 216-219.

-
- Viollet, B., F. Andreelli, S. B. Jorgensen, C. Perrin, A. Geloën, D. Flamez, J. Mu, C. Lenzner, O. Baud, M. Bennoun, E. Gomas, G. Nicolas, J. F. Wojtaszewski, A. Kahn, D. Carling, F. C. Schuit, M. J. Birnbaum, E. A. Richter, R. Burcelin and S. Vaulont (2003). "The AMP-activated protein kinase alpha2 catalytic subunit controls whole-body insulin sensitivity." J Clin Invest **111**(1): 91-98.
- Viollet, B., Y. Athes, R. Mounier, B. Guigas, E. Zarrinpashneh, S. Horman, L. Lantier, S. Hebrard, J. Devin-Leclerc, C. Beauloye, M. Foretz, F. Andreelli, R. Ventura-Clapier and L. Bertrand (2009). "AMPK: Lessons from transgenic and knockout animals." Front Biosci (Landmark Ed) **14**: 19-44.
- Wang, S., G. L. Dale, P. Song, B. Viollet and M. H. Zou (2010). "AMPKalpha1 deletion shortens erythrocyte life span in mice: role of oxidative stress." J Biol Chem **285**(26): 19976-19985.
- Wang, S., B. Liang, B. Viollet and M. H. Zou (2011). "Inhibition of the AMP-activated protein kinase-alpha2 accentuates agonist-induced vascular smooth muscle contraction and high blood pressure in mice." Hypertension **57**(5): 1010-1017.
- Wang, S., M. Zhang, B. Liang, J. Xu, Z. Xie, C. Liu, B. Viollet, D. Yan and M. H. Zou (2010). "AMPKalpha2 deletion causes aberrant expression and activation of NAD(P)H oxidase and consequent endothelial dysfunction in vivo: role of 26S proteasomes." Circ Res **106**(6): 1117-1128.
- Webb, R. C. (2003). "Smooth muscle contraction and relaxation." Adv Physiol Educ **27**(1-4): 201-206.
- Willems, J. M., R. A. Challiss, E. Kelly and S. R. Nahorski (2001). "G protein-coupled receptor kinases 3 and 6 use different pathways to desensitize the endogenous M3 muscarinic acetylcholine receptor in human SH-SY5Y cells." Mol Pharmacol **60**(2): 321-330.
- Woods, A., K. Dickerson, R. Heath, S. P. Hong, M. Momcilovic, S. R. Johnstone, M. Carlson and D. Carling (2005). "Ca²⁺/calmodulin-dependent protein kinase kinase-beta acts upstream of AMP-activated protein kinase in mammalian cells." Cell Metab **2**(1): 21-33.

Woods, A., S. R. Johnstone, K. Dickerson, F. C. Leiper, L. G. Fryer, D. Neumann, U. Schlattner, T. Wallimann, M. Carlson and D. Carling (2003). "LKB1 is the upstream kinase in the AMP-activated protein kinase cascade." Curr Biol **13**(22): 2004-2008.

Wulffele, M. G., A. Kooy, D. de Zeeuw, C. D. Stehouwer and R. T. Gansevoort (2004). "The effect of metformin on blood pressure, plasma cholesterol and triglycerides in type 2 diabetes mellitus: a systematic review." J Intern Med **256**(1): 1-14.

Xiao, B., M. J. Sanders, D. Carmena, N. J. Bright, L. F. Haire, E. Underwood, B. R. Patel, R. B. Heath, P. A. Walker, S. Hallen, F. Giordanetto, S. R. Martin, D. Carling and S. J. Gamblin (2013). "Structural basis of AMPK regulation by small molecule activators." Nat Commun **4**: 3017.

Yeh, L. A., K. H. Lee and K. H. Kim (1980). "Regulation of rat liver acetyl-CoA carboxylase. Regulation of phosphorylation and inactivation of acetyl-CoA carboxylase by the adenylate energy charge." J Biol Chem **255**(6): 2308-2314.

Zhou, G., R. Myers, Y. Li, Y. Chen, X. Shen, J. Fenyk-Melody, M. Wu, J. Ventre, T. Doebber, N. Fujii, N. Musi, M. F. Hirshman, L. J. Goodyear and D. E. Moller (2001). "Role of AMP-activated protein kinase in mechanism of metformin action." J Clin Invest **108**(8): 1167-1174.

Acknowledgements

First of all I would like to thank my supervisor, Professor Ulrich Pohl for the opportunity to work for him and join his laboratory group and for his continuous support, inspiration, guidance and motivation throughout the time of this thesis.

I would also like to thank all the members of our laboratory group, most notably Dr. Michael Schubert, Dr. Holger Schneider and Dr. Jiehua Qiu for their help in finishing my thesis.

Last but not least, I would like to thank my family for always believing in me and for supporting and encouraging me during the difficult and lengthy stages of this thesis.

Eidesstattliche Versicherung

Wiedenmann, Margarethe

Ich erkläre hiermit an Eides statt,
dass ich die vorliegende Dissertation mit dem Thema:

“Differential Role of the AMP-Kinase’s α Subunits in Controlling Microvascular Smooth Muscle Tone”

selbstständig verfasst, mich außer der angegebenen keiner weiteren Hilfsmittel bedient und alle Erkenntnisse, die aus dem Schrifttum ganz oder annähernd übernommen sind, als solche kenntlich gemacht und nach ihrer Herkunft unter Bezeichnung der Fundstelle einzeln nachgewiesen habe.

Ich erkläre des Weiteren, dass die hier vorgelegte Dissertation nicht in gleicher oder in ähnlicher Form bei einer anderen Stelle zur Erlangung eines akademischen Grades eingereicht wurde.

München, den 30.11.2018
Ort, Datum

Margarethe Wiedenmann
Doktorand